Soft-sensor design and dynamic model development for a biomass combustion power plant

Soft-sensor Entwurf und Entwicklung mathematischer Modelle eines Biomasse-verbrennungskraftwerks

Dissertation
zur Erlangung des Grades
des Doktors der Ingenieurwissenschaften
der Naturwissenschaftlich-Technischen Fakultät
der Universität des Saarlandes

von

Fethi Belkhir

Saarbrücken

2017

Tag des Kolloquiums:	11.09.2017
Dekan:	Univ.-Prof. Dr. rer. nat. Guido Kickelbick
Mitglieder des Prüfungsausschusses	
Vorsitzender:	Univ.-Prof. Dr.-Ing. Chihao Xu
Gutachter:	Prof. Dr. Andreas Schütze
	Univ.-Prof. Dr.-Ing. Georg Frey
Akademischer Mitarbeiter	Dr.-Ing. Emanuele Grasso

This thesis is dedicated to my parents Bouzid Belkhir & Souad Haouam for their endless love, support and encouragement. To all great spirits who despite the adversities thrown their way decided not to give up on their definite chief aim.

"Resolve says, 'I will'. The man says, 'I will climb this mountain. They told me it is too high, too far, too steep, too rocky and too difficult. But it's my mountain. I will climb it. You will soon see me waving from the top or dead on the side from trying.'"

Jim Rohn

Abstract

English: From a system theory perspective, a biomass power plant is a nonlinear, coupled multivariate system with multiple inputs (fuel feed, air supply, grate speed) and multiple outputs (gas temperature, oxygen concentration, steam generated), where the different process input-output relationships are difficult to understand due to the large disturbances acting on the combustion process, which emanate mainly from the varying calorific value of fuel delivered to the furnace. Hence, any attempt to maintain stable operating conditions and to design or improve the control strategy being employed will lead to suboptimal solutions, which may jeopardize the commercial character of the combustion site. One possible way to handle such a situation is by improving the combustion performance using advanced model-based control strategies for this aim to further ameliorate the economical aspect of the power plant, while adhering to stringent emission standards. These control techniques explicitly incorporate the available process knowledge, which is represented in terms of an available mathematical model, used by the controller to compute the best control actions to fulfill the multiple conflicting goals in the plant. Therefore, mathematical modeling will be carried out to derive a suitable dynamic model of the power plant. The model is extended by designing a soft-sensor which estimates the energy content of fuel mix.

German: Aus systemetheoretischer Perspektive ist ein Biomassekraftwerk ein nichtlineares, verkoppeltes Mehrgrößensystem mit mehreren Eingängen (Brennstoffzufuhr, Luftzufuhr, Rostgeschwindigkeit) und mehreren Ausgängen (Gastemperatur, Sauerstoffkonzentration, erzeugter Dampfmenge). Dabei werden die unterschiedlichen Beziehungen zwischen Prozesseingängen und -ausgängen von großen Störungen überlagert, die hauptsächlich vom variierenden Heizwert der in den Ofen gelieferten Biomasse herrühren. Deshalb wird jeder Versuch, stabile Betriebsbedingungen aufrechtzuerhalten und die eingesetzte Regelstrategie zu verbessen, zu suboptimalen Lösungen führen, die den kommerziellen Nutzen des Kraftwerks gefährden können. Eine Lösungsmöglichkeit ist die Verbesserung der Verbrennungsleistung unter Verwendung höherer modellbasierter Regelungsstrategien, um den wirtschaftlichen Aspekt des Kraftwerks unter Einhaltung strikter Emissionsnormen weiter zu verbessern. Diese Strategien integrieren explizit das verfügbare Prozesswissen, das durch ein verfügbares mathematisches Modell repräsentiert wird, das vom Regler verwendet wird, um die besten Steuerungsaktionen zu berechnen, die die vielfältigen konkurrierenden Ziele in der Anlage erfüllen. Daher wird eine mathematische Modellierung durchgeführt, um ein geeignetes dynamisches Modell des Kraftwerks abzuleiten. Das Modell wird um einen Softsensor erweitert, der den Energiegehalt des Brennstoffs schätzt.

Acknowledgment

I would like to express my deepest gratitude to my supervisor Prof. Dr.-Ing. Georg Frey. Without his guidance and support, I would not have been able to complete my doctoral thesis.

I would also like to thank my colleagues, with whom I worked during the four years of my research project at the Chair of Automation and Energy Systems, for all the help and support they have provided.

Contents

Abstract **ii**

Acknowledgment **ii**

1 Introduction **1**
1.1 Background . . . 1
1.2 Motivation and target . . . 3
1.3 Organization of the thesis . . . 5

2 Biomass as energy source **7**
2.1 Properties and characterization . . . 8
2.1.1 Chemical composition . . . 8
2.1.2 Moisture content . . . 12
2.1.3 Calorific value . . . 13
2.1.4 Ash content . . . 15
2.2 Biomass properties impact on combustion system . . . 18

3 Power generation from biomass **19**
3.1 Biomass combustion technologies . . . 20
3.1.1 Grate-fired combustors . . . 21
3.1.2 Fluidized-bed combustions . . . 21
3.1.3 Pulverized-fuel combustors . . . 23
3.1.4 Comparison of different technologies . . . 23
3.2 The grate firing system . . . 25
3.2.1 Grate variants . . . 26
3.2.2 Furnace geometry . . . 27
3.2.3 Description of BMK Lünen . . . 29
3.3 Thermochemical conversion processes . . . 32
3.3.1 Drying . . . 33
3.3.2 Pyrolysis . . . 34
3.3.3 Gasification . . . 35
3.3.4 Oxidation . . . 36

4 Mathematical modeling of a biomass power plant **39**
4.1 A review . . . 40
4.2 Combustion furnace . . . 44
4.2.1 Reactor modeling . . . 44
4.2.2 Burning rate . . . 51
4.2.3 Drying process . . . 52
4.2.4 Residence time . . . 54
4.3 Heat transfer mechanisms . . . 56
4.3.1 Radiative heat transfer in furnace . . . 57
4.3.2 Convective heat transfer in bed . . . 62

4.4 Steam boiler . . . 64
4.5 Model calibration . . . 67
4.5.1 The calibration procedure . . . 68
4.5.2 Optimization algorithm . . . 69

5 Biomass calorific value soft-sensing 73
5.1 Existing techniques . . . 75
5.1.1 Direct techniques . . . 77
5.1.2 Indirect techniques . . . 81
5.2 Thermal power estimation . . . 83
5.2.1 Combustion stoichiometry . . . 83
5.2.2 Chemical reactions . . . 84
5.2.3 Combustion air . . . 86
5.3 Static combustion model . . . 87
5.3.1 Mass balance . . . 88
5.3.2 Energy balance . . . 90
5.3.3 Combustion and boiler efficiencies . . . 94
5.4 Fuel calorific value monitoring . . . 100
5.4.1 The monitoring approach . . . 100
5.4.2 Prediction of steam generated . . . 102
5.5 Soft-sensor: A schematic overview . . . 102

6 Simulation results and discussion 105
6.1 Soft-sensor simulation . . . 105
6.1.1 Static combustion model . . . 105
6.1.2 Calorific value estimation . . . 109
6.1.3 Section summary . . . 114
6.2 Understanding the plant dynamics . . . 115
6.2.1 Step response experiments . . . 115
6.2.2 Section summary . . . 119
6.3 Power plant simulation . . . 120
6.3.1 Boiler model . . . 120
6.3.2 Furnace model . . . 122
6.3.3 Section summary . . . 125

7 Summary and future work 127

Bibliography 129

A Nomenclature 141

B Appendix II 145

C Appendix I 147

1 Introduction

1.1 Background

The energy system in the European Union is witnessing a period of fundamental reconstruction and is getting ready for a new "zero-carbon" energy era, where renewables will be a mainstay of future energy supply. This call for an energy transition within EU boarders and other nations has been driven by many facets, with emerging economies like China and India finding that their domestic supply of coal, gas, and oil cannot keep up with the unprecedented demand for energy to fuel their economical growth, the prices have increased drastically over the last few decades. Moreover, the effects of increased greenhouse gas emissions and its environmental impact on global warming can no longer be tolerated. Hence, without a deliberate large-scale shift towards a future low-carbon power system, the emission levels will keep on rising rapidly [Brüggemeier, 2015].

As these challenges continue to grow, so do the opportunities for providing forward-looking innovations and new technologies to establish solutions too. From early on, Germany has recognized these benefits of such a transition and adopted a very ambitious plan among all nations, the Energiewende, to ensure that Germany's future energy system will be not only environmentally cleaner, but also robust and able to adapt itself to future scenarios which will often include a frequent and more unpredictable fluctuating energy market. Strategies for this transformation were initiated in the late 1970's after the oil crisis, and reinforced in the late 1990's by the adoption of Electricity-Feed-in-Act (StrEG). This includes setting ambitious mid and long-term targets over the next four decades, namely, an 80 % renewables contribution in the gross power generation (electricity) by horizon 2050, and also, decommissioning of nuclear power plants[1] by 2022. As a matter of fact, the German energy mix has undergone a significant transformation in the last 3 decades, as seen from Figure 1.1 [Agora, 2015].

Consequently, within the last 25 years, energy from renewables has emerged with a stunning speed (almost exponentially), and the share from renewables in Germany's gross electricity consumption has substantially increased almost by tenfold, from 3.6 % in 1990 up to 29.9 % in 2015. According to the same statistics, biomass[2] contributed with more than 6.8 % in the total power[3] production, which is estimated to be in the range of 645,6 TWh, thereby securing the second position after wind power with 13.3%, and way more than photovoltaics with 5.9% total share (see Figure 1.2).

Based on an annual report done by the German Biomass Research Center, abbreviated DBFZ, about 395 registered combined heat and power (CHP) plants, using

[1] Currently, there are 8 still operating nuclear power plants with an electric gross output of 11,357 MW_{el} in Germany, status: December 2015.

[2] Wood and agricultural biomass.

[3] This embodies only the electricity mix.

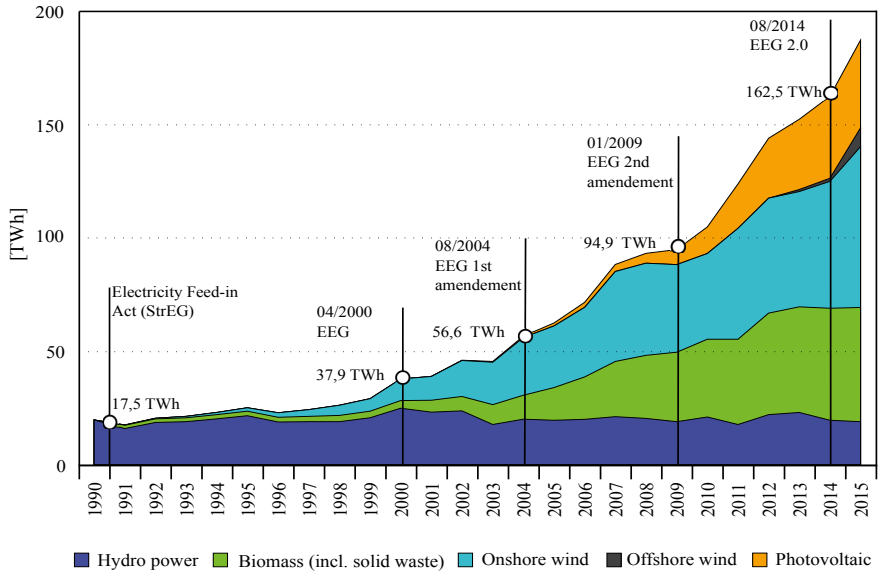

Figure 1.1: Development of power generation from renewables in Germany from 1990 to 2015 [Energiebilanzen, 2016].

solid biomass as a feedstock, were in operation by the end of 2014 (report status 05.2015). The corresponding installed electric capacity amounted to 1,491 MW_{el} and to 1,511 MW_{el} when wood gasification installations were also included, this in total made about 696 installations. The main biomass feedstock used according to a survey among plant operators is demolition wood and additionally natural wood biomass. Finally, compared to the year 2000 when the Renewable Energy Act (EEG) was introduced, the number of biomass CHP plants has increased twentyfold, and the respective installed electric capacity sevenfold [Scheftelowitz et al., 2015].

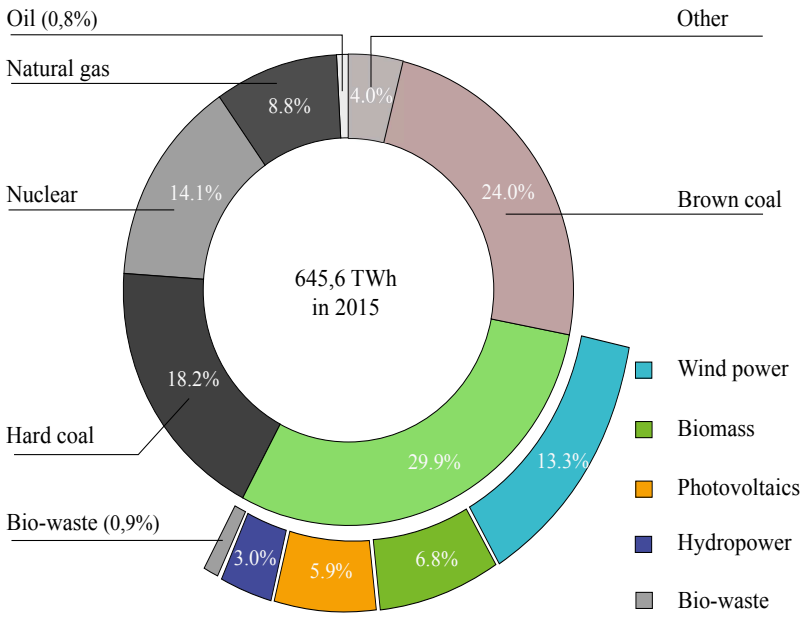

Figure 1.2: Share of renewables in Germany's gross power generation mix production for year 2015 [Energiebilanzen, 2016].

Thus, it can be clearly concluded that biomass took a leading position in the Energiewende and enjoyed a considerable prosperity on the road to a modified energy system paradigm where the energy is mostly supplied by renewables and where flexibility prevails in Germany's future energy system. Additionally, unlike wind and solar energy, which perforce to instant fluctuations, fired biomass for heat and electricity generation will provide a quick balancing supply to offset these fluctuations or changes in demand. Hence, it is more reliable and can be considered as a perfect compliment to intermittent forms of renewables generation.

1.2 Motivation and target

On the road to the green energy system, biomass and biomass-derived fuels combustion for power generation have been an attractive and viable alternative source of energy to fossil fuels and nuclear power. Hence, it is one of the key contributing factors in Germany's gross power generation mix, as it has already been indicated. Moreover, as an energy source, energy from biomass is environmentally friendly, since it is regarded as CO_2 neutral with respect to greenhouse gas emissions and this is deemed to be the main environmental profit of biomass combustion in comparison to fossil fuels, due to the fact that the amount of CO_2 released during biomass combustion does not exceed the amount of the same substance taken in during the plant growth via photosynthesis reaction.

Current technology used in biomass combustion is the state-of-the-art grate-firing system, the most competitive and market-proven technology for supplying district heating and power to the grid, which is offered on the market with capacities that range from 20 up to 50 MW_{el}, and comes with different grate configurations and furnace geometries. Though the grate firing of biomass has been used over many years, there are some problems to be further studied, for instance, stabilizing the combustion process, as a result of the disturbance caused by the unpredictable energy content of biomass blend, which varies even for the same type of biofuel due to harvesting, storing, and transport conditions. Such fluctuations in the calorific value of the fuel fed to the furnace, will consequently prevent an optimal process operation to be achieved, where the main goal is to minimize the emissions at the stack and to maximize the economical aspect of the combustion power plant, i.e. operating the turbine in the most efficient way to maximize production [Yin et al., 2008].

From a system theory perspective, a biomass combustion power plant is a nonlinear, coupled multivariate system with multiple inputs (fuel feed, air supply, grate speed) and multiple outputs (gas temperature, oxygen concentration, steam amount), where the different process input-output relationships are difficult to understand, due to the large disturbances acting on the process emanating mainly from the fuel's calorific value, which often fluctuates between the different batches delivered to the furnace as previously stated. Therefore, any attempt to maintain stable operating conditions of the biomass furnace and to design or improve the adopted process control strategy currently used based upon practical experience will lead to sub-optimal solutions, which may jeopardize the commercial character of the combustion site [Koppejan and Van Loo, 2012].

One possible way to handle such a situation is by improving the combustion control performance using advanced model-based control strategies for this aim, namely the model predictive control (MPC), to further ameliorate the economical aspect of the power plant while adhering to stringent emission standards. Such control techniques explicitly incorporate the available process knowledge, which is represented in terms of an available dynamic mathematical model used by the controller to compute the best control actions to fulfill the multiple conflicting goals in the plant (see Figure 1.3).

While mathematical modeling and CFD simulation helped in developing a detailed understanding of the different thermo-chemical processes involved in biomass combustion inside the furnace, and provided a cost-effective approach to exploit potential areas where the plant can be optimized in terms of a better furnace design and conversion efficiency of the fuel at a low emissions of gaseous pollutant, during the early stages of pre-development to increase the plant's competitiveness, such models are very complex and cannot be applied for model-based control of the biomass combustion power plant [Bauer et al., 2010].

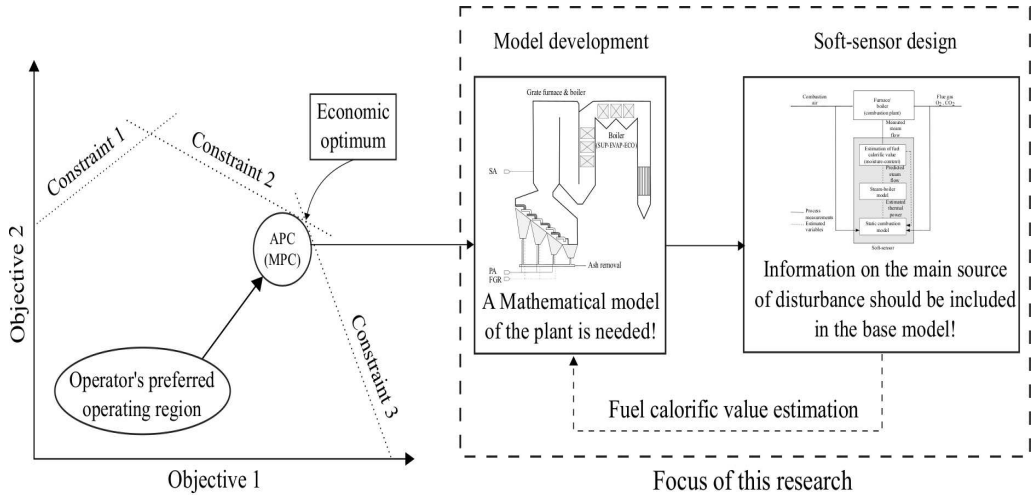

Figure 1.3: Increasing the plant efficiency by advanced model-based control techniques and research focus.

Hence, to further foster and exploit potential benefits of modern model-based control techniques in the field of biomass combustion, this research aims at the following:

(a) Developing a mathematical model for a biomass grate-firing power plant, as a basis for the development of an advanced process control strategy for the plant.

(b) Since the knowledge about the main source of disturbance inside the furnace, that is the energy content of biomass fed to the power plant, has to be incorporated in the dynamic model, a soft-sensor will be designed to monitor the variation of the fuel's calorific value. This information is then integrated in the base model to allow for an improved simulation of the dynamic model of the plant.

1.3 Organization of the thesis

The current section highlights how the thesis is organized and provides an abstract of the content of each chapter. The reminder of this thesis is organized as follows:

Chapter 2 presents an overview of the most important physical and chemical properties of solid biomass that are relevant for its reactivity as a fuel and may impact the whole combustion process. Additionally, based on proximate and ultimate analyses of different biomass-type from literature, an empirical elemental formula for the fuel needed to carry out a common combustion calculation for designing the virtual sensor is derived in this chapter.

In **Chapter 3** different existing combustion systems for firing biomass are discussed, while a focus is put on the grate-firing units, the most widespread technique for converting biomass into power and the main subject of the currently carried research. Moreover, a short technical description for the BMK Lünen power plant as a practical and typical example of a large-scale biomass grate-fired unit, the one from which the measurements were taken for the validation step of both the dynamic model and the designed soft-sensor, is carried out. Finally, the basic combustion route of a biomass particle on the moving grate, namely drying, pyrolysis/gasification, and char burnout, is briefly explained.

In **Chapter 4** an overview on existing approaches in literature for modeling biomass grate fired unit is briefly given, while the main focus is directed to the state-of-the-art reported models that are dictated to the control part of the system. Next, mathematical modeling is carried out to derive a general dynamic model for the system. For this purpose, the heat recovery power plant is divided into two main parts: the combustion furnace and the steam-boiler units. Here, the modeling part of the grate fired furnace involves the development of further submodels for the individual processes and components that comprise the system, such as models for both radiative and convective heat transfer mechanisms inside the furnace, as well as models describing the retention time, the drying process of the fresh fuel and the thermal decomposition of the dry part. Since at BMK Lünen a boiler with natural recirculation is used to generate steam, a dynamic model of this type of steam-boiler taken from the literature will be provided in this chapter.

Next, and in order to integrate the information about the main source of acting disturbances on the process operation in the developed dynamic model for the grate-firing furnace, which is the calorific value of the biomass fuel, a new developed concept of soft-sensing the variations of fuel's energy content inside the furnace is addressed in **Chapter 5**. The energy content of the fed fuel is inferred from both the measured steam amount from the power plant and the predicted one from the steam-boiler dynamic model. This will be based on the calculated value of the released thermal power from the furnace side and by applying an optimization-based scheme, which minimizes the difference between the predicted and measured steam values. Therefore, the estimation loop for the fuel's calorific value is build on two interlinked main components: the thermal power estimation and steam amount prediction.

In **Chapter 6** both the implemented virtual sensor for estimating the calorific value of biomass feedstock and the dynamic model of the grate-fired furnace are simulated using real data gathered from the biomass combustion power plant BMK Lünen. Moreover, to gain an insight on the dynamic behavior of the power plant and answering the question of why the system is behaving that way, step response experiments are applied on the simulation model while the system is at a given operating point. These tests are comprised of stepwise increase on the manipulated variables and observing the corresponding effects on the plant outputs.

At the end, a summary and an outlook on future work are given in **Chapter 7**.

2 Biomass as energy source

The worldwide urge for durable, eco-friendly energy sources to replace the conventional ways, such as fossil fuels and nuclear power, made biomass one of the most utilized renewable energy sources of interest for promoting both sustainability and the economical development. This is not surprisingly new, since mankind for millennia has been exploiting the energy contained in the chemical bonds of biomass to generate heat by combustion and by eating plants for nutrition. Biomass, whether stemming from forest products such as wood, logging residues, sawdust, and bark, or as a by-product of any plant-based activity, is a major source of energy. Indeed, the bond chemical energy stored in the structural components of biomass is the solar energy captured as chemical energy via photosynthesis.

In Germany, there has been a continuous progress to foster the use of biomass as a source of energy instead of classic fossil fuels, such as: brown coal (lignite) and bituminous coal. This is primarily due to the dwindling of federal's fossil fuel reserve, the associated rising transport and costs expenses on the one hand, and to achieve the stipulated objectives set by both the local government and the European Council to increase bioenergy share in the overall primary energy consumption on the other hand. Other important driving factors for the "renewed" interest in biomass can be classified into two main folds McKendry [2002b]:

- The economical factor: new technological developments in the field of energy recovery from biomass promise a low cost and high conversion efficiency, this insures already competitive costs compared to fossil-fuel based power generation. Hence, promoting the usage of renewable energies to meet the short-term objectives of horizon 2020 set by the European Commission, that aim at increasing the share of renewable energy up to 20% by the year 2020.

- The ecological factor: the worldwide climate change concerns, due to greenhouse gas emissions (carbon-dioxide being the most important emitted gas). Hence, the usage of biomass as a renewable energy source does not contribute significantly to carbon dioxide emission, since the biomass is merely the reaction of CO_2 in air with sunlight via photosynthesis, to reproduce the hydrocarbons which are the basic building blocks of biomass. Therefore, the released carbon dioxide during biomass combustion will not exceed the amount as it is taken up during the plant growth.

In this chapter, important physical and chemical properties of biomass, which have a strong impact on its reactivity as a sustainable source of energy, are highlighted. These properties will most likely dictate, on the one hand, the end-use form of recovered energy from biomass, i.e. gaseous, liquid, or heat and electric power, on the other hand, the used biomass conversion technologies which can be classified into two main categories: either combustion-based or biochemical-based. Finally, since the biomass fuel will be exploited using the former one, the impact of these properties on the combustion process are summarized in Section 2.2.

2.1 Properties and characterization

In assessing the suitability of a biomass feedstock as a renewable source of energy, it is essential to define and understand those performance metrics that have an impact on its behavior as a fuel. These fuel-related properties are key driving factors affecting the selection of the conversion technique, its design, operation, as well as the handling, storage and any further pretreatment step that might be required prior to fuel utilization for a particular end-user application [Shastri et al., 2014]. Additionally, within this context, before making any investment decision on developing a new bioenergy project, both the economic viability and the scale of production, either on a small or a large-scale production capacity, and whether the new conversion facility will be designated to provide electricity, heat, or liquid biofuels for transport, will be anticipated by the properties of the available nearby feedstock supply [Kavalov and Peteves, 2004], [Karlen, 2014].

Over the last decades, a considerable body of research has been conducted to gain more insight into the physical characteristics and chemical composition of biomass as an alternative to conventional fuels, therefore, endeavoring to understand not only how the conversion technology can be adapted to fit these properties, but also how the properties of the fuel might be varied to suit the conversion technology of choice, which can be either combustion-based or biochemical-based conversion processes. As a consequence, many standardized methods have been developed for a consistent and accurate characterization of fuel properties, some of them were mainly developed for coal, but have been found to be adequate for biomass as well [Jenkins et al., 1998].

In this section, properties relevant to biomass combustion, which have a strong influence on its reactivity as a fuel, will be further elaborated. Other properties that are influenced by the way the biomass fuel is handled or preprocessed, such as the bulk density, particle size and shape distribution are omitted in the current discussion.

2.1.1 Chemical composition

The most common and useful practice for characterizing the chemical composition of a specific feedstock (see Figure 2.1), or a blend of various biomass types, is by means of two standard analyses methods, these are [McKendry, 2002b]:

- Proximate analysis.
- Ultimate analysis.

Such analytical laboratory methods for evaluating the chemical properties were basically developed for coals and cokes and largely extended in application to include biomass and also waste materials as a potential source of energy. The methods for carrying these chemical, including physical, analyses have been standardized by all major standard institutions particularly in the USA[1], UK[2], and Germany[3]

[1]Americal Society for Testing and Materials (ASTM).
[2]British Standards Institution (BSI).
[3]Deutsches Institut für Normung (DIN).

[Spliethoff, 2010].

These standards, though similar in nature, are different from one another; therefore, it is important to implicitly specify the method used when providing the analysis data of test samples under investigation [Higman and Van der Burgt, 2011].

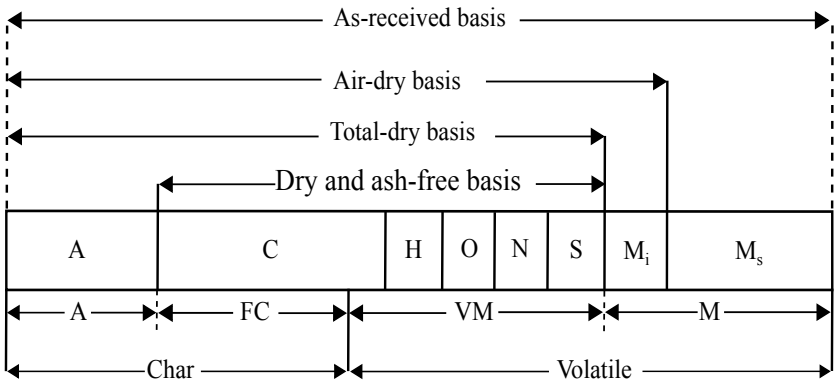

Figure 2.1: Proximate and ultimate composition of biomass: M_s moisture surface, M_i inherent (intrinsic) moisture[4](adapted from [Basu, 2013]).

Proximate analysis

The proximate analysis is used to quantify the following constituents in the solid fuel:

- Moisture content (M)(see Subsection 2.1.2)
- Volatile matter (VM)[5]
- Fixed carbon (FC)
- Ash content (Ash) (see Subsection 2.1.4)

As the name suggests, the method is empirical, and therefore, not exact, but the tests are done quite accurately in that they are carried out using a standard method [Borman and Ragland, 1998]. Here, the volatile matter (VM), which accounts for a significant fraction of all biomass, is the fraction of condensable and noncondensable gases released upon heating of the dry biomass sample in a covered crucible at 550 °C (for coal to 900 °C according to DIN 51720) in an inert atmosphere. What remains after the complex mixture of gases and vapors is released is called char, which consists of fixed carbon and ash (see also Figure 2.2).

The weight difference with the original sample is the fraction of VM content, that can be evaluated according to Eq. (2.1) [De Jong and Van Ommen, 2014]:

$$\gamma_{\mathrm{VM}}^{\mathrm{db}} = \frac{\text{weight loss}}{\text{dry weight}} \tag{2.1}$$

[4]Intrinsic moisture is the water held within the cell walls by hydrogen bonds. It is the removal of this water that causes shrinking of biomass.

[5]Volatile matter refers to that portion of the solid fuel transmuted into gas due to the thermal degradation of the fuel. The volatile gas is mainly composed of carbon monoxide CO, carbon dioxide CO_2, hydrogen H_2 and hydrocarbons (CH_4, C_2H_6).

If the remaining residue from the previous step, i.e. devolatilization, is further combusted in the presence of oxygen at temperature 815 °C according to DIN 51719 standard, then the amount of ash can be determined. Consequently, the weight loss after combustion at elevated temperatures of char will represent the fixed carbon fraction contained in the solid fuel, which is estimated experimentally by difference as follows:

$$\gamma_{\text{ash}}^{\text{db}} = \frac{\text{weight ash}}{\text{dry weight}} \tag{2.2}$$

$$\gamma_{\text{FC}}^{\text{db}} = 1 - \gamma_{\text{VM}}^{\text{db}} - \gamma_{\text{ash}}^{\text{db}} \tag{2.3}$$

The residue left over after the biomass is totally converted does not entirely come from the mineral matter of biomass (inherent), but also from those added to the fuel during the harvesting. The latter is adventitious materials (extraneous), such as soil, rock and other impurities, which often constitute the major fraction of ash content of biomass fuels used in power plants and originate from scrapping off the fuel from the forest floor, which leads to the attachment of these inorganic matters to the surface of the feedstock [Jenkins et al., 1998]. Other ash-related properties, such as its composition, ash fusion as well as its impact on the process operation during biomass thermochemical conversion will be treated separately in Subsection 2.1.4.

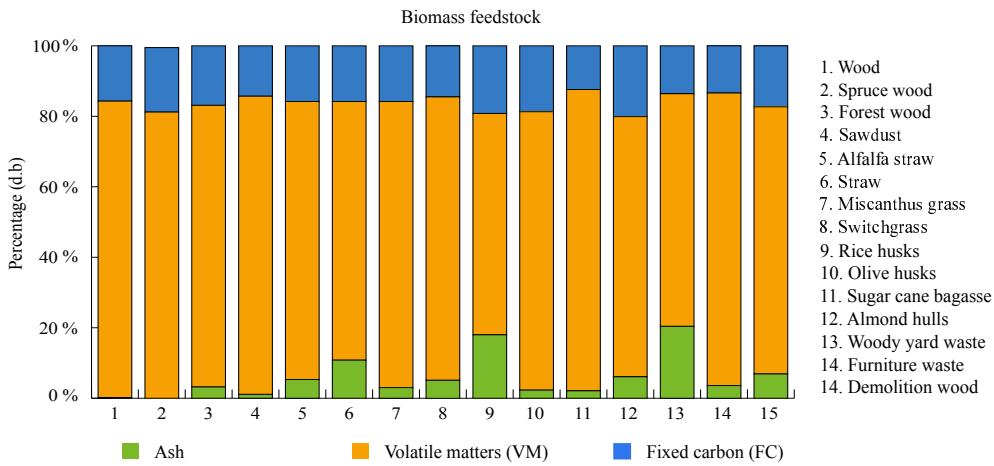

Figure 2.2: Proximate analysis for a wide variety of biomass fuels on dry basis (d.b) based on data from [Vassilev et al., 2010].

Because of the associated labor and time required to perform proximate analysis based on the aforementioned standards, [Klass, 1998] suggested an alternative, which consists of using thermogravimetry (TG) or differential thermogravimetry (DTG) techniques, for proximate analysis of biomass and the rapid estimation of their conversion characteristics. In this techniques, a biomass substance is heated at specific atmosphere and desired conversion rate in a pan supported by a microbalance, which continuously monitors the weight change of the sample during the experiment. Therefore, from the measured weight loss versus time graphs, one can determine the moisture content, volatile matters, and ash content [Basu, 2013]. A detailed description of the thermal analysis by thermogravimetrical techniques can be found in [Kemp, 1999].

Ultimate analysis

The ultimate analysis states the chemical composition of the biomass fuel in terms of its elementary constituents (see Figure 2.1). The analysis involves the measurement of carbon, hydrogen, nitrogen and sulfur based on the gaseous mixture emanating from the total combustion of the fuel. The oxygen content, however, is most commonly determined by difference. For feedstocks containing high moisture content such as biomass, special care should be taken in using ultimate analysis for describing the fuel's basic composition, because the hydrogen and oxygen reported in this step is in addition to the physical moisture determined in the proximate analysis. Therefore, the carried elemental analysis on the fuel sample is usually performed and reported on dry basis, to ensure that the hydrogen determined is only the one chemically bound to the biomass fuel [Kishore, 2010]. A typical ultimate analysis (dry basis) is as follows:

$$\gamma_{\mathrm{O}}^{\mathrm{db}} = 1 - \gamma_{\mathrm{C}}^{\mathrm{db}} - \gamma_{\mathrm{H}}^{\mathrm{db}} - \gamma_{\mathrm{N}}^{\mathrm{db}} - \gamma_{\mathrm{S}}^{\mathrm{db}} - \gamma_{\mathrm{ash}}^{\mathrm{db}} \tag{2.4}$$

The carbon, hydrogen, nitrogen, and sulfur content are determined using a CHNS gas analyzer apparatus. Here, the biomass solid sample is thermochemically decomposed in presence of oxygen as an oxidizer. The resulting gaseous products are then analyzed using gas chromatography techniques, in which the gas mixture is carried by helium as a carrier gas and introduced into thermal conductivity detector (TCD) or flame ionization detector, where the basis fuel's components are determined quantitatively according to, for example, DIN 51721, DIN 51722, and DIN 51724 standards [Stevens and Brown, 2011].

Figure 2.3 depicts the major components of biomass fuel resulting from elemental analysis of various biomass types (see also Appendix B). Here, the carried analysis on different biomass sources reveals that the chemical composition is fairly constant regardless on the biomass origins, with C $\simeq$ 50%, H $\simeq$ 6%, and O $\simeq$ 44%, which is equivalent to the empirical formula $CH_{1.44}O_{0.66}$. This formula will be employed in stoichiometric combustion equations in Chapter 5 to develop a calorific soft-sensor for the biomass combustion power plant [Belkhir and Frey, 2016a].

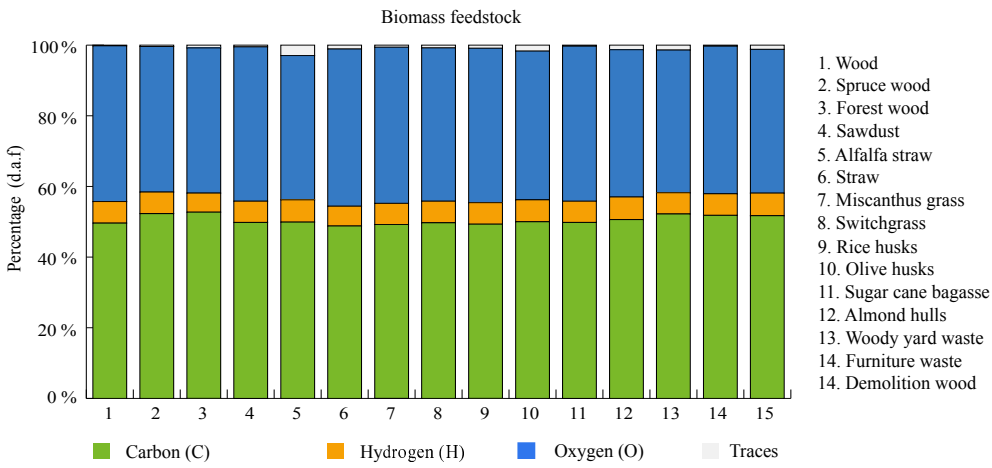

Figure 2.3: Ultimate analysis for a wide variety of biomass fuels on dry ash-free basis (d.a.f) based on data from [Vassilev et al., 2010].

With respect to conventional fossil fuels, the ultimate analysis reveals that the biomass is highly oxygenated. As it will be seen in Subsection 2.1.3, the high oxygen content will have a negative impact on its calorific value. Moreover, biomass fuels are almost devoid of nitrogen, sulfur and chlorine, which are usually less than 1 %, and are important in the pollutant formation during biomass combustion, namely, NO_x and SO_x [Jenkins et al., 1998]. Coupled with the low ash-content, these two properties make biomass a highly desirable fuel for energy recovery via combustion [Brown et al., 2011].

2.1.2 Moisture content

The moisture content is probably the most important physical property of a feedstock as it will influence any subsequent processing of the freshly harvested biomass prior to further exploitation and the form in which the energy is required, hence, the conversion technology [McKendry, 2002b]. In many combustion power plants, moisture content of biomass is an undesirable burden, which has to be reduced to a feasible extent before usage, as a biomass fuel with a high moisture-content makes its ignition very difficult prior to combustion and has a negative impact on the thermal efficiency of the system [Kishore, 2010].

With wood and wood-derived biomass are hygroscopic in nature and absorb or adsorb water, the moisture can be present in two forms: (a) free, or extrinsic water, and (b) bound, or intrinsic water. The former one is the water absorbed by the capillary uptake in the cell cavities (lumen) of biomass structure, the latter is the sorption of water into the biomass cell walls. Therefore, due to the hygroscopic property of biomass fuels, the moisture content will vary substantially between the different biomass species and even for the same type of biomass depending on the prevailing weather and harvesting conditions of the solid fuel [Tillman, 1981].

When a biomass with a high moisture content is used, a part of the released energy will be diverted to vaporization of water it contains, energy which would otherwise be useful in the steam generation by the boiler. It follows that the drier the biomass is, the more useful energy, in form of heat, can be used. Literally, the moisture content will determine the energy value of the biomass [Rosillo-Calle and Woods, 2012]. Furthermore, a high moisture content in the feedstock will need a longer residence time for drying prior to actual burning, which means a bigger combustion furnaces will be required [Koppejan and Van Loo, 2012].

As the moisture content linearly impacts the fuel's energy content, it is necessary to quantify the amount of dry biomass for setting the purchasing price of a certain shipment for power generation. This is achieved by measuring the weight fraction of moisture, which can be described in two ways [Brown et al., 2011]:

- Dry basis

$$\gamma_{\mathrm{w}}^{\mathrm{db}} = \frac{\text{wet weight} - \text{dry weight}}{\text{dry weight}} \tag{2.5}$$

- Wet basis

$$\gamma_{\mathrm{w}}^{\mathrm{wb}} = \frac{\text{wet weight} - \text{dry weight}}{\text{wet weight}} \tag{2.6}$$

The moisture content is usually determined using standard gravimetric measurement method (oven-drying method) according to test protocols in DIN 51718 or ASTM D4442-15 for wood and wood-based materials. In these protocols, a fuel sample or a set of samples are electrically heated and weighed in air-oven at temperature equal to 106 ± 2 °C. The process is then repeated for 30 min until the weight remains unchanged ($< 0.05\%$). The difference in weight between the fresh sample before heating and the dried one gives the moisture content in the fuel [Basu, 2013]. The accuracy of this standard method is very important as it will have an implication on the calibration and validation of other instrumental methods for moisture determination [Dahlquist, 2013b]. These techniques will be reviewed in Section 5.1.

2.1.3 Calorific value

A key property of biomass is its energy value or heating value, also referred to as the fuel's calorific value. By definition, the calorific value is a measure of the thermal energy being released from the bond chemical of solid fuel upon complete combustion with oxygen in air under specific conditions. The calorific value is usually measured in terms of the energy content per unit mass, i.e. in [kJ/kg] or [MJ/kg]. In determining the heat given up by a unit of solid biomass, one can generally distinguish between two forms of calorific value, the higher heating value (HHV), also expressed as upper or gross calorific value (GCV), and the lower calorific value (LCV), also named the net calorific value (NCV) [McKendry, 2002b].

If the combustion is carried out at either a constant volume or constant pressure, with the former being more commonly reported for solid biomass feedstock, the internal energy change measured by a bomb calorimeter with water being condensed is the HHV, while the LCV at constant volume measures the internal energy change if product water is in the vapor phase [Jenkins et al., 1998]. Therefore, the difference between these two values corresponds to the latent heat of vaporization, or similarly the latent heat of condensation, at standard temperature of 25 °C ($\Delta h_v^{\mathrm{w}} = 2441,7\,\mathrm{kJ/kg}$) [Baehr and Kabelac, 2012]. Similar to the moisture content, the relations used to estimate these quantities, which describe the energy content of fuel, are also reported on dry basis (d.b) or on wet basis (w.b) and they will be described below.

Estimation of HHV

The heating value of biomass fuel can be experimentally determined using a so-called bomb calorimeter, which measures the enthalpy change between reactants and products. However, due to the time-consuming process that requires the set-up measurement and calculation procedure, and to circumvent this problem, many attempts have been made to find empirical correlations between this value and the conventional analysis of the fuel, i.e. proximate and ultimate analyses (Subsection 2.1.1). Following this direction, other empirical formulae were also proposed to correlate the HHV with biomass chemical composition, i.e. cellulose, hemicellulose, lignin and extractives [Sheng and Azevedo, 2005].

One of such established correlations used for predicting the HHV ($H_{U,\mathrm{db}}$) in [kJ/kg], based on the ultimate analysis can be found in [Gaur and Reed, 1995], which is given below:

$$H_{U,\mathrm{db}} = 34.91\,\gamma_{\mathrm{C}} + 117.83\,\gamma_{\mathrm{H}} + 10.05\,\gamma_{\mathrm{S}} - 1.51\,\gamma_{\mathrm{N}} - 10.34\,\gamma_{\mathrm{O}} - 2.11\,\gamma_{\mathrm{Ash}} \tag{2.7}$$

Other empirical correlations that were reported in literature for estimating the HHV based on proximate/ultimate analyses, as well as the chemical analysis, can be found tabulated in [Sheng and Azevedo, 2005], [Yin, 2011] and [Kieseler et al., 2013]. As it can be seen from this relation, the variation in calorific value of biomass fuel depends strongly on the composition of the fuel as well as its moisture and ash content [Dahlquist, 2013b]. Namely, the constituents C, H, and S contribute positively to HHV, while contents N, O, and ash have a negative impact on it.

Estimation of LHV

The LHV of biomass fuel is directly related to the dry basis higher heating value and the hydrogen content through the following relation [De Jong and Van Ommen, 2014]:

$$H_{L,\mathrm{db}} = H_{U,\mathrm{db}} - \Delta h_v^{\mathrm{w}}\,\frac{M_{\mathrm{H_2O}}}{2\,M_{\mathrm{H}}}\,\gamma_H \tag{2.8}$$

If, instead of expressing $H_{L,\mathrm{db}}$, in [kJ/kg], on dry basis, the wet basis is used, Eq. (2.8) can be re-formulated, by taking into account the fuel's moisture content γ_{w}:

$$H_{L,\mathrm{wb}} = H_{L,\mathrm{db}}\,(1-\gamma_{\mathrm{w}}) - \Delta h_v^{\mathrm{w}}\,\gamma_{\mathrm{w}} \tag{2.9}$$

Since the temperature of the exhaust flue gas is usually between 120-160 °C, the water in the flue gas does not condense. Therefore, the latent heat of condensation cannot be recovered in the energy conversion process, which leads to consider for most cases the LHV instead of HHV in the combustion calculations [Basu, 2013]. Table 2.1 illustrates the estimated values for these two important characterizing properties of biomass fuels from the basic analysis data, i.e. proximate and ultimate analyses, obtained from open literature and the correlation relationships presented by Eq. (2.7) and Eq. (2.8).

Table 2.1: Heating values based on ultimate and proximate analyses (wt%) of various biomass fuels obtained from [Vassilev et al., 2010].

Fuel type	Proximate analysis [a]			Ultimate analysis [b]					Heating value [c]	
	VM	FC	Ash	C	O	H	N	S	LHV	HHV
Wood	84.1	15.7	0.2	49.6	44.1	6.1	0.1	0.06	18.58	19.90
Wood residue	78.0	16.6	5.4	51.4	41.9	6.1	0.5	0.08	18.30	19.56
Sawdust	84.6	14.3	1.1	49.8	43.7	6.0	0.5	0.02	18.39	19.68
Spruce wood	81.2	18.3	0.5	52.3	41.2	6.1	0.3	0.10	19.75	21.07
Spruce bark	73.4	23.4	3.2	53.6	40.0	6.2	0.1	0.10	19.81	21.12
Pine bark	73.7	24.4	1.9	53.8	39.9	5.9	0.3	0.07	19.99	21.25

[a] Dry basis (d.b).
[b] Dry, ash-free basis (d.a.f).
[c] Evaluated according to Eq. (2.7) and Eq. (2.8) in [MJ/kg].

According to [Jenkins et al., 1998], each 1% increase in ash translates roughly into a decrease of 0.2 MJ/kg of LHV, and therefore ash can be seen as a heat sink, similar to the moisture; hence, it does not contribute to the heat released by combustion. On the contrary, each 1% increase in carbon content will elevate the fuel's heating value by approximately 0.39 MJ/kg. Finally, it should be noted that the estimation result will be always significantly influenced by the moisture content, the fuel type and its composition, also on the accuracy of the empirical correlation methods used, which are still an open subject of further research that aim at deriving more statistical formulae for an accurate evaluation, but such approaches can by no means replace the more reliable experimental methods.

2.1.4 Ash content

The complete breakdown of the solid biofuel by thermo-chemical conversion, here combustion, will result in an inorganic yield solid residue called "ash"[Jenkins et al., 1998]. Depending on the magnitude of the ash and its chemical composition, this fraction negatively affects the energy density of the feedstock, and can often pose serious operational problems in the firebed, especially if it contains alkali and alkali metals as its principle ash-forming constituents, which react with other fuel elements such as silica and sulfur, and facilitated further by the presence of chlorine, will lead to slagging, fouling and corrosion on the metal part of the furnace and boiler [Karlen, 2014].

Furthermore, fly ash formation, ash deposit formation, as well as logistics related to ash utilization and/or disposal depend also on the ash content [Obernberger et al., 2006]. Moreover, high ash content in the fuel will usually lead to an increased dust emission and consequently to the associated expenditure for the dust percipitation technology. This is particularly relevant for the biomass fuel in the grate-firing system which is continuously subject to mechanical influences [Döring, 2012].

The ash, as a by-product, originates simultaneously from natural and anthropogenic (technogenic) matter during biomass combustion [Vassilev et al., 2010]. The former is inherent inorganic constituents that are essential for the plant growth, and they are required in varying amount in the plant tissue. These mineral nutrients can be further divided into macronutrients, which include mineral nutrient elements necessary for plants to complete their growth cycle, and those micronutrients elements that are benificial to plants but not necessarily essential. The latter class of inorganic material entails the extraneous material, such as soil, dust and other impurities, added to solid biomass during harvesting, handling, or a subsequent processing, and often comprises the bulk of ash content in a power plant [Baxter, 1993]. The ash content and composition varies considerably between different feedstocks, ranging from 0.5 wt%(d.b) for wood up to 12 wt%(d.b) in agricultural residues such as straw (see Figure. 2.4).

Ash fusibility

In a high temperature environment such as the combustion chamber, physical changes of ash content occur in the firebed. Depending on both the temperature levels and ash composition, and thus mainly on the biomass type, either slagging or fouling

mechanisms may occur on the different parts of heat transfer surfaces in the furnace [Döring, 2012].

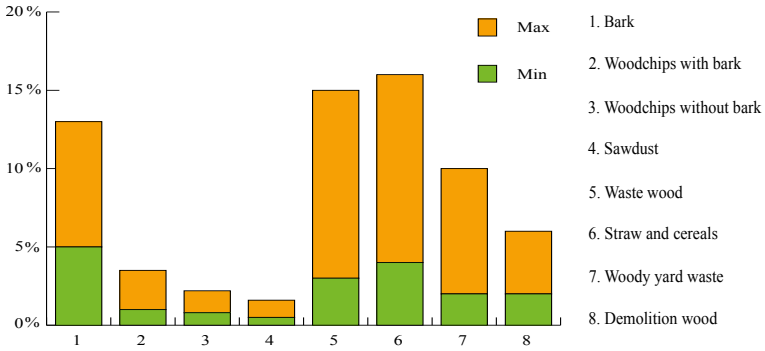

Figure 2.4: Ash content in wt%(d.b) of various biomass fuels (adapted from [Koppejan and Van Loo, 2012]).

By definition, fouling is the formation of ash deposit on the convective heat transfer sections in the boiler, e.g superheater and reheaters, whereas slagging is the ash deposited on the heating surfaces that are exposed to flame radiation [Rosendahl, 2013]. As a consequence, both deposition mechanisms will result in a limited heat transfer efficiency, reduction in a safe and reliable unit operation, and in extreme cases to a complete shut down of the power plant unit [Shastri et al., 2014]. Therefore, beside the biomass's ash content, the ash fusion behavior is a critical property for an efficient process design. According to DIN 51730, or ASTM standard D-1102 for wood, the ash melting behavior is characterized by preparing ash samples in specific shapes, cubic form for the former, and triangular cone for the latter. The ash fusibility is then characterized by defining temperatures at which changes of sample shape occur. These temperatures are described below and shown graphically in Figure 2.5 [Kitto and Stultz, 1992], [Spliethoff, 2010]:

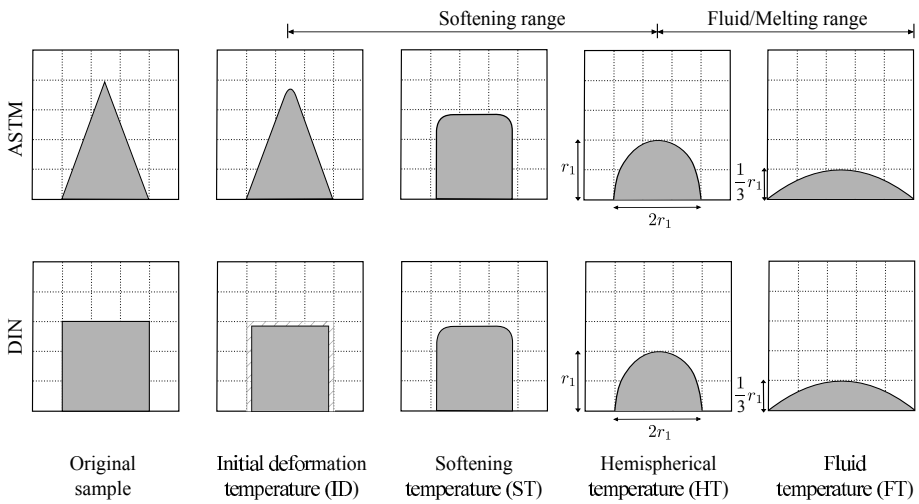

Figure 2.5: Ash fusion characterization according to DIN and ASTM standards.

- **Deformation temperature (DT)**: the temperature at which the first signs of shape changes of the test sample occurs.

- **Spherical temperature (ST)**: the temperature at which the top part of the test sample starts exhibiting a spherically formed geometry with the height equal the width at the shape's bottom.

- **Hemispherical temperature (HT)**: the temperature at which the test sample is hemispherical with a geometry that is characterized by a height equal to the half of the width.

- **Fluid temperature (FT)**: the temperature at which the ash is molten and spread out to an extent at which the maximum height is reduced to one third of that at the hemispherical phase.

As already stated, the ash melting behavior is influenced by the chemical composition of its forming constituents which are often classified into either major or minor elements. Calcium (Ca) and magnesium (Mg) tend to increase the ash melting point; however, potassium (K) in combination with silicon (Si) and sodium (Na) can lead to formation of low melting silicates in fly ash particles [Obernberger et al., 2006]. Typical concentration ranges of selected ash elements depending on the origin and type of biomass are shown in Table 2.2.

Table 2.2: Concentration ranges of major ([wt%(d.b)]) and minor ash-forming elements ([mg/kg (d.b)]) for different biomass fuels [Koppejan and Van Loo, 2012].

	Ash element	Woodchips (spruce)	Bark (spruce)	Straw (wheat, rye, barley)	Cereals (tricate)
Major	Si	4.0-11.0	7.0-17.0	16.0-26.0	0.3-4.9
	Ca	26.0-38.0	24.0-36.0	4.5-8.0	3.0-7.0
	Mg	2.2-3.6	2.4-5.6	1.1-2.7	1.2-2.6
	K	4.9-6.3	5.0-9.9	10.0-16.0	11.0-18.0
	Na	0.3-0.5	0.5-0.7	0.2-1.0	0.2-0.5
	P	0.8-1.9	1.0-1.9	0.2-6.7	4.5-6.8
Minor	Fe	64-340	280-1,200	42-860	37-150
	Al	79-580	330-1,500	11-810	42-93
	Mn	63-900	430-1,300	14-44	27-31
	Zn	7-90	90-200	11-57	10-25
	Cu	0.3-4.1	1.5-8.0	1.1-4.2	2.6-3.9

Depending on the major ash forming elements concentrations, particularly potassium (K), calcium (Ca), and magnesium (Mg), [Kaltschmitt et al., 2009] suggested empirical equations in order to approximate both the deformation temperature (DT) and the fluid temperature (FT), these are:

$$\mathrm{DT} = 1172 - 53.9\,\mathrm{K} + 252.7\,\mathrm{Ca} - 788.4\,\mathrm{Mg} \tag{2.10a}$$

$$\mathrm{FT} = 1369 - 43.4\,\mathrm{K} + 192.7\,\mathrm{Ca} - 698\,\mathrm{Mg} \tag{2.10b}$$

Table C.1 in Appendix C.1 gives an overview of the ash melting behavior of different biomass types, indicating that ash contained in herbaceous fuels start to sinter at low temperature levels in comparison to woody biomass. Therefore, solid fuels that are characterized by low ash content and high melting temperature, particularly wood-type fuels, are better suited for thermal utilization in order to avoid many ash-related problems in the combustion power plant.

2.2 Biomass properties impact on combustion system

As stated previously in this chapter, the entire biomass processing chain as a renewable energy source from the collection up to the combustion site is influenced by its physico-chemical properties. Table 2.3 gives a summary of the most important properties of biomass and their corresponding impact on its behavior from harvesting to the combustion process.

Table 2.3: Combustion-relevant characteristics of solid biomass fuels (adapted from [Koppejan and Van Loo, 2012] and [De Jong and Van Ommen, 2014]).

	Characteristics	Effect
Physical properties	Moisture content	- Storage durability, HHV, self-ignition, plant design
	LHV, HHV	- Fuel utilization, plant design
	Volatiles	- Thermal decomposition behavior
	Ash content	- Dust emission, ash manipulation, ash utilization/disposal, combustion technology
	Ash melting behavior	- Operational safety, combustion technology, process control system, hard deposit formation
	Bulk density	- Fuel logistics (storage, transport, handling)
	Particle density	- Thermal conductance, thermal decomposition
	Particle porosity	- Formation of fines in processing, interparticle heat and mass transfer
Chemical properties	C, Carbon	- Heating value, possibly emission of CO
	H, Hydrogen	- Heating value
	O, Oxygen	- Heating value (negatively impacting)
	N, Nitrogen	- Emission of NO_x and N_2O
	Cl, Chlorine	- Emission of HCl and polychlorinated dibenzo-p-dioxin/furan (PCDD/F) causing corrosion and catalyst poisoning, also it lowers ash-melting temperature
	S, Sulfur	- Emission of SO_x causing corrosion and catalyst poisoning
	F, Fluor	- Emission of HF causing corrosion
	K, Potassium	- Corrosion (heat exchanger, superheaters), lowering ash-melting temperature, aerosol formation
	Na, Sodium	- Corrosion (heat exchanger, superheaters), lowering ash-melting temperature, aerosol formation
	Mg, Magnesium	- Increase of ash-melting temperature, ash ultilization (plant nutrient)
	Ca, Calcium	- Increase of ash-melting temperature, ash ultilization (plant nutrient)
	P, Phosphorus	- Ash utilization and deposit formation
	Trace element	- Emission, ash utilization and aerosol formation

3 Power generation from biomass

The use of biomass, in lieu of fossil fuels for energy generation, has become one of the key factors in promoting a sustainable energy policy worldwide for the socio-economical development and the reduction of greenhouse gas emissions that cause the global warming as a side effect. This revived interest in biomass stems from the incentive environmental and economic benefits, biomass offers when exploited. The exploitation of the latent chemical energy contained in biomass depends generally on the end-use requirements, i.e. the desired form of the energy to be harvested, usually as electricity and/or as a fuel for power. Consequently, such a choice influences the type of conversion methods, which can be classified into the following two main process technologies: thermo-chemical and bio-chemical/biological McKendry [2002a].

Within the class of thermochemical processes, combustion is the most direct and widespread method used for converting biomass into a useful form of energy. This is not surprisingly new, because the humankind since the prehistoric times has been exploiting, based on small-scale, the latent energy stored in the chemical bounds of biomass by burning the fuel to generate heat (fire) for warmth and cooking, as an end-use application of biomass. Notwithstanding, power generation from biomass involves various physical/chemical aspects, including successive homogeneous and heterogeneous reactions, of high complexity, the advances in both scientific knowledge of solid fuels combustion theory and technology have enabled the development of different sophisticated biomass-based commercial systems, for a maximum exploitation of the biofuel and for large-scale applications, i.e. industrial-scale. Within this context, one of the most competitive and market-proven technologies in biomass combustion being currently used in Europe for power production, either as electricity and/or steam for district heating, is the state-of-the-art grate-firing systems. These systems are offered on the market with capacities ranging from 20 up to 50 MW_{el} and can fire a wide range of biomass fuels with different physical properties and a varied moisture content [Yin et al., 2008].

In a first step, this chapter aims at providing a brief overview of the different existing conventional combustion technologies for power generation from biomass, whereas a particular emphasis will be placed on the popular grate-firing units, the main subject of this thesis, which come with different furnace designs and different grates mechanical configuration depending on the manufacturer own experience. Additionally, a short technical description of the BMK Lünen as a practical and typical example of a large-scale biomass grate-firing unit, and the one from which the measurements are taken for the validation step for both the dynamic model of the system and the designed soft-sensor, is given. Besides the apparatus where the fuel is being combusted, the different thermochemical conversion processes taking place on the moving grate, which consist of fuel drying, pyrolysis, gasification, and the oxidation of the gaseous products emanating from the burning the fuel bed on the grate, are described.

3.1 Biomass combustion technologies

Various technologies for energy recovery from biomass are currently commercially available, while others are less mature and only at the beginning of the research and development stages. In general, four types of biomass thermal conversion technologies that convert the energy stored into a useful form of energy exist; this includes combustion, pyrolysis, gasification and liquefaction [McKendry, 2002a], with the combustion being the most advanced and market-proven application, making from it a dominant conversion technology at present and in the near future. Consequently, various combustion technologies for a wide range of biomass fuels (woody biomass, herbaceous biomass fuels and biodegradable waste and residues) covering a wide range of plant capacity are offered in the market [Obernberger, 2009].

In principle, the following combustion technologies for biomass can be distinguished [Koppejan and Van Loo, 2012]:

- grate-fired/fixed-bed combustion,
- fluidized-bed combustion,
- pulverized fuel combustion.

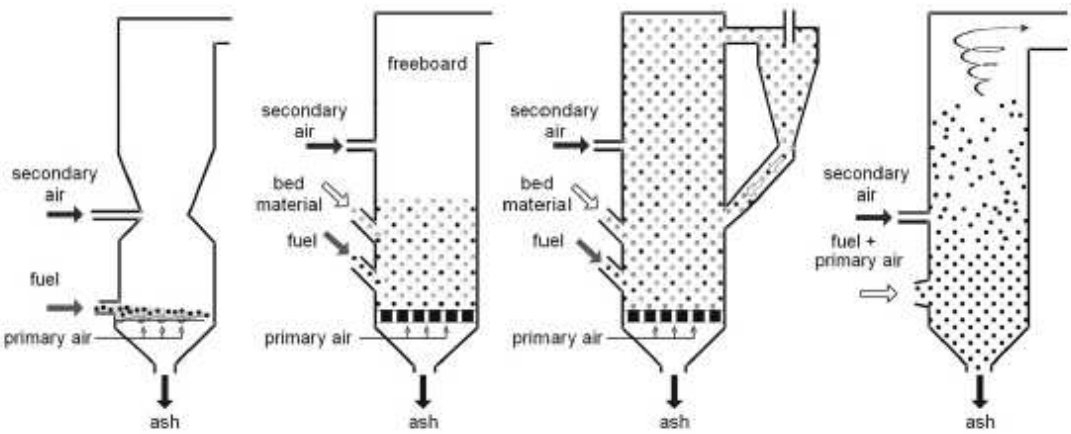

Figure 3.1: Overview of the different biomass combustion technologies [Koppejan and Van Loo, 2012]

The first category covers the different moving-grate systems such as the forward acting, the reverse acting, and roller type grates (Subsection 3.2.1). Within the fluidized bed combustion, two classes can be distinguished, these are: the bubbling-fluidized bed (BFB) and the circulating-fluidized bed (CFB) (Subsection 3.1.2). The last category, which is more reported for biomass co-firing with coal, is the pulverized-fuel combustion or suspension firing (Subsection 3.1.3). All of the aforementioned technologies will be briefly explained in the following, whereas, as mentioned in the introduction, the primary focus will be given to the first category, i.e. the grate-firing unit, which is the subject of study in this research.

3.1.1 Grate-fired combustors

The grate-fired combustors, being the first combustion systems used for burning solid fuels, are now mainly used for burning biomass for power production and district heating. These systems are offered on the market with capacities ranging from 20 up to 50 MW_{el}, and the heat release rate per grate area may be up to about 4 MW_{th}/m^2 [Yin et al., 2008]. The State-of-the-art grate-fired systems consist of 4 key elements: the furnace, the grate assembly, the flue gas cleaning unit, and the ash discharge system. This combustion system will be much more elucidated in Section 3.2.

3.1.2 Fluidized-bed combustions

The 1970s saw the introduction of a new combustion method: the fluidized-bed firing, which was firstly used for energy production from coal. Since then, it has been expanded to cover firing/co-firing of biomass and other low-grade fuels [Grammelis, 2010]. Here, the key idea of fluidized-bed technology is the burning of the fuel in a bed of hot inert particles, which is kept suspended by the upward flow of combustion air injected through the bottom of the furnace. Heat and mass transfer are enhanced due to the hot bed material inside the furnace. As a result of the intense heat transfer and mixing, a good condition for complete burnout with low excess air demand (λ between 1.2 and 1.3) is achieved, which prevents ash sintering problems in the bed [Koppejan and Van Loo, 2012].

The fluidized-bed consists of a rectangular/cylindrical furnace filled with bed materials in the bottom. The fuel amounts only to 1-2 % of the total mass and the rest is inert material such as ash, silica sand or delomite. A primary air is supplied over the perforated plat which supports the bed material and a secondary air flow dosed at the upper part through horizontally arranged nozzles to ensure staged-air supply [Obernberger, 1998]. An increase in the air flow rate/velocity at the bottom of the bed through the air distributor ducts will exert a counteracting force (drag force) on the particle compared to the gravitational ones, until the so called maximum fluidization condition is reached, where the bed starts to behave like a fluid. Therefore, depending on the air velocity two types of fluidized bed combustors can be distinguished:

Bubbling-fluidized bed (BFB)

In bubbling-fluidized bed, a further increase in the air velocity in the range of 1.0-2.5 m/s will result in a substantial increase in the air/solid volume and an obvious distinct transition between the bed and the void space above it, due to the increasing distance between the particles. Therefore, bubbles begin to form and the bed becomes violent, less uniform, and the point at which the bed starts to behave as a fluid is called the minimum fluidization condition [Kitto and Stultz, 1992].

The fuel feeding is done through a number of ports in the furnace side wall, and a good fuel distribution is essential in order to reach a low excess air. The biomass particle size is in the order of 80-100 mm. Hence, a very limited pre-treatment of the biofuel before being fed to the furnace is necessary [Rosendahl, 2013]. The tem-

perature in the bed is typically controlled and maintained in the range of 650-850 °C through sub-stoichiometric bed operation (λ[1] about 0.35), that allows for the burning of fuels with low-ash melting temperature without any sintering problems, which may lead to a complete plant shutdown for manual cleaning in the bed.

The burnout of volatiles and fine particles is achieved in the postcombustion phase (freeboard) through the injection of secondary air, which is introduced from inlets of horizontally arranged nozzles at this upper part of the furnace. For BFB typical excess air ratios are between 1.2 and 1.3 [Koppejan and Van Loo, 2012]. Similar to the grate-firing unit, the BFB combustion employs staged combustion, with a clear separation of primary and secondary air dosage. The main difference lies in the use of fluidized bed suspension rather than a grate to support the fuel during the combustion [Rosendahl, 2013].

Circulating-fluidized (CFB)

Contrary to the BFB case, where the increase in the bed volume is almost insignificant when compared to the non-fluidized case, a further increase in the primary air flow between 3.0-10 m/s, and using smaller sand particles (0.1-0.4 mm in diameter) with a pretreated fuel of particle size ranging from 0.1-40 mm, a circulating-fluidized bed is achieved. As a consequence to the high fluidization velocity, the fuel particles will be blown away leading to a dispersed bed over the entire volume of the furnace. Hence, there will be no clear distinction between the bed material zone and the dilute upper zone as for the BFB case [Koppejan and Van Loo, 2012].

The solid particles carried with the gas flow, will be captured by a filtering device, usually a cyclone filter or a U-beam separator, before they are fed back again into the combustion chamber (see Figure.3.1(c)) [Kitto and Stultz, 1992]. As a matter of fact, the re-circulation of the solid particles will ensure a long residence time for the burnout of the fuel in the furnace. The bed temperature is typically between 750-900 °C, and it is not controlled by bed combustion stoichiometry as for the CFB case, but rather by cooling through heat exchange surfaces, flue gas recirculation, water injection in water-cooled walls [Grammelis, 2010],[Rosendahl, 2013]. Moreover, as a result of the high turbulence that characterizes CFB combustors, better mixing and heat transfer are achieved, which lead to a very homogeneous temperature distribution in the furnace, and a stable combustion condition due to the hot inert material [Koppejan and Van Loo, 2012].

The high mixing inside the combustion chamber provides good combustion condition for a complete burnout, with less excess air required between 1.1-1.3, and low CO emissions in comparison to the BFB case. In addition, the low excess air ratio, and consequently the low combustion temperature, allows for low levels of NO_x emission and high conversion efficiency. Here, staged-combustion is also applied with primary air split that can be up to 70 % [Rosendahl, 2013]. Finally, the key characteristic differences in those two biomass combustion technologies can be summarized in Table 3.1.

[1]Excess air λ is the ratio of the actual air-fuel ratio to the stoichiometric air-fuel ratio [McAllister et al., 2011].

Table 3.1: The different characteristics of BFB and CFB combustion technologies [Koppejan and Van Loo, 2012], [Rosendahl, 2013].

	BFB	**CFB**
Air velocity	Typically 2-3m/s	About 5-10m/s
Excess air	1.2-1.3	1.1-1.2
Fuel particle size	<80 mm in diameter is recommended	Smaller fuel particles of 0.1-40 mm are required
Bed material	Usually silica sand of about 0.5-1.0 mm in diameter	Smaller silica sand of about 0.2-0.4 mm in diameter
Air flow split	About 50% of the combustion air is fed from bottom, the rest is fed above	50-70% of the combustion air is fed from bottom, the rest is fed above
Bed temperature	650-850 °C	750-900 °C
Combustion process	Mostly occurs in the bed due to the lower air velocity	Not only limited to the bed but the entire furnace volume
Plant efficiency	High (typically >90% on lower heating value)	Very high (higher than BFB)
Unit capacity	Can be offered up to 100 MW_{th}	Can be offered up to 500 MW_{th}
Investment	Lower	higher

3.1.3 Pulverized-fuel combustors

Pulverized-fuel (PF) is a widely used technology for large-scale coal-fired power plant, yet also, for biomass co-firing applications in particular when the fuel is already fine after preprocessing it. Such a system, which is quite similar to the CFB case, the milled fuel is pneumatically injected and mixed; thereafter, the particles will be carried along the high velocity gas flow and the combustion will take place while the fuel is in suspension. The gas burnout of the remaining uncombustible gases will be achieved by applying air-staging, i.e. the injection of secondary air [Obernberger, 2009]. As a matter of fact, the combustion will be distributed over the entire volume of the furnace, so higher load capacities are also possible than in grate or fluidized bed firing systems [De Jong and Van Ommen, 2014].

Due to the fibrous nature of the biomass, the fuel has to be a pretreated biofuel, which further requires additional milling and feeding devices, in order to bring the biomass fuel particles to a suitable size for pulverized combustion to achieve a complete burnout. As a prerequisite, a maximum fuel particle size of 10-20 mm has to be maintained and the fuel moisture content should not exceed 20 wt%(w.b) [Koppejan and Van Loo, 2012], meaning that the biomass fuel has to be within a specified range of properties and of a constant quality to ensure a good combustion [Jones et al., 2014].

3.1.4 Comparison of different technologies

Table 2.3 gives an overall overview of the main characteristics of each previously discussed combustion system. The choice of the appropriate combustion technology will depend always on the targeted capacity for power production that has to be covered by the power plant. Other influencing aspects that have to be thought of when selecting which firing technique to employ is the quality (possible pretreatment) and the availability (storage and management) of the feedstock to be combusted [Rosendahl, 2013].

Table 3.2: Comparison of industrial-scale biomass combustion technologies [Rosendahl, 2013],[Obernberger, 2009].

	Grate firing	Bubbling fluidized bed (BFB)	Circulating fluidized bed (CFB)	Pulverized fuel (PF)
Fuel requirements				
Max. particle size	300mm	80-100mm	40mm	10-20mm
moisture content	$10-60\%$	$10-55\%$	$10-55\%$	$< 20\%$
other requirements	limited fines content	limited alkali content	limited alkali content	limited alkali content
Boiler efficiency	low	medium-high	high	high
Excess air ratio	1.3-1.5	1.15-1.3	1.1-1.2	1.25-1.4
Uncontrolled emissions				
CO,VOC	medium-high	low	low	low
NO_x	high	low	low	low
Load stability and control	poor	very good	very good	very good
Capacity range	100 kW-50 MW	20 MW-several 100 MW	20 MW-several 100 MW	500 kW-several 100 MW
Cold start-up time	long, due to the slow heating of refractory. Start-up burner mainly needed for ignition	long (8-15h or longer), due to heating of bed and refractory. Start-up burner required until the bed is close to normal operating temperature	long (8-15h or longer), due to heating of bed and refractory. Start-up burner required until the bed is close to normal operating temperature	long (8-15h or longer), due to heating of bed and refractory. Start-up burner required until the bed is close to normal operating temperature
Capital cost	low-medium	medium-high	high	high
Operating costs				
Fuel consumption	high	low	low	low
Fuel preparation costs	low	medium	high	high

3.2 The grate firing system

Power recovery from biomass using the grate-type boilers is one of the oldest combustion still in use in today's life. There exists a variety of grate types offered by different manufacturers, that have been enhanced, re-designed and optimized over the years; however, the same principles apply with the exception that the different processes differ slightly from one another. Nowadays, these sophisticated modern grate-firing systems, as shown in Figure 3.2, are mainly composed of [Kitto and Stultz, 1992],[Spliethoff, 2010]:

- a stoker or fuel feeding system,
- a moving grate assembly to support the burning mass of fuel and admit undergrate air to the fuel,
- an overfire system to complete combustion and limit atmospheric pollutant emissions,
- a natural-circulation boiler for steam generation,
- a flue gas cleaning system,
- an ash or residual discharge system.

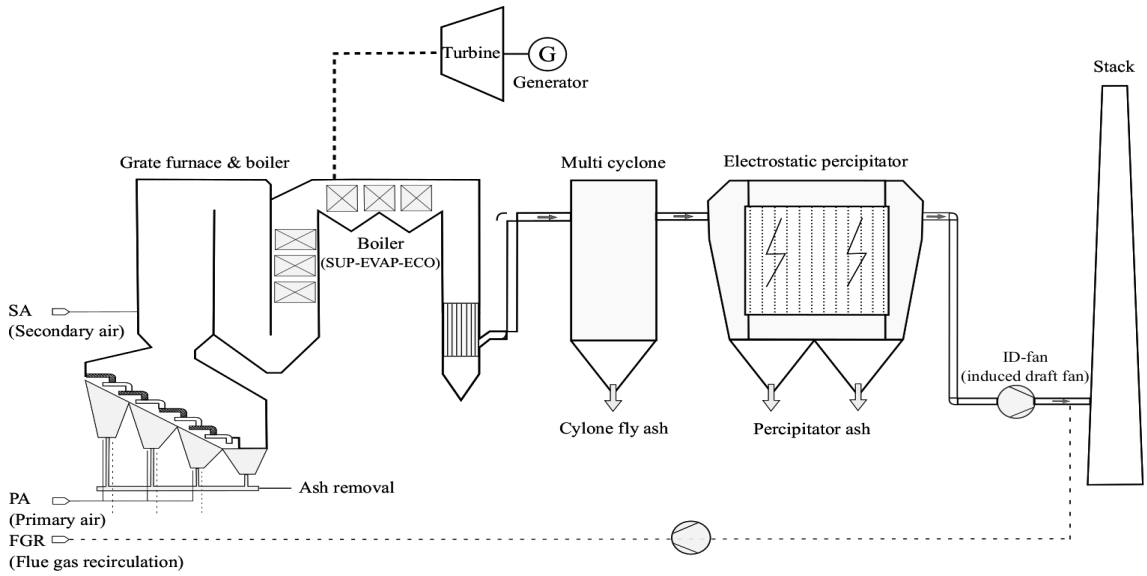

Figure 3.2: Typical plant scheme of a large-scale biomass grate-firing system with its main units: the grate, the boiler for electricity/steam generation, and the flue gas cleaning unit (adapted from [Obernberger, 2009])

In this section, and before introducing the power plant BMK Lünen as a practical and a typical example of such technology in biomass combustion for heat and power production, the main characteristics of grate firing system are briefly explained, whereas an emphasis is put on the furnace part only, i.e. grate types and different furnace design topologies, and excluding the flue gas treatment part, since it is out of the scope of this thesis. However, a detailed discussion of the overall system, including the flue gas treatment part, can be found in [Yin et al., 2008],[Carlsson, 2008].

3.2.1 Grate variants

In the last decades, one of the breakthrough technologies, that aims at exploiting the bond chemical energy in a more efficient and reliable way to a useful form of energy, is the grate assembly technology, a key element in any grate-fired power plant, which is offered in many mechanical configurations depending on the manufacturer experience [Kitto and Stultz, 1992].

Being located within the lower part of the furnace, the grate is designed not only for the lengthwise transportation of the fuel through the furnace and the removal of the remaining ash residues after the combustion, but also for the distribution of the undergrate air (UGA) passing through it and to some extent to the mixing of the fuel [Yin et al., 2008]. The grate assembly can be either air-cooled (more indicated for dry biomass fuels with low ash-sintering temperatures) or water-cooled (more indicated for wet bark, saw dust and woodchips)[Dahlquist, 2013a].

Grates can be further classified into two main categories, these are [Yin et al., 2008]:

- **Stationary grates**: where the grate is principally fixed inside the combustion chamber and the fuel motion is driven by the gravity (caused by the inclination of the grate). This technology is no longer applied in modern biomass combustion power plants.

- **Moving grates**: where the grate transports the fuel through the combustion chamber as a result of the mechanical movement induced. These grates come with different configuration depending on the mechanical principle (forward acting reciprocating, reverse acting, or roller-type grate) that moves the fuel along the furnace. The aforementioned grate assemblies can be well illustrated in Figure 3.3.

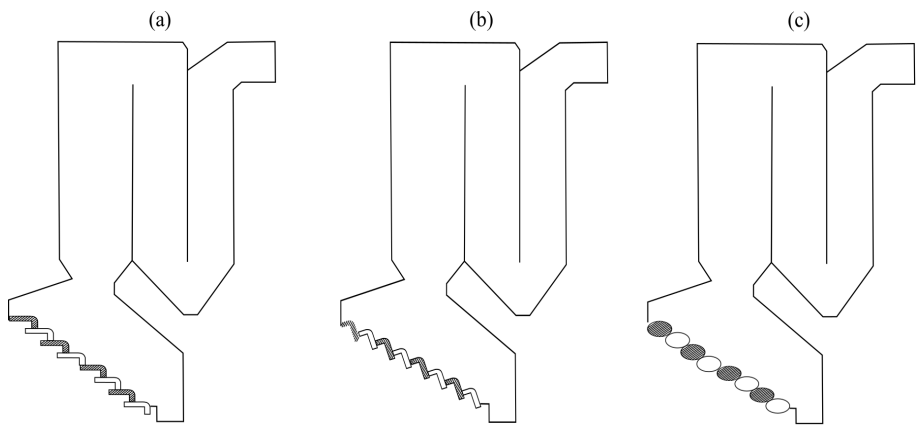

Figure 3.3: The various grate assemblies used in modern grate furnaces: (a) forward acting grate, (b) reverse acting grate, (c) roller-type grate.

Finally, a summary of the key characteristics of different types of grates technology for biomass combustion is given in Table 3.3.

Table 3.3: The different grate types and their key characteristics according to [Yin et al., 2008] and [Lackner et al., 2013].

Grate type	Major characteristics
Stationary sloping grate	The grate does not move. The fuel burns as it slides down the slope under gravity. The degree of sloping is an important characteristic of this kind of grate. Disadvantages: (1) difficult control of the combustion process, (2) risk of the fuel avalanching.
Traveling grate	The fuel is fed onto one side of the grate and burns while the grate transports it to the ash pit. Compared to a stationary sloping grate, it has improved control and a better carbon burnout efficiency (due to the small layer of the fuel on the grate).
Reciprocating grate	The grate tumbles and transports fuel by reciprocating (forward and reverse) movements of the grate rods as combustion proceeds. The solids are finally transported to the ash pit at the end of the grate. Carbon burnout is further improved due to the better mixing.
Roller grate	A series of rollers turning in the direction of fuel transportation characterized by good mixing capabilities and mainly used for high throughputs of up to 40 t/h. Since only approx. one-third of the roller surface is exposed to the hot fuel bed and the other part is cooled by primary air, roller type grate can cope with higher calorific fuels and the resulting higher fuel bed temperatures.
Vibrating grate	The grate has a kind of shaking movement, which spreads the fuel evenly. This type of grate has fewer moving parts than other moveable grates (and thus lower maintenance and higher reliability). Carbon burnout efficiency is also further improved

3.2.2 Furnace geometry

A central part in any biomass heat recovery power plant, beside the grate topology used, is the combustion chamber where all the thermo-chemical processes take place. Different combustion furnaces, with different design and geometries, are offered on the market depending on the supplier specific experience [Spliethoff, 2010].

Usually, as the biomass fuel is characterized by the high volatile matter, only a small fraction of the released gaseous mixture will be oxidized on the grate, the larger part will take place in the upper zone (freeboard). Therefore, the incineration chamber is designed, on the one hand, in a way to ensure that a good gas mixing with the secondary air and a sufficient residence time are achieved in the post-combustion zone, on the other hand, to suit the grate and the gas flow above it. In practice, three main furnace designs are reported for grate combustion plants, as it can be also seen schematically in Figure 3.4, these are:

(a) co-current flow,

(b) counter-current flow,

(c) cross-current flow.

The current nomenclature for furnace classification stems basically from the flow of the flue gases in the furnace relative to the movement of the fuel layer on the grate [Kaltschmitt et al., 2009],[Spliethoff, 2010],[Koppejan and Van Loo, 2012].

Co-current

In a co-current furnace operation, the combustion air and the fed biofuel are in the same flow direction through the incineration furnace, and the flame will be in the same direction as the fuel. Consequently, the flue gas outlet is located at the back end of the grate. For this type of furnaces, there will be less contact between the hot flue gas and the fuel on the grate, and therefore, preheated combustion air should be expected to facilitate the ignition.

Counter-current

Contrary to the previous case, in the counter-current furnace arrangement, the combustion air and fuel on the moving grate are in opposite direction to each other, and the flow gas outlet is located at the front end of the grate. Therefore, due to the fact that the hot flue gas passes over the fresh and wet biomass at the furnace entrance, the drying as well as the ignition of the solid bed are facilitated by convection (in addition to the radiant heat transfer to the solid surface).

According to [Koppejan and Van Loo, 2012], this arrangement is most suitable for fuels with low heating values such as wet bark and woodchips or sawdust, and requires a good mixing of flue gas and secondary air in the upper zone in order to avoid flows with unburned gases and thereby increased emissions.

Cross-current

The cross-current furnace arrangement can be considered as a compromise between the co-current and the counter-current designs. In this case, the flue gas outlet is located in the middle of the grate. According to [Spliethoff, 2010], this arrangement is suitable for a wide range of fuel properties.

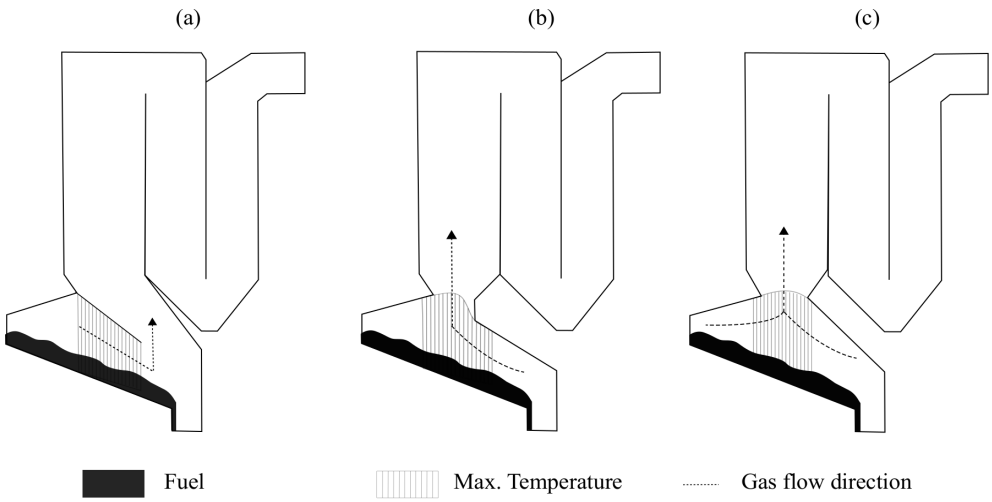

Figure 3.4: Different furnace types in biomass combustion: (a) co-current, (b) counter-current, and (c) cross-current.

3.2.3 Description of BMK Lünen

The biomass power plant BMK Lünen, located in the state of North Rhine-Westphalia, northeast of the city of Dortmund, can be regarded as one of the modern grate-fired units for generating power from biomass. The construction of the combustion unit started in September 2004 and it was officially in operation on June 9th, 2006, with the following technical aspects that characterize the power plant:

Table 3.4: The key technical data of BMK Lünen power plant.

Fuel		
Type	wood (A1-A4)	-
Lower heating value	10,0/13,4/16,0 (min/nom/max)	MJ/kg
Grate		
Type	reciprocating	-
Length	9,9	m
Width	6,9	m
Inclination	16	°deg
Surface	68	m^2
Furnace		
Type	counter-current	-
Fuel throughput	15/18/24 (min/nom/max)	t/h
Volume	1360	m^3
Rated thermal input	67	MW
Flue gas volume	101,000	Nm^3/h
Flue gas temperature	160/180 (at the boiler exit)	°C
Steam boiler		
Type	Natural circulation	-
Steam capacity	80	t/h
Feedwater temperature	130	°C
Steam temperature	462	°C
Steam pressure	79	bar
Turbine		
Electrical output	20	MW_{el}

The plant generates 150,000 MWh of electricity per year, enough to supply 39,000 households with electric power. For this, the biomass combustion power plant approximately requires 135,000 tons annually of pretreated woody biomass. The collected biomass fuel, mainly composed of demolition wood, pallets, fiber boards, residues from the wood processing industry, railway sleepers, telephone masts, etc, is firstly classified and assigned to one of the four categories (A1-A4) in accordance with the German Ordinance on the Management of Waste Wood (Altholzverordnung- AltholzV). This task is done at the Lippe plant, Europe's largest industrial recycling

park located also in Lünen, and owned by the Remondis group.

The shredded woody biomass is stored into a bunker, where it gets homogenized, and possibly mixed with other biomass fuels having a lower energetic value, by means of a crane. The mix is then transported by a long conveyor belt (178 meters long) to the combustion site, where a reception hopper (charging chute) maintains a regular supply of fuel inside the furnace via an integrated special feeding mechanism installed at its bottom, called feed pusher, which operates hydraulically in proportion to the load conditions and the capacity being covered by the combustion power plant, shown in Figure 3.5.

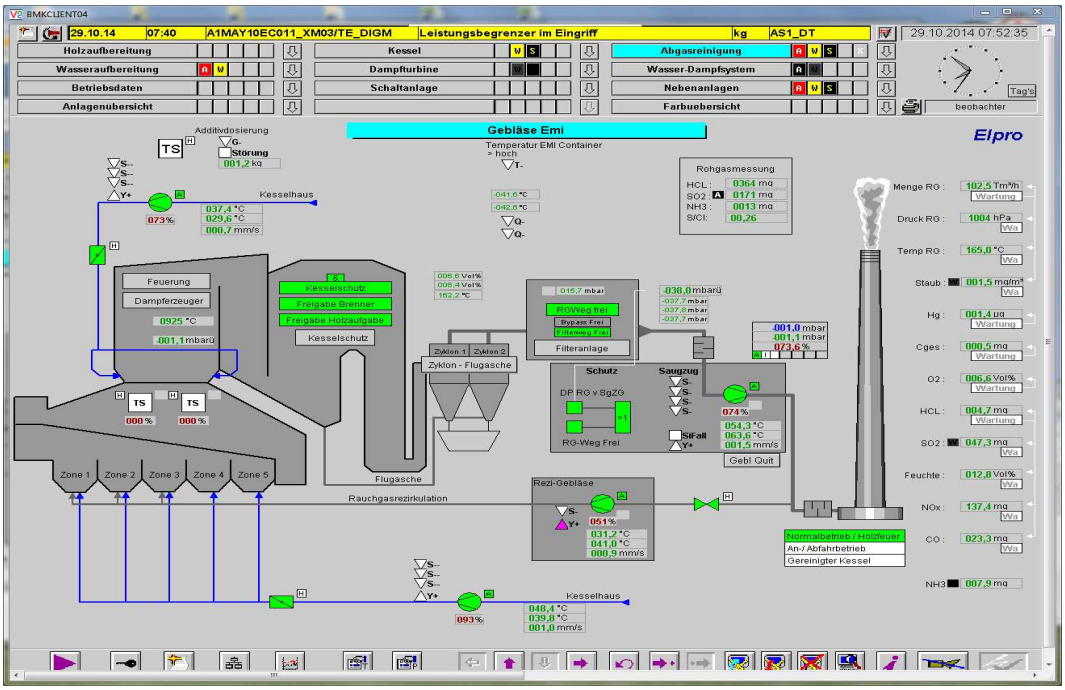

Figure 3.5: Schematic screen of the overall combustion process at BMK Lünen.

Once the solid fuel is dosed inside the furnace, a horizontal reciprocating grate assembly (see also Subsection3.2.1), which serves as a support for the combustion, will transport the biomass through the different zones of thermo-chemical degradation of the biofuel (drying, pyrolysis and gasification, char combustion), while also ensuring its mixing due to the consequent grate movement. The burning bed of fuel reacts then with the combustion air, which is introduced primarily from below the grate and it is sectionalized along the grate into different compartments (five zones) depending on the requirements of the individual combustion zones, as shown in Figure 3.6.

Moreover, a part of the exhaust gas is tapped off from the total exhaust gas being released to the atmosphere and returned to the combustion process in order to compensate for the vaporization heat of the fuel moisture. On the average, the fuel will remain on the grate until its complete combustion about an hour. At the end of the combustion process, the solid residues (ash and unburned char) falls into basin filled with water, called ash discharger, where it could be subject to further treatment.

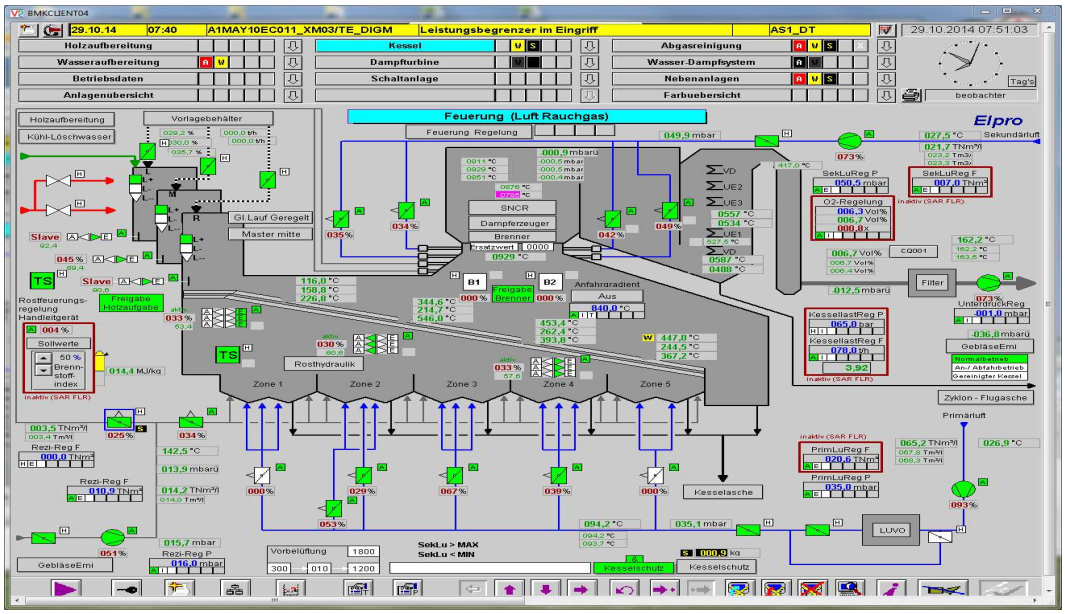

Figure 3.6: Schematic screen of the combustion chamber at BMK Lünen.

The gas mixture being released from the solid bed (together with some fly ash), as a result of the thermal degradation processes during the combustion, will be entrained by the primary flow on top of the bed, and mixed with secondary air to form a hot flue gas mixture that leaves the combustion section and flows to the boiler section formed by several bundles of heat exchanger tubes, where the outer surface of the tubes receives the thermal energy primarily by convection and radiation, then gets absorbed by the working medium inside the tubes (water/steam), as seen from Figure 3.7.

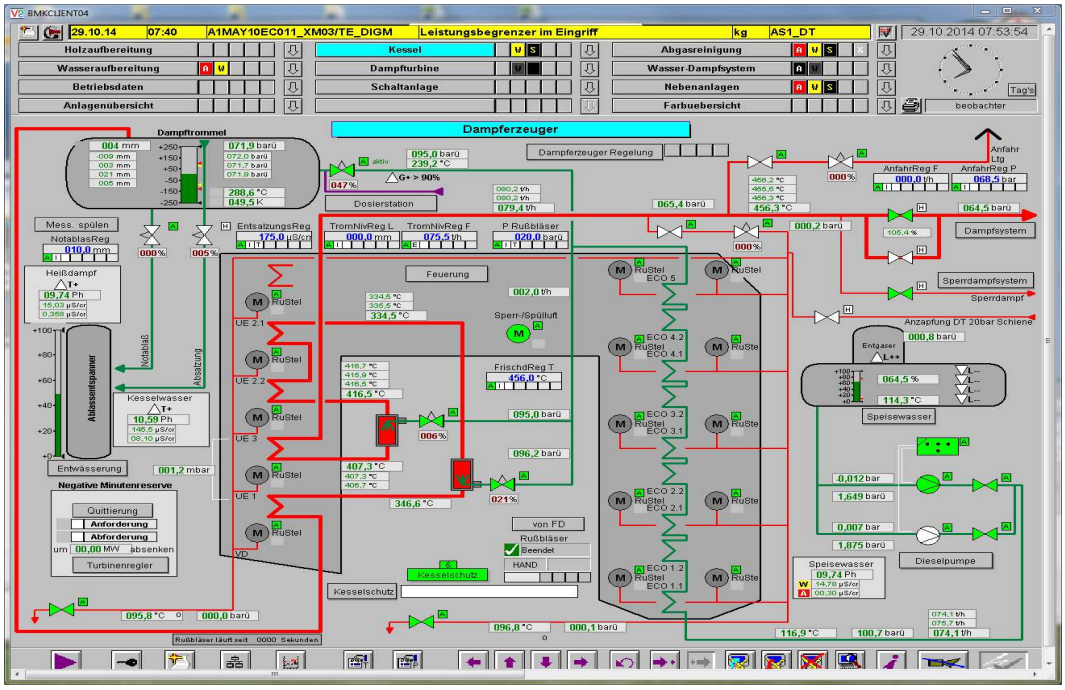

Figure 3.7: Schematic screen of the natural-circulation boiler at BMK Lünen.

Finally, the cooled flue gas at the boiler exit is treated in the flue gas cleaning system, where the fly ash and particles are removed by an Electrostatic Precipitator Unit (ESP), water soluble gases (such as SO_2, HCL, HF and NH_3) are removed by wet/dry scrubbing. Moreover, the nitrogen oxides NO_x are removed by a Selective Catalytic Reduction (SCR). A detailed discussion of such flue gas cleaning systems can be found in [Carlsson, 2008].

3.3 Thermochemical conversion processes

As soon as the fresh biomass solid fuel enters into the hot combustion chamber, heat transferred by the reflected radiation from the hot flame and the furnace refractory walls, as well as convection from the circulating flue gas on top of the solid bed, will be absorbed by the biomass particles from the outside surface of biomass particles to their inner core. In fact, the biomass fuel temperature will increase (abruptly in the outer surface but slowly toward the core of particles), and henceforth initiating the combustion process of biomass on the moving grate, which involves a series of partial fuel degradation processes of high complexity, namely, preheating and drying, pyrolysis, gasification, and combustion (oxidation), as depicted in Figure 3.8, which will be further explained in the upcoming subsections.

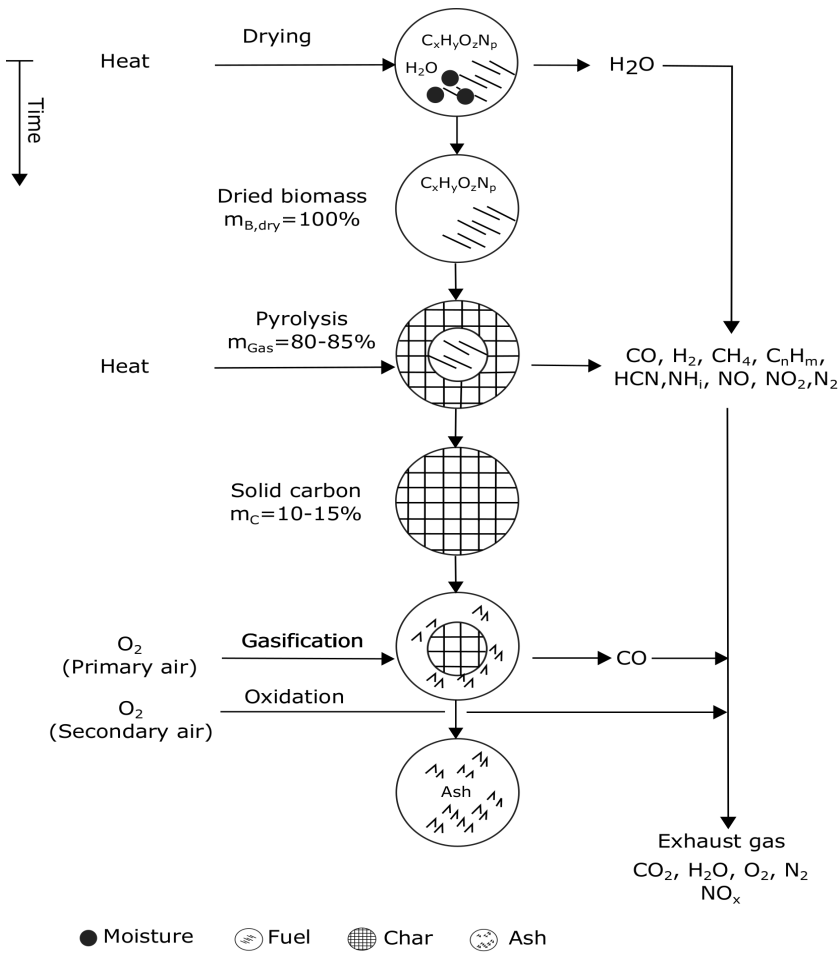

Figure 3.8: Thermal decomposition phases of biomass particle on the moving grate and combustion products [Kaltschmitt et al., 2009].

3.3.1 Drying

Drying, or the moisture evaporation process, is a very crucial part of thermochemical processing of biomass inside the grate firing unit and a complex process that involves simultaneous heat and mass transfer. It is the exsiccation process through which the water content of the biomass fuel is vaporized and swept away from its surface by means of a carrier fluid passing through the porous bed, without being associated to any chemical reaction. With biomass being a hygroscopic, capillary-porous material, the water in biomass can exist in three forms, free water (capillary) in the cell cavities and inside the pores that form a complex network of capillary paths, as a vapor in the cell cavities, and finally as a bound (hygroscopic) water in the cell walls [Peishi and Pei, 1989], [Skaar et al., 1988].

When the fresh porous biomass fuel enters the combustion system, heat will be conducted and radiated toward the surface of the biomass particle, and two simultaneous processes will proceed, these are: (a) the internal heat transfer from the particle's surface toward its interior (heating) and (b) moisture evaporation at the surface of the particle. In this case, the movement of the water from the inner core to the outer surface of biomass fuel, as a liquid or vapor, will be primarily attributed to the capillary forces due to the water gradients, meaning that the surface has to be drier than the interior if the moisture is to be exsiccated from the solid fuel [Asli, 2013]. The heating and drying phases can be seen from a thermogravimetric analysis, which shows the mass loss as a function of temperature during combustion of wet biomass fuel (see Figure 3.9).

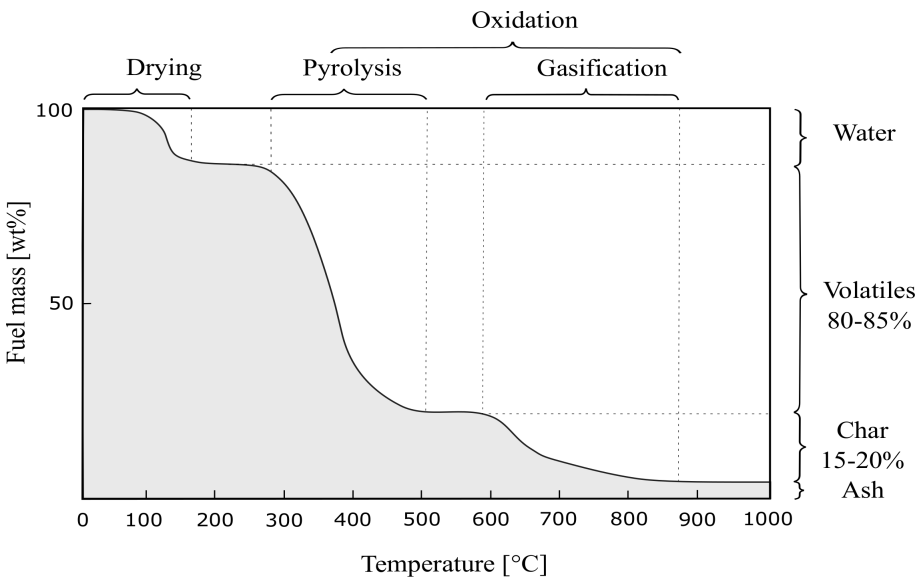

Figure 3.9: Thermal degradation of wet biomass as a function of time and temperature from thermogravimetrical analysis (TGA), adapted from [Kaltschmitt et al., 2009] and [Nuusbaumer, 2002].

In grate or fluidized bed systems, where the furnace is fed with moisture-containing fuel and without pre-treatement, it has been found that the combustion process cannot be self-sustained if the moisture content exceeds 60 wt%(w.b). This implies that the heat generated should be larger than the energy required to evaporate the contained moisture in the biomass fuel, as the drying process is an endothermic reaction

that requires energy. Consequently, moisture content is a key controlling variable for an appropriate operation of the heat recovery power plant [Koppejan and Van Loo, 2012].

3.3.2 Pyrolysis

After the drying is completed, the fuel temperature starts to increase, and another intermediate step towards a full oxidation of the biofuel begins to occur, namely the pyrolysis reaction. By definition, pyrolysis is the thermochemical decomposition of biomass under the influence of heat and in an oxygen-deficient environment ($\lambda = 0$). The pyrolysis can convert up to 80-85 wt%(w.b) of the biomass into volatile compounds, char and tar[2]under an endothermic reaction where heat is required to accomplish the pyrolytic decomposition process [Kaltschmitt et al., 2002].

The mechanistic step of this reaction can be generally described by the following equation [Tong et al., 2015]:

$$\text{Biomass} \xrightarrow{+\text{heat}} \text{Gases } (H_2 + CO + H_2O + CH_4 + C_nH_m) + \text{tar} + \text{char} \tag{3.1}$$

In this process, at a fuel temperature of about 200 °C, the complex macromolecules of biomass, which are made of three major polymers: cellulose, hemicellulose and lignin, start to break down into relatively smaller and simpler molecules of gas, liquid, and char. The decomposition process becomes progressively more rapid and complete as the temperature reaches 400-500 °C (see Figure 3.10).

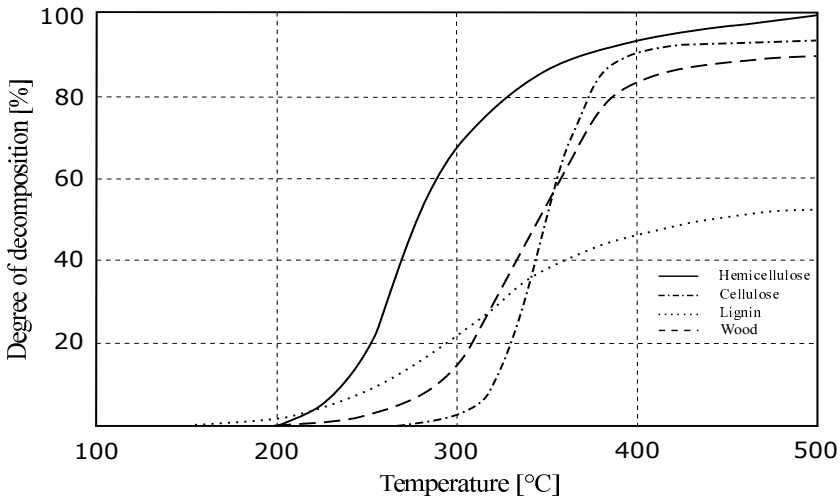

Figure 3.10: Thermal decomposition of wood and its cellulose, hemicellulose and lignin components as a function of temperature [Kaltschmitt et al., 2009].

Each of these three ligno-cellulosic biomass components has a different thermal decomposition behavior and preferred temperature ranges of decomposition [Basu, 2013]. An analysis of data from thermogravimetric analyzer (TGA) based on various selected biomass species indicates different temperature ranges for cellulose, hemicellulose, and ligning, in order to undergo the pyrolytic decomposition process, these are [Pandey et al., 2015]:

[2]Tar is all organic contaminants with a molecular weight larger than benzene [Devi et al., 2003].

- **Hemicellulose**: 150-350 °C
- **Cellulose**: 275-350 °C
- **Lignin**: 250-500 °C

Upon the completion of the pyrolytic decomposition phase, a mixture of volatile gases, light hydrocarbons and high molecular weight (condensable) compounds, as well as a carbonaceous solid fraction known as char are formed [Stevens and Brown, 2011]. Volatile gases include H_2, CO_2, CH_4, H_2O (steam), and light hydrocarbons such as C_2H_6, C_2H_4, and C_2H_2. The high molecular weight hydrocarbons will contribute to the formation of tars, that have an organic structure similar to the base fuel; tars evaporate from biomass at a temperature between 400 and 600 °C, or can be condensed if they are cooled below 200 °C.

For generating such pyrolytic products, the cellulose is pyrolyzed in a multistage process, according to Broido-Shafizadeh model, via both depolymerization and dehydration. In dehydration, which dominates at low temperature and slow heating rate, anhydrocellulose is formed, which is later degraded to produce noncondensable gases, char, and tar. In depolymerization, which is favored under fast heating rates, the levoglucosan as an intermediate product is formed, which then decomposes into tar and condensable gases. Hemicellulose yields more noncondensable gases and less tar in comparison to cellulose. Degradation products from lignin typically will include char (50-65%), tar (10-15%), and (10-12%) gases [Cheng, 2009],[Basu, 2013].

3.3.3 Gasification

Similar to the pyrolytic decomposition, the gasification process represents an intermediate step toward a full oxidation of the biofuel. Unlike the pyrolysis, gasfication of biomass is a thermochemical conversion process in the presence of restricted supply of oxygen ($0 < \lambda < 1$), i.e. partial oxidation, and at high elevated temperatures (700-1500 °C)[Kaltschmitt et al., 2002].

Essential in the gasification process is the conversion of the solid carbon remaining from the pyrolytic decomposition phase as a byproduct (see also Eq.(3.1)), at sufficiently high solid surface temperature, into lower molecular-weight gaseous products, with the gas mixture will predominantly be composed of CO_2 and H_2, as a result of the several heterogeneous solid-gas reactions between the char and the gasifiying agents like oxygen, carbon dioxide and steam. Hence, gasification can be said to be an extension of pyrolysis, and thereby, together with pyrolytic products a so called producer gas[3] is formed [Baskar et al., 2012].

Depending on the temperature at the solid surface, the pressure condition, and supplied gasifying agents from the pyrolysis phase, four major reactions by which solid carbon is further upgraded into gaseous product can be distinguished. These are: partial combustion (carbon-oxygen reaction), hydrogenation, water-gas, and

[3]This term is used in different ways. Some use it as interchangeable with cleaned syngas, others to describe a particular industrial fuel. Here, this term is used to describe uncleaned gases resulting from biomass gasification.

finally Boudouard, which can be respectively given by the following Eq. (3.2a)- Eq. (3.2d) [Christensen et al., 2011]:

$$C + \frac{1}{2}O_2 \longrightarrow CO \qquad +110{,}6 \quad kJ/mol \tag{3.2a}$$

$$C + 2\,H_2 \longrightarrow CH_4 \qquad +79{,}9 \quad kJ/mol \tag{3.2b}$$

$$C + H_2O \longrightarrow CO + H_2 \qquad -131{,}4 \quad kJ/mol \tag{3.2c}$$

$$C + CO_2 \longrightarrow 2\,CO \qquad -172{,}6 \quad kJ/mol \tag{3.2d}$$

As the drying and pyrolytic decomposition phases are endothermic processes, requiring an external source of heat to drive them. The required energy more typically will be supplied by the highly exothermic carbon-oxygen reaction, which releases sufficient energy to accomplish them. This exothermic reaction also helps in providing thermal energy to activate the Boudouard and carbon-water reactions, that are of great significance in gasifying char into CO and H_2. Furthermore, the hydrogenation helps in providing energy for the endothermic reactions, but its contribution is small in comparison to the carbon-oxygen reaction, due to the relatively low concentration of H_2 [Stevens and Brown, 2011].

3.3.4 Oxidation

Within the last step of the thermochemical combustion processes of solid biomass, and with respect to the thermal decomposition of the molecular structure of biomass fuel, the gases that are formed during the gasification will move away from the char particle and combine with the volatile gases released in the devolatilization phase. These resulting combustible gases will be usually further oxidized by applying staged combustion (see Figure 3.11), where oxygen is carried with air injected in a consecutive phase on top of the fuel bed [Nuusbaumer, 2002].

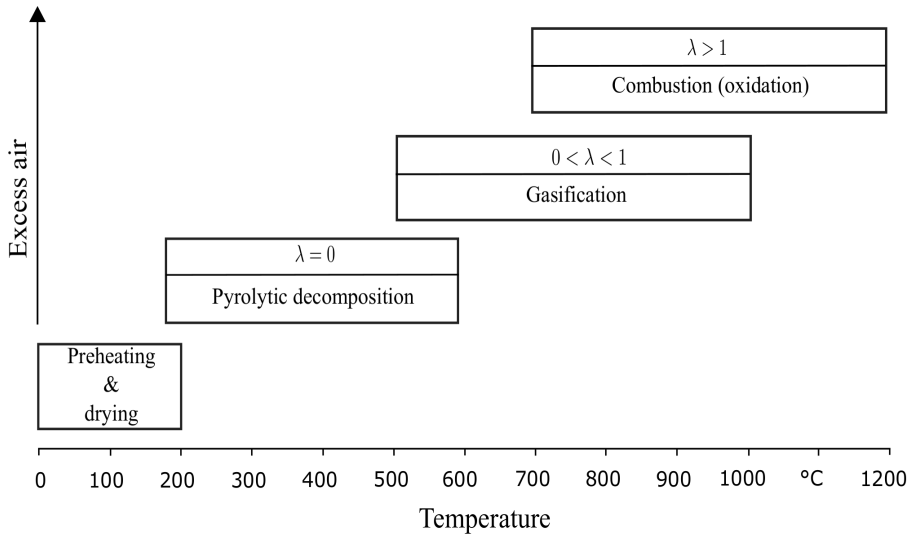

Figure 3.11: Oxygen supply levels during staged-combustion of the fuel inside the furnace [Kaltschmitt et al., 2009].

During the homogeneous exothermic reaction, the three Ts of combustion are very critical, these are: temperature, time and turbulence. A high combustion temper-

ature will assure that the chemical reactions proceed at high reaction rates. The turbulant mixing of combustion gases with oxygen will make certain that every fuel molecule will come into contact with oxygen molecules. Long residence time in the post-combustion phase will allow for the complete consumption of the volatile gases and none will escape the post-combustion phase without being fully oxidized to the desirable combustion products [Goswami and Kreith, 2007].

It is only under such conditions that a complete burnout is achieved with the ultimate combustion products from burning the solid biomass, according to the following oxidation reactions scheme, will be CO_2 and H_2O [Baskar et al., 2012]:

$$C + O_2 \longrightarrow CO_2 \qquad +393{,}5 \quad \text{kJ/mol} \tag{3.3a}$$

$$H_2 + \frac{1}{2}O_2 \longrightarrow H_2O \qquad +241{,}8 \quad \text{kJ/mol} \tag{3.3b}$$

In the absence of good combustion conditions, the biomass will not be fully oxidized into its final products, i.e. CO_2 and H_2O. As a consequence, products of incomplete combustion will be inevitably present in the exhaust flue gas, this includes, CO, volatile organic compounds (VOC), polycyclic aromatic hydrocarbon (PAH), and soot.

4 Mathematical modeling of a biomass power plant

The development of mathematical models for complex physical systems has been always an integral tool and an important activity in many science and engineering fields, aiming at understanding the current real-world situation, i.e., the system, or the observed phenomena being modeled, as a prerequisite to approach optimality in either the system design or operation [Klee, 1987]. Although using mathematics in problem solving has been practiced for a very long time, a strong stride in the area of model development for dynamic systems has become conspicuous in the last five decades, due to the emergence of powerful computer simulators and simulation software packages to mimic the reality.

Thereupon, model development could be defined as a way of casting the real world problem by a modeler into a set of mathematical equations, which has to be solved and then interpreted, to gain an insight into the real world situation [Rasmuson et al., 2014]. However, in doing so, only a "chunk of reality", or in other words certain characteristics of the system, are captured by the model, either because of the limited knowledge on the system, or the intended use and the purpose for which the model has to be constructed [O'Shea, 1992]. Hence, only a subset of the essential process characteristics will be included in the model. Consequently, besides the physical system to be modeled, the purpose for which the model is developed will influence the level of included mathematical details, this can be restated as follows [Cameron and Hangos, 2001]:

> "*The modeling enterprise links together a purpose $\mathcal{P}$ with a subject or physical system $\mathcal{S}$ and the system of equations $\mathcal{M}$ which represent the model. A series of experiments $\mathcal{E}$ can be applied to $\mathcal{M}$ in order to answer questions about the system $\mathcal{S}$.* "

In this chapter, and based on the last statement, a mathematical model is developed for predicting the dynamic behavior of a biomass heat recovery power plant. The model is comprised of three main units: the production of thermal energy, the production of steam using a boiler with a natural circulation for generating steam based on the released thermal energy from the furnace part, and finally the pollutant reduction unit, which is responsible for the flue gas aftertreatment and it will be omitted in the modeling task; therefore, an emphasis will be only put on the first two units. The aforementioned units that constitute the power plant are illustrated in Figure 4.1. Finally, in order to keep the modeling task at moderate level, a balance between simplicity and accuracy of the model has to be kept in mind, since the intended purpose will be directed to the model-based control of the power plant unit. Furthermore, the model should have a valid structure that is capable of representing the right behavior of the system, which means finding the correct relationships between the inputs, outputs and the internal variables, that will govern the right response of the power plant's outputs as the inputs are changed.

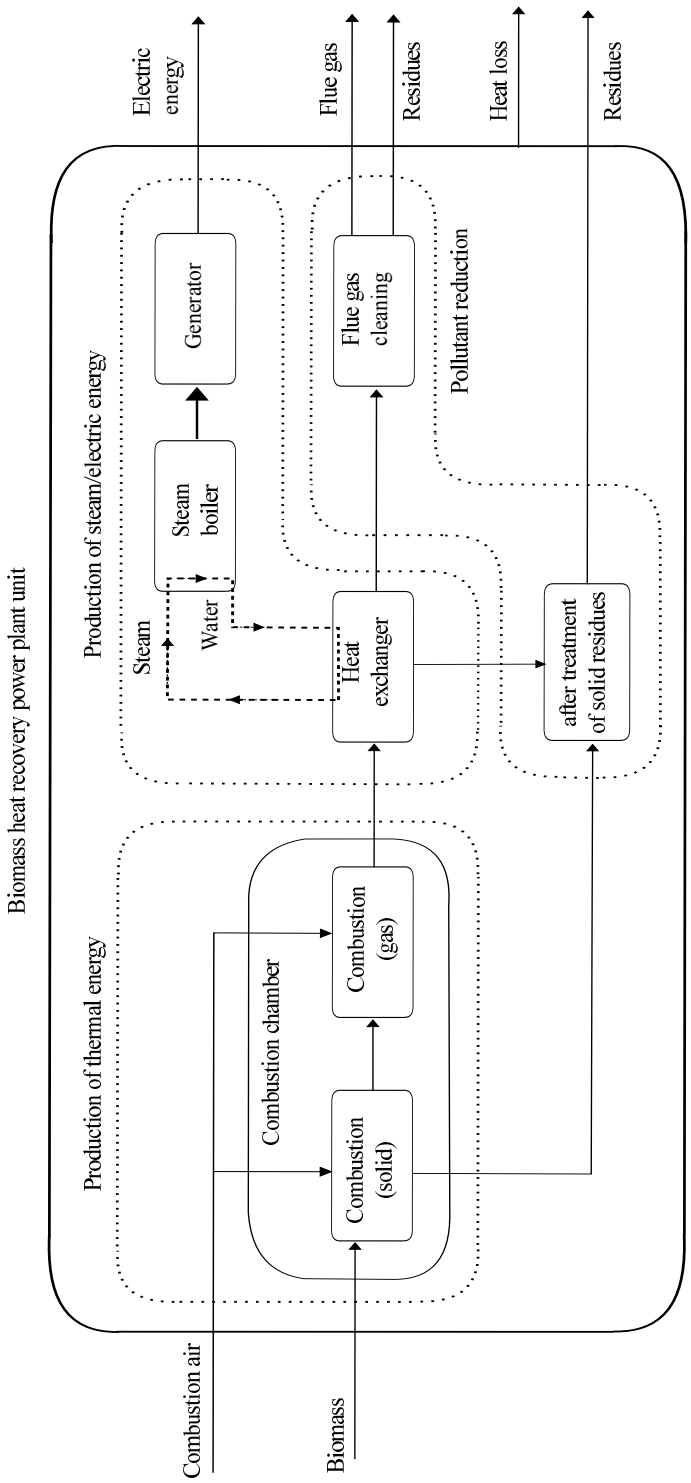

Figure 4.1: Biomass heat recovery power plant with the different main units: (a) production of thermal energy, (b) production of steam/electric energy, and (c) pollutant reduction [Belkhir et al., 2015b].

4.1 A review

In the last two decades, there has been an intensive ongoing work in modeling both the thermo-chemical phenomena in the fuel bed on the grate and in simulating biomass grate fired furnaces overall. In general, the existing modeling approaches

can be classified into two categories, distributed models, which constitute the bulk of reported models in literature and are dedicated to CFD (Computational Fluid Dynamics) simulations, and to a lesser extent control oriented models.

[Yin et al., 2008] gave an excellent overview on modeling and developed CFD simulation models of biomass grate firing systems, in which these models were classified into five main categories depending on the purpose of the carried research. Within the suggested classification, two main modeling efforts prevail, namely, modeling of biomass conversion in the fuel bed on the grate, and modeling of mixing and combustion in the gas phase. Here, a common modeling concept is to couple these "sub-models", i.e. the bed model and the gas phase model, into one coherent simulation model that represents the entire combustion furnace.

As a consequence, the bed model is used to solve the thermal conversion of biomass in the fuel bed, and CFD is used for the gas phase simulation. These separate submodels are coupled with each other by the heat and mass transfer at the interface, which is here the top surface of the fuel bed, with the former providing boundary conditions such as the distribution of gas species concentration, velocity, and temperature along the grate to the CFD gas phase simulation, while in return the gas phase simulation provides the heat flux released from the flame and furnace walls to the fuel layer in the bed model. Concerning the bed model which provides the inlet conditions to the gas phase simulation, two main approaches exist: the first straightforward approach is based on empirical bed models that are built from both experience and measurements in the solid bed, the second approach is developing mathematical models of the solid phase, either separately or directly integrated in the CFD simulation, based on distributed mass, momentum, and energy balance equations.

Even though, the reported CFD models for the biomass grate-firing plant form a helpful tool in understanding the different reciprocal relationships between the relevant thermo-chemical phenomena in biomass combustion, and provide a good platform for a further understanding of combustion-related problems at a detailed level, as well as help in optimizing the plant operation and coming with new plant's design, these models, while also tailored to specific combustion furnace, they are too complex and very detailed, typically consisting of many partial differential equations, which prevent their consideration for further development of a control strategy for the biomass combustion power plant. Contrary to the mature area of designing grate combustion based on CFD simulation, only a few control-oriented models have been reported in the literature for the grate combustion with natural biomass (wood chips) as a fuel for power generation.

A nonlinear model for a medium scale biomass control was developed at the research center BIOENERGY2020+ in coorporation with the institute of Automation and Control of Graz University of Technology. In order to reduce the complexity of the model, separate modeling of the relevant parts of the medium scale grate combustion of biomass were carried independently. [Bauer et al., 2010] derived a simplified model for the fuel bed. Prior to the modeling, the present combustion situation at

the pilot plant[1] was assessed. The detailed investigation of the fuel bed revealed that the plant shows a co-current combustion behavior with the ignition at the bottom of the bed. Based on this fact, a simple co-current combustion model for the fuel bed was developed. The fuel bed was divided into a dead zone in which the wet fuel is heated up, due to heat conducted from the hot grate bars, but it remains almost unchanged, a water evaporation zone begins with the emergence of the heated wet fuel and ends with the fuel moisture being evaporated, and a thermal decomposition zone where fuel devolatilization and char burnout take place. Finally, the resulting mathematical model consisted of two ordinary differential equations, which represent mass balance for water in the water evaporation zone and the dry substance in the thermal decomposition zone. Also, the model gave an empirical correlation between the provided fuel and air mass flows to close the balance equations.

In the PhD thesis of [Gölles, 2008], and in order to complement the work done by [Bauer et al., 2010], a static combustion model was developed for the primary and secondary combustion zones, as well as a model for the heat exchanger for the small-scale biomass boiler. The model describing the combustion zone is a common stoichiometric combustion calculation, with the oxygen necessary for oxidizing the carbon and hydrogen in the fuel to carbon dioxide and water. Here, the resulting evaporated water and the devolatilized dry biomass from the fuel bed model, as well as the supplied primary and secondary air are taken into account. Consequently, this allows for the calculation of the mass flow rate of the flue gas and its chemical decomposition, as well as the adiabatic combustion temperature, which is the maximum achievable temperature under the assumption that there will be no heat transfer to the environment, and neglecting the kinetic and potential energy in the energy balances.

Although, the overall resulting model found application in designing a control strategy for a small-scale biomass grate system, such as in [Gölles et al., 2014] and [Schörghuber et al., 2015] where a controller based on input-output linearization and an extended Kalman filter to estimate the current state of the furnace were designed in order to control the oxygen content in the flue gas and the water feed temperature in the heat exhanger, and more recently, the model has been used by [Kortela and Jämsä-Jounela, 2015] for the design of fault-tolerant model predictive controller for an underfeed rotating grate boiler; the described model cannot be considered here, as the combustion situation at the BMK Lünen power plant shows a counter-current combustion behavior (ignition from the top of the fuel bed), which is totally different from the co-current case (ignition from the bottom). In addition, the model does not include the grate speed and its geometry. These two elements influence the time biomass will spend inside the furnace, and therefore, its reactivity.

[Strzalka et al., 2013] presented an equilibrium mathematical model for a counter-current biomass combustion plant. The biomass furnace is equipped with an inclined moving grate of a total length of 6 m and width of 1.85 m, and utilizes woodchips gathered from landscape residues as a fuel to produce a maximum thermal output capacity of 8 MW_{th}. Here, the methodology for the model development assumes

[1] A down scale version 180 kW_{th} of a typical medium scale furnace equipped with a horizontally moving grate, and two primary air zones with flue gas recirculation above the grate.

no accumulation in both solid and gas phases, while a dynamic model takes the capacity of the system into consideration. In addition to this, the modeling concept separates the thermal decomposition stages of solid biomass on the grate, i.e., drying, devolatilization, and char burnout, into different sequencing steps depending on the primary air requirement of the individual zones. Based on these assumptions, mass and energy balances for each of the individual combustion subprocesses, as well as for the gas phase, which was also divided into two zones depending on the secondary air supply, were drawn.

Whilst the developed equilibrium model was beneficial to estimate optimized control parameter settings for the flue gas recirculation fans in order to reduce the recirculated gas rate to the furnace, hence, increasing the gas temperature to optimal values and the overall efficiency of the combustion appliance, modern model-based control strategies for nonlinear system, such as biomass grate combustion case, require a dynamic model that is able to predict the dynamic response of the system as a prerequisite for their application, which can be considered a limitation for this model. Furthermore, both oxygen concentration in the flue gas and the influence of the grate speed are not modeled. Beside this, the model does not consider the variation in the energy content of the fuel, and takes only the average value of fuel's moisture content, as an input for the model into account.

In [Paces and Kozek, 2011] a detailed dynamic model of grate-fired biomass furnace suitable for control application has been presented. The mathematical model was derived based on first-principle considerations in both solid and gas phases inside the furnace. Here, the biomass bed on the grate was divided into five different sections depending on the air requirements of each zone, with each section further including one solid phase and another gas phase that represents the void space inside the fuel bed only, while the gas phase above the bed is regarded as a single volume.

The biomass fuel is assumed to be composed of four fractions, mainly, moisture, volatile matter, fixed carbon, and inert ash. The thermal decomposition rates for these components were given under the form of a linearized Arrhenius equations. The oxygen concentration in the flue gas was modeled by using a grey-box model, which represents a second-order all pass filter with the transfer function coefficients have to be determined experimentally. For the generated steam amount a black-box model was identified. The resulting model is characterized by its high order, and the considerable tuning effort required to fit the model parameters to the experimental data. As a consequence, model reduction technique, namely, balanced truncation, was applied in order to reduce the complexity of the model. This resulted in a linearized model around only a single operating point, and therefore, cannot cover the whole operating region of the plant.

Based on the insight gained from the presented overview on the current state-of-the art models, a general dynamic model for biomass grate-fired power plant will be developed. The model is characterized by a small number of parameters to be identified and takes also into account the variation of the energy content of the fuel. The model parameters will be tuned by comparing the measured data to the modeled response using a robust global optimization algorithm for this goal.

4.2 Combustion furnace

The modeling of the combustion process of the virgin woody biomass fuel in a furnace is fairly a very difficult and elusive task that requires an exorbitant time for its accomplishment. In this section, an effort will be made to derive a suitable mathematical model, which will be able enough to characterize and capture the dynamic behavior of a real combustion furnace, and for a wide variety of operating conditions, while keeping this modeling task at an acceptable moderate level of complexity in order to make the problem amenable to a numerical solution. This goal will be achieved through approximations and by assuming some simplifications to lessen the confronted complexity.

As it will be seen later, one of such assumptions that will simplify this task, and hence, the number of equations describing the system, is to consider the furnace as a reactor with one solid and one gas phase, thereby displaying the principle of parsimony that underlies the model.

4.2.1 Reactor modeling

As it has been mentioned earlier, the furnace is regarded as a continuous stirred tank reactor, abbreviated CSTR, with two phases, a solid and a contiguous gas phase. Usually, in many modeling tasks in chemical engineering, where such a CSTR model is used to predict the system's behavior, a common simplifying assumption is that the performance of the reactor is approximated by that of an ideally stirred tank reactor, and hence, all performed calculations assume a complete mixing in the vessel [Denbigh and Turner, 1984].

The perfect-mixing assumes that the composition as well as the temperature have a uniform value throughout the reactor volume. Therefore, there will be only a dependency on time for these fundamental quantities, and a set of balance equations, which describes the dynamics of both the solid and gas phases, are obtained, when the conservation principles are applied on these quantities. Consequently, the solid bed temperature is considered to be homogeneous along the grate length and described by the temperature T_s [K], this also holds true for the gas phase temperature T_g [K], since the secondary air is usually injected at high speeds through the air nozzles to insure that a perfect mixing of the gaseous species from the burning solid bed is achieved.

A schematic drawing of a typical CSTR is depicted in Figure 4.2, along with the entering and leaving flows in and out the system boundary. This scheme is used as an approximation for the combustion furnace for the modeling task. Here, the biomass solid fuel is assumed to be composed of two main fractions: a combustible fraction (including inert), as well as the moisture fraction (free water) similar in [Van Kessel, 2003]. The recirculation gas is divided into two portions, a part that goes to the post combustion phase, and a part that is fed into the fuel bed. The primary air is fed under the grate through an air preheater, whereas a secondary air is injected in the gas phase to achieve a complete burnout.

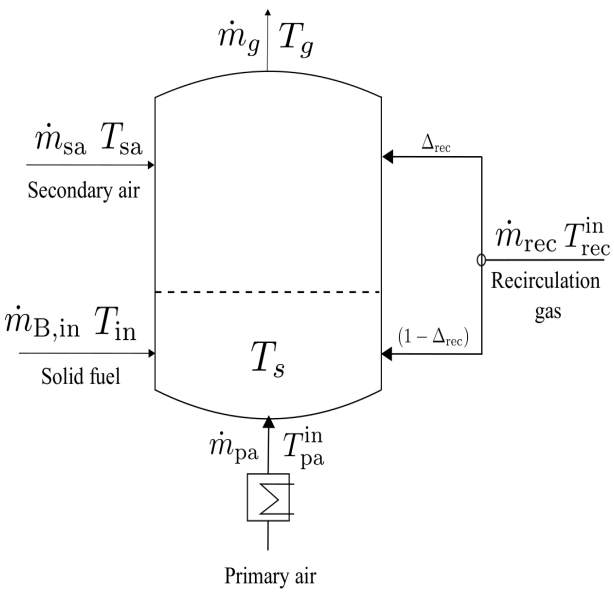

Figure 4.2: Continuous stirred tank reactor scheme.

Mass transport dynamics

The formulation of the model for solid thermal decomposition inside the reactor can be obtained by a simple mass balance for the dry biomass m_{ds} [kg] inside the reactor. This, can be expressed as:

$$\frac{dm_{\mathrm{ds}}(t)}{dt} = (1-\gamma_{\mathrm{w}})\,\dot{m}_{B,in} - \dot{m}_{out}(t) - \dot{m}_{\mathrm{thd}}(t) \tag{4.1}$$

with the thermal decomposition rate $\dot{m}_{\mathrm{thd}}$ can be expressed according to the biomass solid conversion model in [Van Kessel et al., 2004b]:

$$\dot{m}_{\mathrm{thd}}(t) = R_{\mathrm{thd}} \cdot a \cdot m_{\mathrm{ds}}(t) \tag{4.2}$$

with a [m^2/kg] denotes the solid surface renewal area due to the grate movement, and R_{thd} [kg/(m^2.s)] is the thermal decomposition rate which can be described by first order combustion kinetics dominated by oxygen diffusion towards the flame surface, which will be further discussed in Subsection 4.2.2.

The biomass flow rate at the exit can be linked to the solid mass hold-up and the residence time of the reactor τ [s], which will be discussed in Subsection 4.2.4, via the following relation:

$$\dot{m}_{out}(t) = \frac{m_{\mathrm{ds}}(t)}{\tau} \tag{4.3}$$

Similar to the thermal decomposition model of the dry fuel, the evaporation model of the wet fuel inside the reactor is obtained by a simple mass balance as follows:

$$\frac{dm_{\mathrm{w}}(t)}{dt} = \gamma_{\mathrm{w}}\,\dot{m}_{B,in} - \dot{m}_{\mathrm{evap}}(t) \tag{4.4}$$

with the evaporation rate of the biomass fuel is expressed as:

$$\dot{m}_{\text{evap}} = K_{\text{evap}} \cdot \frac{m_{\text{w}}(t)}{m_{\text{tot}}(t)} \tag{4.5}$$

and

$$m_{\text{tot}}(t) = m_{\text{ds}}(t) + m_{\text{w}}(t) \tag{4.6}$$

Here, K_{evap} [kg/s] denotes the evaporation rate of the moisture from the fuel. The evaporation rate is strongly linked to the mass and heat transfer phenomena acting on the solid fuel on the burning bed, as it will be discussed in Subsection 4.2.3.

The total mass balance of the gas phase can be obtained based on an instantaneous rate of change, i.e., by considering the mass rates entering and leaving the gas phase, as well as the fraction of oxygen consumed in the post-combustion zone to burn the biomass fuel. Hence, the gas mass balance dynamics is given by:

$$\frac{dm_{\text{g}}(t)}{dt} = \dot{m}_{\text{pa}} + \dot{m}_{\text{sa}} + \dot{m}_{\text{rec}} + (1 - \nu_{\text{O}_2})\, \dot{m}_{\text{thd}} + \dot{m}_{\text{evap}} - \dot{m}_{\text{g,out}} \tag{4.7}$$

Here, ν_{O_2} [$\text{kg}_{\text{O}_2}/\text{kg}_{\text{B}}$] denotes the specific oxygen demand to burn 1 kg of the biomass fuel. This value will be fitted to measurement data, or can be also estimated from molecular formula if the stoichiometric coefficients of the fuel are known, as it will be shown in Subsection 4.2.2.

Solid and gas temperature dynamics

Similar to the solid phase, the energy balance can be obtained by an integral balance on the total energy flows entering and leaving solid and gas phases, as shown in Figure 4.3. Again, the gas temperature as well as the solid temperature are both assumed to be homogeneous within the compartments formed by these phases, as a result of the perfect mixing assumption [Stadler et al., 2011].

In addition to this, it assumed that both the primary and the recirculated air flows traversing the bed from below the grate exchange heat with the solid bed via convective heat transfer (see Subsection 4.3.2), and leave the porous bed along with the combustion products at the same exit temperature T_{fg} [K], as shown in Eq. (4.8):

$$T_{\text{pa}}^{\text{out}} = T_{\text{rec}}^{\text{out}} = T_{\text{fg}}^{\text{out}} \tag{4.8}$$

According to Figure 4.3, the equation describing the dynamics of the solid bed temperature is given by:

$$\bar{c}_{p,s}\, m_{B,in} \frac{dT_s(t)}{dt} = \dot{Q}_{B,in} + \dot{Q}_{\text{pa}}^{\text{in}} + \Delta'_{\text{rec}} \dot{Q}_{\text{rec}}^{\text{in}} + \dot{Q}_s - \dot{Q}_{\text{fg}}^{\text{out}} - \dot{Q}_{\text{ash}} - \dot{Q}_{\text{evap}} \tag{4.9}$$

Here, the average specific heat capacity of the solid biomass $\bar{c}_{p,s}$ [J/(kg.K)] varies considerably with the moisture content of the biomass fuel as shown by Eq. (4.10) [Kollmann and Côté Jr, 1968]:

$$\bar{c}_{p,s} = [\gamma_{\text{w}} c_{p,\text{w}} + (1 - \gamma_{\text{w}}) c_{p,wood}] \tag{4.10}$$

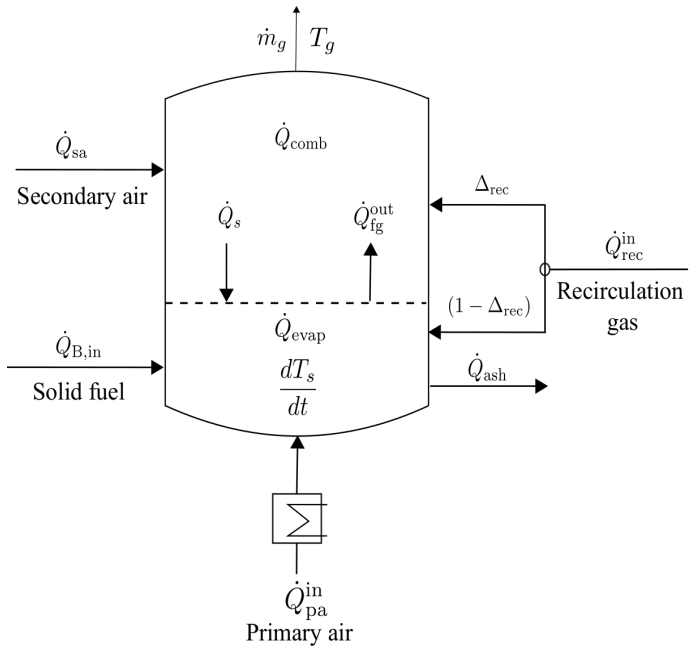

Figure 4.3: Energy flows entering and leaving the CSTR.

The specific heat capacity of wood $\bar{c}_{p,wood}$ [J/(kg.K)] at a given temperature T [K] is evaluated according to [Dunlap, 1912]:

$$c_{p,wood}(T) = 4186.8\,[0.266 + 0.00116 \cdot T] \tag{4.11}$$

The energy streams entering and leaving the solid bed on the left-hand side of Eq. (4.9), can be individually given as follows:

$$\dot{Q}_B^{\text{in}} = \bar{c}_{p,s}\,\dot{m}_{B,in}\,(T_0 - T_s) \tag{4.12}$$
$$\dot{Q}_{\text{pa}}^{\text{in}} = \bar{c}_{p,air}\,\dot{m}_{pa}\,(T_s - T_{\text{pa}}) \tag{4.13}$$
$$\dot{Q}_{\text{rec}}^{\text{in}} = \Delta'_{\text{rec}}\,\dot{m}_{\text{rec}}\,c_{p,\text{fg}}(T_s - T_{\text{rec}}^{\text{in}}) \tag{4.14}$$
$$\dot{Q}_{\text{ash}}^{\text{out}} = \dot{m}_{\text{ash}} c_{p,\text{ash}}(T_{\text{ash}} - T_0) \tag{4.15}$$
$$\dot{Q}_{\text{pa}}^{\text{out}} = \dot{m}_{\text{pa}} c_{p,\text{fg}}(T_g - T_{\text{pa}}^{\text{out}}) \tag{4.16}$$
$$\dot{Q}_{\text{rec}}^{\text{out}} = \Delta'_{\text{rec}} \dot{m}_{\text{rec}} c_{p,\text{fg}}(T_g - T_{\text{rec}}^{\text{out}}) \tag{4.17}$$
$$\dot{Q}_{\text{fg}}^{\text{out}} = \dot{m}_{\text{fg}} c_{p,\text{fg}}(T_g - T_{\text{fg}}^{\text{out}}) \tag{4.18}$$

The gas temperature T_g [K] can be drawn from a total energy balance in the gas phase and by defining the energy streams in and out the control volume within the corresponding compartment.

Similar to [Stadler et al., 2011], the main assumption here is that the energy input of the fuels occurs into the gas state only. Therefore, the equation that describes the gas temperature state is straight forward and can be given by:

$$\bar{c}_{p,g}\,m_g\,\frac{dT_g(t)}{dt} = \dot{Q}_{\text{sa}}^{\text{in}} + \dot{Q}_{\text{fg}}^{\text{out}} + \Delta_{\text{rec}}\dot{Q}_{\text{rec}}^{\text{in}} + \dot{Q}_{\text{comb}} - \dot{Q}_s - \dot{Q}_g^{\text{out}} \tag{4.19}$$

Here, the first term on the left-hand side in Eq. (4.19) denotes the energy flow of the secondary air that is given by Eq. (4.20):

$$\dot{Q}_{\text{sa}}^{\text{in}} = \bar{c}_{p,air}\,\dot{m}_{\text{sa}}\,(T_s - T_{\text{sa}}) \tag{4.20}$$

The rate of the total heat generated from the latent chemical bond energy in the bio-fuel by combustion $\dot{Q}_{comb}$ [W] is calculated as follows [Baukal Jr, 2003]:

$$\dot{Q}_{comb} = \dot{m}_{\text{thd}} \cdot (-\Delta h_R) \tag{4.21}$$

with

$$-\Delta h_R = H_L(T_0) \tag{4.22}$$

Here, $\Delta h_{\text{R}}\ (T_0) < 0$ [J/kg] denotes the enthalpy of reaction that is equal to the lower calorific value of the biomass fuel $H_L(T_0)$, and which will be further estimated in Chapter 5.

Finally, the energy flow that goes to the boiler section for a heat exchange with the boiler's tube for steam production reads:

$$\dot{Q}_g^{\text{out}} = \bar{c}_{p,g}\dot{m}_g(T_g - T_{g,out}) \tag{4.23}$$

Where, $T_{g,out}$ [K] is the temperature at the boiler exit, and $\bar{c}_{p,g}$ [J/(kg.K)] is the specific heat capacity of the gas mixture.

Gas specific heat capacity

In order to calculate the specific heat capacity of the gas mixture, the combustion products are assumed to be composed solely of the following gaseous species O_2, N_2, CO_2, and H_2O. Therefore, a complete combustion of the biomass fuel is assumed, and the computation proceeds quite similar to the one done in Subsection 5.2.2, where the amounts of the individual gaseous species in the flue gas can be given by [Langeheinecke et al., 1993]:

$$n_{\text{O}_2}^{\text{fg}} = (\lambda - 1) \cdot n_{\text{O}_2}^{+} \tag{4.24a}$$

$$n_{\text{N}_2}^{\text{fg}} = \frac{0.79}{0.21} \cdot \lambda \cdot n_{\text{O}_2}^{+} \tag{4.24b}$$

$$n_{\text{CO}_2}^{\text{fg}} = \left(\frac{\gamma_{\text{C}}(1-\gamma_{\text{w}})}{M_C}\right) m_B \tag{4.24c}$$

$$n_{\text{H}_2\text{O}}^{\text{fg}} = \left(\frac{\gamma_{\text{w}}}{M_{\text{H}_2\text{O}}} + \frac{\gamma_{\text{H}}(1-\gamma_{\text{w}})}{2M_{\text{H}}}\right) m_B \tag{4.24d}$$

With M_C, M_H, M_{H_2O} are the molar masses [kg/mol] and m_B the fuel mass [kg]. The total number of moles of the gas mixture n_{fg} [mol] is:

$$n_{\text{fg}} = n_{\text{O}_2}^{\text{fg}} + n_{\text{N}_2}^{\text{fg}} + n_{\text{CO}_2}^{\text{fg}} + n_{\text{H}_2\text{O}}^{\text{fg}} \tag{4.25}$$

Since the composition of a gas mixture is usually expressed in mol fraction of species i, where $\text{i} = \text{O}_2, \text{N}_2, \text{CO}_2, \text{H}_2\text{O}$, then:

$$x_i = \frac{n_{\text{i}}^{\text{fg}}}{n_{\text{fg}}} \tag{4.26}$$

The specific heat capacity of gas mixture $\bar{c}_{p,g}$ [J/(kg.k)] can be given as follows:

$$\bar{c}_{p,g} = \sum_i c_{p,gi} \cdot x_i \tag{4.27}$$

and

$$\frac{c_{p,gi}}{c_{p0}} = \left(\frac{T}{T_0}\right)^{\mathrm{n_{cp}}} \tag{4.28}$$

with the specific heat capacity for the different gaseous species c_{p0} and the exponent $\mathrm{n_{cp}}$ are evaluated according to Table. 4.1.

Table 4.1: The specific heat capacities of the different gaseous species with the corresponding exponent parameters [Specht, 1993].

Gas	c_{p0} (kJ/kg K)	$\mathrm{n_{cp}}$ (−)
O_2	0.90	0.15
N_2	1	0.11
CO_2	0.84	0.30
H_2O	1.75	0.20

Oxygen concentration

Similar to the solid phase, the oxygen concentration in the furnace can be obtained from a component material balance over the gas phase control boundary. Consequently, the general form of the material balance of a given component inside the reactor is given by [Emig and Klemm, 2006]:

$$\frac{\partial c_i}{\partial t} = -\mathrm{div}(c_i \vec{\mathbf{w}}) + \mathrm{div}(\mathrm{D_{eff}}\ \mathrm{grad}\ c_i) + \sum r_i \tag{4.29}$$

Where, $\vec{\mathbf{w}}$ is the speed vector of the turbulent flow, and $\mathrm{D_{eff}}$ refer to as the effective diffusion (mixing) coefficient that depends on the kind of turbulence and flow as well as the direction of concentration gradients. As a simplifying assumption, the gas phase is regarded again as a perfectly mixed tank reactor (CSTR) with a constant reactor volume. Therefore, the second term on the right hand side of Eq. (4.29), which includes the diffusion coefficient, can be omitted.

If one integrates over the control volume of the gas phase reactor (see Figure 4.4), then:

$$-\int_{V_R} \mathrm{div}(c_i \vec{\mathbf{w}}) = c_i^{in} V_R - c_i^{out} V_R = \dot{n}_i^{in} - \dot{n}_i^{out} \tag{4.30}$$

By taking into account Eq. (4.30) and the aforementioned assumptions, and by integrating the general equation that describes the mole balance of a oxygen substance over the reactor volume, the latter can be reformulated as follows:

$$V_R \cdot \frac{dc_{\mathrm{O_2}}}{dt} = \dot{n}_{\mathrm{O_2}}^{\mathrm{in}} - \dot{n}_{\mathrm{O_2}}^{\mathrm{out}} - r_{\mathrm{O_2}}^{\nu_{\mathrm{O_2}}} \tag{4.31}$$

According to the control volume shown in Figure 4.4, the oxygen molar flow rates entering and leaving the control volume boundary are:

$$V_R \cdot \frac{dc_{\mathrm{O_2}}}{dt} = \dot{n}_{\mathrm{O_2}}^{\mathrm{pa}} + \dot{n}_{\mathrm{O_2}}^{\mathrm{sa}} + \dot{n}_{\mathrm{O_2}}^{\mathrm{rec}} - \dot{n}_{\mathrm{O_2}}^{\mathrm{fg}} - r_{\mathrm{O_2}}^{\nu_{\mathrm{O_2}}} \tag{4.32}$$

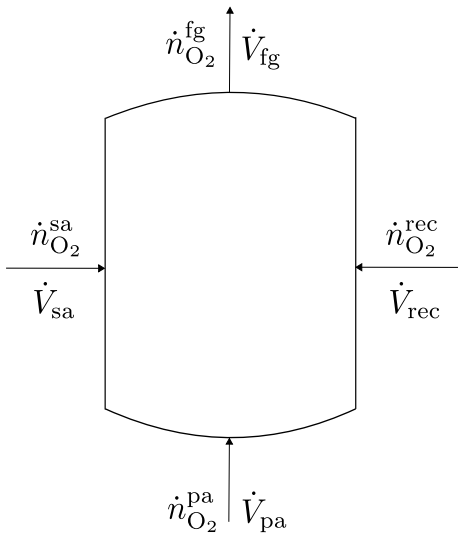

Figure 4.4: Oxygen mole balance inside the combustion furnace.

With the concentration is related to the molar flow rate via the following equation:

$$\dot{n}_i = c_i \cdot V_i \tag{4.33}$$

By substituting Eq. (4.33) into Eq. (4.32), and by taking the assumption that there is no accumulation due to the gas phase fast dynamics Eq. (4.32) can be written as follows [Wolf, 2005]:

$$V_R \cdot \frac{dc_{O_2}}{dt} = 0 = c_{O_2}^{pa}\,\dot{V}_{pa} + c_{O_2}^{sa}\,\dot{V}_{sa} + c_{O_2}^{rec}\,\dot{V}_{rec} - c_{O_2}^{fg}\,\dot{V}_{fg} - r_{O_2}^{\nu_{O_2}} \tag{4.34}$$

The perfect mixing assumption leads to consider that:

$$c_{O_2} = c_{O_2}^{fg} = c_{O_2}^{rec} \tag{4.35}$$

If the mass flow rate is used instead of the volume flow rate, which are both linked by the following equation:

$$\dot{m}_i = \rho_i\,\dot{V}_i \tag{4.36}$$

Then, the oxygen concentration in the flue gas at the exit c_{O_2} [mol/m^3] can be given under its final form:

$$c_{O_2} = \frac{\rho_{fg}}{\dot{m}_{fg}}\left[c_{O_2}^{pa}\left(\frac{\dot{m}_{pa} + \dot{m}_{sa}}{\rho_{pa}}\right) - r_{O_2}^{\nu_{O_2}}\right] \tag{4.37}$$

where ρ_{fg} is the flue gas density [kg/m^3] and $r_{O_2}^{\nu_{O_2}}$ is the consumption rate of oxygen [mol/s].

Density of the gas mixture

The gas mixture can be well approximated by an ideal gas for a gas at a relatively low pressure. Here, the mol fraction of the individual gas species is evaluated using Eq. (4.26). Therefore, the molar mass of the mixture is given by:

$$M_{mean} = \sum_i x_i \cdot M_i \tag{4.38}$$

By the substitution of Eq. (4.26) into Eq. (4.38), the latter can be reformulated as follows:

$$M_{mean} = \frac{n^{\mathrm{fg}}_{\mathrm{O_2}} M_{\mathrm{O_2}} + n^{\mathrm{fg}}_{\mathrm{N_2}} M_{\mathrm{N_2}} + n^{\mathrm{fg}}_{\mathrm{CO_2}} M_{\mathrm{CO_2}} + n^{\mathrm{fg}}_{\mathrm{H_2O}} M_{\mathrm{H_2O}}}{n_{\mathrm{fg}}} \tag{4.39}$$

with the ideal-gas equation of state, which reads:

$$p_{\mathrm{tot}} V = nRT \tag{4.40}$$

From Eq. (4.38) and Eq. (4.40), the density of the gas mixture can be consequently given as follows:

$$\rho_{\mathrm{fg}} = \frac{p_{\mathrm{tot}} \cdot M_{mean}}{R \cdot T_g} \tag{4.41}$$

Where p_{tot} is the pressure inside the furnace, which can be taken equal to 1 bar, and R [J/(mol.K)] is the universal gas constant.

4.2.2 Burning rate

In literature, the thermal decomposition rate of the dry fraction of the solid fuel is computed according to the oxygen mass transfer from the bulk gas to the fuel surface. Consequently, the overall reaction rate will be only diffusion limited. A typical model for describing the thermal decomposition that is dominated by the rate the oxygen diffuses toward the surface, and therefore, it is only a mass transfer controlled reaction, can be found in [Rovaglio et al., 1998] or [Van Kessel, 2003]. Here, the latter model is being selected and it is given as follows:

$$R_{\mathrm{thd}} = k_d \frac{c^{\mathrm{fg}}_{\mathrm{O_2}} \cdot M_{\mathrm{O_2}}}{\nu_{\mathrm{O_2}}} \tag{4.42}$$

where k_d [m/s] is the mass transfer coefficient and and $\nu_{\mathrm{O_2}}$ [$\mathrm{kg_{O_2}/kg_B}$] is the amount of oxygen consumed during combustion.

Many different possibilities for modeling the mass transfer coefficient k_d [m/s] exists in literature. One possibility is [Borman and Ragland, 1998]:

$$k_d = \frac{D}{d_p} \cdot (2 + 1.1 Sc^{1/3} Re^{0.6}) \tag{4.43}$$

with D in [$\mathrm{m^2/s}$] is the diffusion coefficient of O_2 in N_2 and can be given by [Van Der Lans et al., 2000]:

$$D = 0.207 \cdot 10^4 \left(\frac{T}{100}\right)^{1.75} \tag{4.44}$$

with the Reynolds number Re [-]:

$$Re = \frac{d_p}{\nu_{\mathrm{pa}}} \cdot u_{\mathrm{eff}} \tag{4.45}$$

Where ν_{pa} is the kinematic viscosity of air [$\mathrm{m^2/s}$].

The effective velocity of fluid in bed u_{eff} [m/s] can be given by Eq. (4.46) as a function of the fluid superficial velocity u and bed porosity (void fraction) Ψ [-] as follows [Kind et al., 2005]:

$$u_{\text{eff}} = \frac{u}{\Psi} \tag{4.46}$$

The Schmidt number Sc [-] can be given as follows:

$$Sc = \frac{\nu_{\text{pa}}}{D} \tag{4.47}$$

Finally, the amount of oxygen needed ν_{O_2} to burn 1 kg of biomass can be either fitted to measured data or evaluated according the following global combustion reaction:

$$\text{C}_\text{a}\text{H}_\text{b}\text{O}_\text{c} + (\text{a} + \frac{1}{4}\text{b} - \frac{1}{2}\text{c})\text{O}_2 \xrightarrow{\nu_{O_2}} \text{aCO}_2 + \frac{1}{2}\text{bH}_2\text{O} \tag{4.48}$$

Consequently,

$$\nu_{\text{O}_2} = \text{a} + \frac{1}{4}\text{b} - \frac{1}{2}\text{c} \tag{4.49}$$

with a,b,c are the stoichiometric coefficients that depend on the fuel's chemical composition.

4.2.3 Drying process

As mentioned earlier in Subsection 3.3.1, when the wet porous biofuel is subject to thermal drying two processes will occur in parallel, the transfer of heat to warm up the inner core of the fuel, and the evaporation of the water at the solid surface. Hence, it can be concluded that the evaporation rate will be governed by the rate at which these two processes will proceed.

Since the drying process is strictly coupled to the heat transfer mechanisms occurring in the solid bed on the grate, which will be thoroughly and separately treated in Section 4.3, two modes will influence its course these are: (a) the convective drying due to the fluid motion through the capillary-porous bed, and (b) the radiative drying as a consequence of the acting electromagnetic energy on top of the bed.

When the water in the porous medium is subject to the convective drying, the drying rate will proceed according to three different stages [Asli, 2013]:

1. **Stage I**: the fuel consists initially of much moisture, that the surface is covered with a continuous layer of free water, and the evaporation takes place at the surface with a constant rate. This constant rate is maintained only if there is enough internal moisture transfer to the surface by capillary flow through the void.

2. **Stage II**: if the surface moisture content cannot be maintained above the fiber saturation point (FSP), which is defined as the point where there is no free water in lumens and only bound water in the cell walls exist, then neither the drying rate nor the solid surface temperature remain constant, and the first falling drying rate period starts.

3. **Stage III**: in the second falling rate period there will be no more liquid water, and the drying rate will be only diffusion controlled and decreases until an equilibrium moisture content is reached.

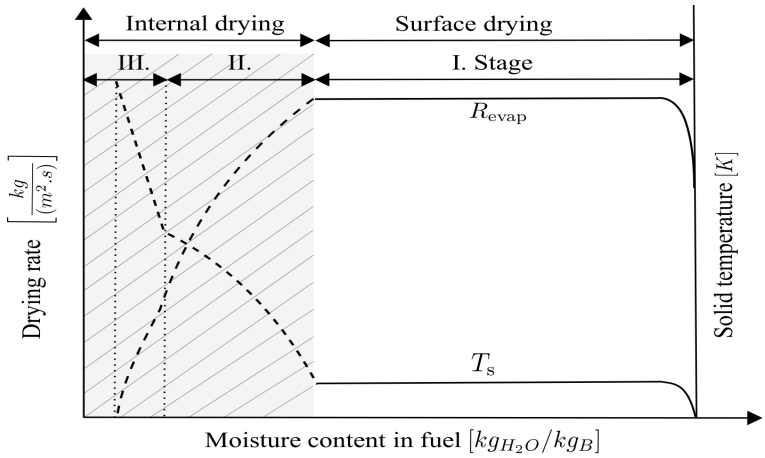

Figure 4.5: The evaporation rate curves for the different stages [Gnielinski et al., 2013].

Since the drying is fundamentally a problem of simultaneous heat and mass transfer, this will result in complex nonlinear differential equations, such as when modeling the fluid flow in the medium [Peishi and Pei, 1989], or the diffusion mass transfer for the last drying stage. To simplify this complexity, the water is assumed to be lying only on the surface of the solid biofuel. Consequently, this will lead to consider only the first drying stage (see Figure 4.5). Such an assumption is adopted in[Krüll, 2001],[Van Kessel et al., 2004b],[Wolf, 2005],[Epple et al., 2009] for the modeling of the drying process in a grate firing unit.

Convective drying rate

According to [Gnielinski et al., 2013], the drying rate for first convective drying stage can be modeled as follows:

$$K_{\text{evap,I}} = \frac{M_{\text{H}_2\text{O}}}{R \cdot T_{\text{s}}} \, \beta \, \text{k}_{s,p} \, (p_{\text{w}}^{sat}(T_{\text{s}}) - p_{\text{w},g}) \, A_p \tag{4.50}$$

With the coefficient $\text{k}_{s,p}$ [-] defined as:

$$\text{k}_{s,p} = \frac{p}{p_{\text{w}}^{sat}(T_{\text{s}}) - p_{\text{w},g}} \ln \left\{ \frac{p - p_{\text{w},g}}{p - p_{\text{w}}^{sat}(T_{\text{s}})} \right\} \tag{4.51}$$

The mass transfer coefficient β [m/s] expressed as:

$$\beta = \frac{Sh \cdot D_{\text{w},g}}{\text{d}_{\text{p}}} \tag{4.52}$$

The diffusion coefficient $D_{\text{w},g}$ [m^2/s] can be given by the following formula [Ouelhazi et al., 1992]:

$$D_{\text{w},g} = 4,52 \cdot 10^{-7}. \left(\frac{T_{\text{s}}}{273} \right)^{1,81} \tag{4.53}$$

The dimensionless Sherwood number in Eq. (4.52) can be given by [Wakao and Kagei, 1982]:

$$\mathrm{Sh} = 2 + 1.1\, Re^{0.6}\, Sc^{1/3} \tag{4.54}$$

Radiative drying rate

Unlike in [Krüll, 2001],[Van Kessel et al., 2004b],[Wolf, 2005], where for the modeling of the drying process only the convective part is considered. Here, the drying rate in Eq. (4.56) will be extended to include also the radiative part. Therefore, the overall drying rate of the wet solid fuel in the furnace can be described as the sum of the convective and the radiative drying rates as follows:

$$K_{\mathrm{evap}} = K_{\mathrm{evap,I}} + K_{\mathrm{evap,II}} \tag{4.55}$$

where the drying rate $K_{\mathrm{evap,II}}$ [kg/s], due to the radiation, can be written as:

$$K_{\mathrm{evap,II}} = \frac{\dot{Q}_{\mathrm{s}}}{\Delta h_v^{\mathrm{w}}} \tag{4.56}$$

Here, Δh_v^{w} is the latent heat of vaporization in [J/kg] (see Subsection 2.1.3), and $\dot{Q}_{\mathrm{s}}$ [W] is the radiation heat flow to the solid bed, which will be separately treated in Subsection 4.3.1.

4.2.4 Residence time

The fed solid biofuel goes through the combustion chamber for a certain period of time called residence or retention time. Thus, it can be defined as the average time the solid biomass spends in the furnace for its complete thermal degradation. As a consequence, the residence time will have a direct impact on the conversion behavior of the solid fuel in the reactor. If this time is too short, there will be a risk of not completing the thermo-chemical conversion phases, the biofuel undergoes on the moving bed. As a matter of fact, a considerable amount of combustible will exit the furnace without being exploited, which will represent a loss.

Therefore, an adequate description of the residence time, as an influencing parameter on the course of combustion, plays a critical role in the mathematical modeling of conversion of the biomass fuel in the reactor. In a grate-firing unit this time will depend on the constructive parameters that define the grate geometry [Scholz et al., 2001], these parameters are, for example, the length and the inclination angle of the grate. In order to simplify the illustration, the solid fuel is assumed to move horizontally with a grate speed v_G [m/s], in reality the grate is inclined by an angle δ [°deg], and the effective distance a biomass particles travels along the grate is denoted by L_{eff} [m] (c.f Figure 4.6).

The solid holdup and volume according to Figure 4.6 are defined as:

$$m_b(t) = V_b(t) \cdot \rho_B \tag{4.57}$$

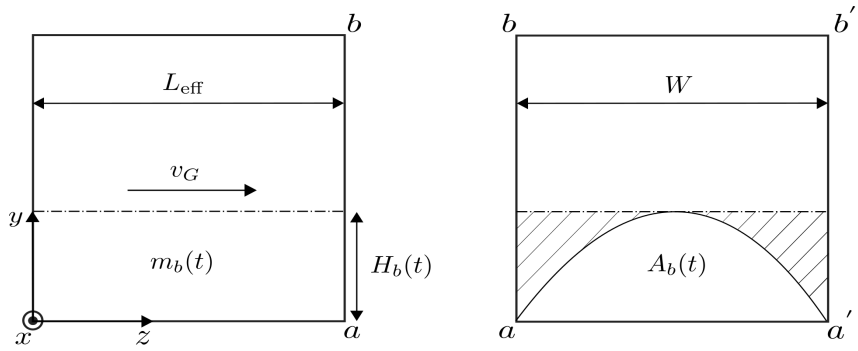

Figure 4.6: Residence time of the grate firing unit. v_G is the grate speed [m/s], L_{eff} is the effective distance traveled by a biomass particle in [m], $H_b(t)$ is the bed height [m], W the furnace width [m], ρ_B the solid fuel density [kg/m^3], and $A_b(t)$ is the cross-sectional area [m^2] [Belkhir et al., 2015b].

and

$$V_b(t) = A_b(t) \cdot L_{\text{eff}} \tag{4.58}$$

with the bed cross section $A_b(t)$ is given as follows:

$$A_b(t) = H_b(t) \cdot W \tag{4.59}$$

Substituting Eq. (4.58) in Eq. (4.57), and by taking also Eq. (4.59) into account, Eq. (4.57) can be reformulated as follows:

$$m_b(t) = H_b(t) \cdot W \cdot L_{\text{eff}} \cdot \rho_B \tag{4.60}$$

The output mass flow $\dot{m}_{out}$ [kg/s] that falls into the ash-pit can be estimated by Eq. (4.61):

$$\dot{m}_{out}(t) = A_b(t) \cdot v_G \cdot \rho_B \tag{4.61}$$

inserting Eq. (4.59) into Eq. (4.61), Eq. (4.61) reads:

$$\dot{m}_{out}(t) = W \cdot H_b(t) \cdot v_G \cdot \rho_B \tag{4.62}$$

The bed height can be as well estimated as follows:

$$H_b(t) = \frac{\dot{m}_{out}(t)}{W \cdot v_G \cdot \rho_B} \tag{4.63}$$

The substitution of Eq. (4.63) into Eq. (4.60) leads to:

$$\dot{m}_{out}(t) = \frac{m_b(t)}{\tau} \tag{4.64}$$

With the residence time of the reactor τ [s] is given by:

$$\tau = \frac{L_{\text{eff}}}{v_G} \tag{4.65}$$

It turns out to be that the residence time of the reactor is the inverse of grate speed multiplied by the effective length, this length is defined as the distance traveled by a biomass particle along the grate, and it depends strongly on the grate geometry being used (see Table 4.2).

Table 4.2: Dependency of the effective length on the grate geometry for the different grate types [Wolf and Koralewska, 2005].

Grate type	Schematic diagram	Trigonometric diagram	Effective length
Forward acting	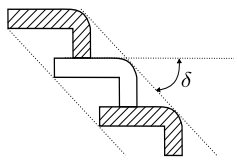	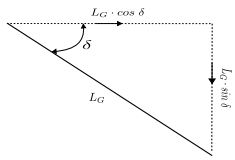	$L_{\text{eff}} = L_G(\cos\delta + \sin\delta)$ (4.66)
Reverse acting	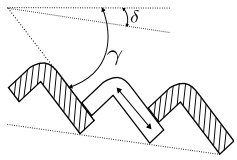	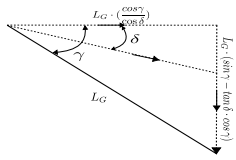	$L_{\text{eff}} = L_G(1 + \frac{\cos\gamma}{\sin\delta})$ (4.67)
Roller grate	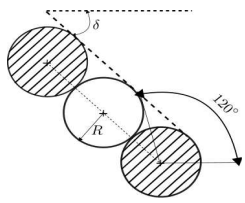	-	$L_{\text{eff}} = 2 \cdot \pi \cdot n_G \; r \cdot \frac{120}{360}$ (4.68)

4.3 Heat transfer mechanisms

A key cornerstone in any industrial combustion process for power generation is the heat transfer mechanisms that occur within the furnace enclosure, which have basically a twofold function to perform, the first and the obvious one is to transfer thermal energy from hot combustion gases to a product or a load, such as the boiler's water tubes for steam production, the second one is to serve as a catalyst for thermal degradation and drying of biomass solid fuel on the moving grate.

Whenever there is a temperature difference within a system, heat transfer must occur between the interacting bodies forming the system. Therefore, the field of heat transfer is the science concerned with the governing rules that describe the transfer of heat between these bodies within a given system [Von Böckh and Wetzel, 2011]. In this context, three modes of heat transfer mechanisms can be distinguished, these are: radiation, convection, and conduction. Whereas conduction can be considered of less importance, especially when describing heat transfer in solid bed, due to the slow propagation speed of the reaction front, the most dominating mode is the radiative heat transfer and to less extent the convective one in an industrial furnace.

In this section, the modeling part of both the radiative heat transfer in the combustion chamber, as well as the convective one between the solid biofuel on the moving grate and the fluid which is the combustion air, is carried out. Here, a balance is made between the level of complexity and the required accuracy in describing the complex heat transfer interaction inside the reactor, by imposing some assumptions and simplifications, as it will subsequently be seen in Subsections 4.3.1 and 4.3.2.

4.3.1 Radiative heat transfer in furnace

In high-temperature applications such as in pyrometallurgy, cement kilns as well as in large-scale combustion furnaces for power generation, the thermal radiation is considered to be the most relevant heat transfer mechanism over the other two possible modes, i.e. conduction and convection, for transferring energy to the load or the burning layer of solid biomass on the moving grate [Viskanta and Mengüç, 1987]. Therefore, thermal radiation can directly or indirectly be considered as a key controlling factor for determining the product quality or in achieving a high conversion efficiency in any industrial furnace which operates at elevated temperature [Jenkins and Mullinger, 2011]. This explains the reason why many commercially available furnaces are offered with different shapes and geometries, since during the development and design phase an emphasis is put on maximizing the radiation heat transfer to the load [Niessen, 2010].

Unlike the conduction and convection heat transfer mechanisms, which both occur whenever there exists a temperature gradient in a medium or between media, and hence, can be considered as a "short-range" phenomena for energy transfer, thermal radiation requires no medium for transferring energy. Rather, the energy will be transferred, and in contrast to convection and conduction over a long distance, by electromagnetic waves, or photons, which are characterized by their wavelength and frequency.

In reality, these propagating electromagnetic waves emanate from the stored internal energy of a warmer body and it will be intercepted and absorbed by the cooler solid surface or gas body, and reconverted again into an internal energy by the absorbing matter, while the rest will be scattered from or transmitted through the body. The strength and wavelength of emission will depend strongly on the temperature of the emitting material [Bergman et al., 2011]. The spectrum these electromagnetic waves scan can be illustrated in Figure 4.7.

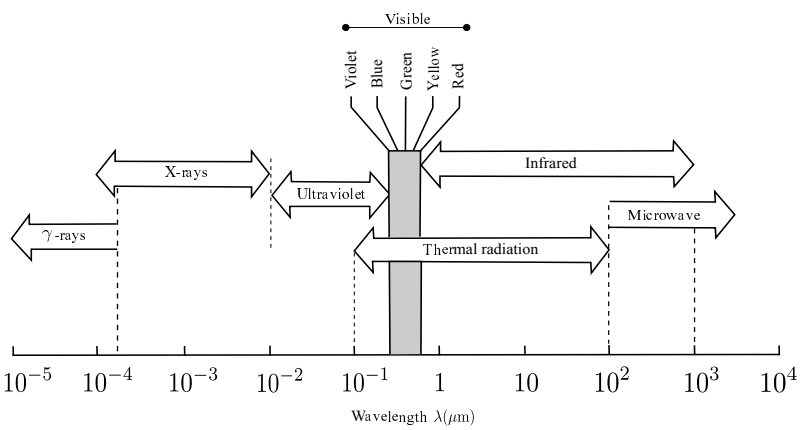

Figure 4.7: Electromagnetic waves spectrum [Baukal Jr, 2012].

The mathematical modeling of the thermal radiation in combustion furnaces is very complex and it is not a trivial task, since, on the one hand, thermal radiation involves complex interaction between different surfaces of different shapes and geometries forming the furnace enclosure, on the other hand, the combustion of solid

fuel on the grate will yield a mixture of diatomic and triatomic gaseous species. Whereas, diatomic molecules such as: O_2, N_2, and H_2 are essentially transparent to incident thermal radiation, i.e., they neither absorb nor emit radiation, the triatomic molecules such as CO_2, H_2O, and to less extent CO and hydrocarbon gases, absorb and emit radiation at specific bands [Bergman et al., 2011]. At other wavelength intervals, no emission or absorption are observed, which further complicates the computation of the radiative properties of the gas mixture.

In literature, different mathematical radiation models have been reported, each of which with different levels of complexity and details. The modeling approaches vary from zero-dimensional up to three-dimensional for a CFD simulation. These radiation models can be further classified into two categories: (a) zone models and (b) flux models and depending on the modeler intent one of these models can be selected for solving the problem at hand [Viskanta and Mengüç, 1987].

Stirred tank radiation model

Generally speaking, in gas filled enclosure, such as in the case of industrial furnaces and combustion chambers, it is evident that a complex heat transfer via radiation will occur between three different interacting main parts, these are: the flue gas suspension, the surrounding walls and finally the thermal load (heat sink).

Despite the fact that such interaction is extremely complex to be described mathematically, as the radiative properties of combustion products and gas temperature vary locally within the enclosure, yet, [Jeschar et al., 1990] developed a simplified stirred tank radiation model (also referred to as 3-exchange model) for computing the effective heat exchange between the gas suspension and the solid bed, which includes also the secondary radiation from the surrounding walls (see Figure 4.8). Such simplification is attributed to the following assumptions [Viskanta and Mengüç, 1987]:

- The refractory wall as well as the load both have a uniform temperature T_w [K] and T_s [K] respectively.
- The gas phase is well mixed with temperature T_g and has an emissivity ϵ_g [-].
- Combustion products are assumed to be gray [2].

Inside the combustion furnace, the transferred heat flow between gas and fuel bed can be described according to Stefan-Boltzmann law as follows [Jeschar et al., 1990]:

$$\dot{Q}_{gs} = \epsilon_{gs} \cdot \sigma \cdot A_s \cdot (T_g^4 - T_s^4) \tag{4.69}$$

Similarly, the radiation exchange flow between gas and furnace refractory wall is given by:

$$\dot{Q}_{gw} = \epsilon_{gw} \cdot \sigma \cdot A_w \cdot (T_g^4 - T_w^4) \tag{4.70}$$

[2] A gas having an absorption coefficient that is independent of wavelength is called a gray gas [Siegel and Howell, 1971].

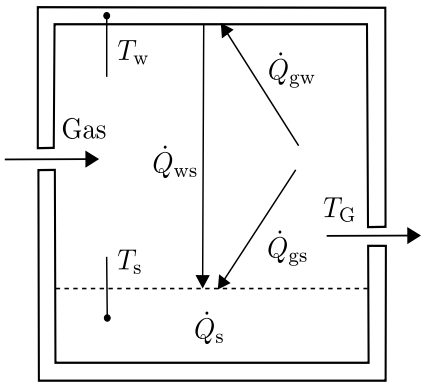

Figure 4.8: Stirred tank radiation model between: (a) gas-wall $\dot{Q}_{gw}$, (b) gas-solid $\dot{Q}_{gs}$, and (c) wall-solid $\dot{Q}_{ws}$ according to [Jeschar et al., 1990].

Finally, the radiation heat flow between furnace refractory wall and the biomass solid bed is described by:

$$\dot{Q}_{ws} = \epsilon_{ws} \cdot \sigma \cdot A_s \cdot (T_w^4 - T_s^4) \tag{4.71}$$

The total transferred heat flow to the solid bed will be the sum of the radiative heat from gas and wall as can be deduced from Figure 4.8:

$$\dot{Q}_s = \dot{Q}_{ws} + \dot{Q}_{gs} \tag{4.72}$$

According to [Jeschar et al., 1990], if an adiabatic furnace is assumed, then:

$$\dot{Q}_{ws} = \dot{Q}_{gw} \tag{4.73}$$

By substituting Eq. (4.70) into Eq. (4.71), the wall temperature T_w can be eliminated. Consequently, it follows:

$$\dot{Q}_{ws} = \frac{1}{\dfrac{1}{\epsilon_{ws}} + \dfrac{A_s}{A_w} \cdot \dfrac{1}{\epsilon_{gw}}} \cdot \sigma \cdot A_\mathrm{s} \cdot (T_\mathrm{g}^4 - T_\mathrm{s}^4) \tag{4.74}$$

Substituting Eq. (4.74) in Eq. (4.72), and by considering also Eq. (4.69), the total radiation heat flow to the solid bed can be rewritten as follows:

$$\dot{Q}_s = \epsilon_\mathrm{eff} \cdot \sigma \cdot A_w \cdot (T_g^4 - T_s^4) \tag{4.75}$$

With the effective emissivity ϵ_eff is given by:

$$\epsilon_\mathrm{eff} = \epsilon_{gs} + \frac{1}{\dfrac{1}{\epsilon_{ws}} + \dfrac{A_s}{A_w} \cdot \dfrac{1}{\epsilon_{gw}}} \tag{4.76}$$

In order to compute the effective emissivity given by the previous equation, the emissivity factors ϵ_{gs}, ϵ_{gw} and ϵ_{ws} are needed, which can be evaluated as follows [Schupe and Jeschar, 1975]:

$$\epsilon_{gs} = \frac{\epsilon_g \cdot \alpha_s \cdot [1 + \phi_s \cdot (1 - \epsilon_g) \cdot (1 - \alpha_w)]}{1 - U} \tag{4.77}$$

$$\epsilon_{gw} = \frac{\epsilon_g \cdot \alpha_w \cdot [1 + \phi_s \cdot (1 - \epsilon_g) \cdot (1 - \alpha_s)]}{1 - U} \tag{4.78}$$

and

$$\epsilon_{ws} = \frac{\epsilon_w \cdot \alpha_s \cdot (1 - \epsilon_g)}{1 - U} \cdot \varphi_{sw} \tag{4.79}$$

Finally,

$$U = (1 - \epsilon_g) \cdot (1 - \alpha_w) \cdot [\phi_s \cdot (1 - \epsilon_g) \cdot (1 - \epsilon_s) + (1 - \phi_s)] \tag{4.80}$$

with

ϵ_{gs}	emissivity coefficient between gas and solid [-].
ϵ_{ws}	emissivity coefficient between wall and solid [-].
ϵ_{gw}	emissivity coefficient between gas and wall [-].
σ	Stefan-Boltzmann constant [W/(m^2.K^4)].
A_s	Solid bed surface [m^2].
A_w	wall surface [m^2].
α_s, α_w	Solid und wall absorption coefficients [-].

Here, the parameter denoted by ϕ_s, that defines the ratio between the furnace wall A_w surface and the solid bed A_s surface, has a value range between $0 \leq \phi_s \leq 1$, and can be given by Eq. (4.81):

$$\phi_s = \varphi_{sw} \cdot \frac{A_s}{A_w} \tag{4.81}$$

Weighted Sum of Gray Gases Model (WSGGM)

For diatomic gases the dependency on the wavelength is fairly smooth, whereas for grate furnaces burning biomass fuels, the combustion products are likely being composed of vapor water and carbon dioxide. These constituents show different emission and absorption characteristics at different spectra, due to the different energy level transitions within the molecules, a fact which leads to a less continuous spectrum compared to the former case [Siegel and Howell, 1971]. Consequently, the emission as well as absorption of thermal radiation by the gas mixture, referred to as non-gray gas [3], will be limited only within a specific narrow wavelength intervals called bands.

Despite the spectral complication non-gray gases exhibit, methods were developed for computing the radiant heat flux from gas to the contiguous surface [Bergman et al., 2011], and further requiring the evaluation of the total emissivity and absorptivity of the combustion flue gases. While, the total emissivity can be evaluated analytically using wide band models [Modest, 2013], [Hottel and Sarofim, 1970] and [Leckner, 1972] gave a simple procedure for determining approximately these two parameters. This requires, in a first step, the separate evaluation of both carbon dioxide and water vapor emissivities that can be obtained from experimentally compiled charts, then both the total emissivity and absorption of the flue gas suspension are computed based on the correlating available data [Stephan et al., 2010], which are related also to the gas temperature, the mean beam length (path length), partial

[3] In contrast to a gray gas, the absorption coefficients have a strong variations with wavelength and often varies substantially with temperature and pressure [Siegel and Howell, 1971].

pressure of the major radiating components (CO_2, H_2O), and total pressure in the furnace [Hottel, 1954],[Bejan and Kraus, 2003].

The weighted-sum-of-the-gray gases model has been proposed in [Hottel and Sarofim, 1970], within the context of zonal method, as an alternative to the previously discussed method for determining the total emissivity in a non-gray gas mixture due to its computer-based simple implementation and reasonable accuracy. As the name already indicates, the WSGG method based upon the postulate that a non-gray gas can be presented by a small number of gray ones with constant absorption coefficients [Modest, 1991].

According to this WSGG model, the total gas emissivity ϵ_g [-], and for a total pressure in the furnace of 1 bar, is evaluated from the following expression [Stephan et al., 2010]:

$$\epsilon_g = \sum_{i=1}^{3} a_i(T_g) \left[1 - e^{(-k_i(p_{\mathrm{H_2O}}+p_{\mathrm{CO_2}})s_{eq})}\right] \tag{4.82}$$

With the emissivity weighting factors for the i-th gray gas in Eq. (4.82) expressed as:

$$a_i(T_g) = b_{1i} + b_{2i}\frac{T_g}{1000\ \mathrm{K}} \tag{4.83}$$

and

$$\sum_{i=1}^{3} a_i(T_g) = 1 \tag{4.84}$$

where the value of the coefficients b_{1i}, b_{2i}, as wells as k_i, which denotes the absorption coefficient of the i-th gray gas, are presented in Table 4.3.

Table 4.3: Coefficients for gas emissivity computation according to Eq. (4.82) for a total pressure in the furnace $p_g = 1$bar [Stephan et al., 2010].

i	$b_{1i}(-)$	$b_{2i}(1/\mathrm{K})$	k_{Gi} (1/(mbar))
1	0.130	0.265	0
2	0.595	-0.15	0.824
3	0.275	-0.115	25.91

The partial pressures of water and carbon dioxide are similar to the approach done for computing the composition of gas mixture in Section 4.2.1. Therefore, the partial pressure of these species in the mixture can be found from the corresponding mole fraction as follows [McAllister et al., 2011]:

$$p_{\mathrm{H_2O}} = x_{\mathrm{H_2O}} \cdot p_{\mathrm{tot}} \tag{4.85}$$

and

$$p_{\mathrm{CO_2}} = x_{\mathrm{CO_2}} \cdot p_{\mathrm{tot}} \tag{4.86}$$

The mean beam length s_{eq} [m], defined as the directional average of the thickness of the medium (gas) as seen from the point on the surface wall [Bejan and Kraus,

2003], is a function of the furnace geometry, and can be considered as a characteristic size of the furnace. The mean beam lengths for known geometries have already been tabulated in [Modest, 2013], and for geometries not listed the following formula can serve as a good approximation for its value [Von Böckh and Wetzel, 2011].

$$s_{eq} = 3.6\,\frac{V_g}{A_w} \tag{4.87}$$

where V_g [m^3] is the gas volume under consideration and A_w [m^2] is the wall area around the gas body.

4.3.2 Convective heat transfer in bed

Another important heat transfer mechanism, which takes place inside the combustion furnace, is the convection due to fluid movement traversing the solid fuel layer on the moving grate. At a macroscopic level, this thermal transport mode occurs as a consequence of the molecular conduction at the solid surface and the fluid motion past the solid boundary layer when the two are at temperature difference [Jenkins and Mullinger, 2011]. Hence, the convection heat transfer will be sustained both by the random molecular motion and the bulk motion of the fluid at the solid boundary layer. The fluid temperature can be either at higher or lower temperature than the solid [Bergman et al., 2011].

As a consequence, the convective heat transfer will be governed by Newton's law of cooling or heating, i.e., if the solid surface is hotter than the fluid passing it, then heat will be convected away from the surface by the fluid, a second alternative if the fluid is hotter than the solid surface then heat will be convected into the surface by the fluid [Baukal Jr, 2012].

In grate fired unit, the fluid will be the preheated atmospheric air, as well as the recirculated flue gas fed to the furnace from beneath the moving mechanical part of the grate. Since the fuel bed is usually divided into two parts: an active burning layer at the top, and fresh inactive fuel layer at the bottom, the convective heat transfer interaction between the wet biomass particles and the fluid allows for the drying of the wet fuel in this part, which further explains the importance of the convective heat transfer and the reason why the primary air is preheated before being injected into the furnace to help accelerate the drying process of the wet solid fuel in the inactive fuel layer part prior to ignition [Petchers, 2003].

In all textbooks covering heat transfer fundamentals and applications, the convection process falls in one of the three heat transfer regimes, namely, the pure forced convection regime, mixed convection regime and pure natural (free) convection regime [Nakayama and Shenoy, 1993]. In natural convection, the fluid motion is associated with the density difference caused by the temperature change in the fluid. In other words, the fluid motion is attributed to the buoyancy forces, and thus, the heat transfer itself induces the flows which carry away the energy at the contact point between the fluid and the surface.

In contrast to the natural convection, the forced convection regime, which is considered to be one of the most important convective modes in industrial combustion

systems, the fluid motion is a result of an external influence such as a fan, a blower, or a pump [Bejan and Kraus, 2003]. Therefore, the fluid is forcefully directed at or through a solid medium giving rise to a turbulent fluid flow. In the mixed convection regime, as the name already indicates, both forced and free convection regimes are present. Here, if one mode is more dominant than the other, then a simplification can be made by ignoring the weaker one [Baukal Jr, 2012].

Since in almost all heat recovery plants, a primary air blower is used to provide air to the combustion grate in the combustion chamber, the governing heat transport mode in the fuel bed will be the forced one, and therefore, in the modeling part of heat transfer between air and solid in bed, the natural convection regime is not taken into account and only the former one will be considered, the same is assumed by [Krüll, 2001] for describing the heat transfer between fluid and particle when developing a continuum mathematical model for the grate-firing unit.

The convective heat transfer between particles and fluid passing the packed bed can be given by [Stephan et al., 2010]:

$$\dot{Q}_{\mathrm{conv}} = \kappa \cdot \mathrm{A_p} \cdot \Delta T_{\mathrm{LM}} \tag{4.88}$$

with the mean logarithmic temperature difference is defined as:

$$\Delta T_{\mathrm{LM}} = \frac{(T_{\mathrm{s}} - T_{\mathrm{pa}}^{\mathrm{in}}) - (T_{\mathrm{s}} - T_{\mathrm{pa}}^{\mathrm{out}})}{\ln \dfrac{T_{\mathrm{s}} - T_{\mathrm{pa}}^{\mathrm{in}}}{T_{\mathrm{s}} - T_{\mathrm{pa}}^{\mathrm{out}}}} \tag{4.89}$$

The heat transfer coefficient (κ) [W/(m^2.K)] in Eq. (4.88) can be expressed using dimensionless relationships. Therefore, the heat transfer coefficient can be given as a function of the dimensionless Nusselt number Nu [-], the air thermal conductivity λ_{pa} [W/(m.K)], the particle diameter (d_p) [m] and the fluid properties (air) as follows [Bauer et al., 2010]:

$$\kappa = \frac{Nu \cdot \lambda_{\mathrm{pa}}}{d_p} \tag{4.90}$$

According to the semi-empirical method proposed by [Gnielinski, 1975], the Nusselt number for a flow around a single sphere and a form factor $f(\Psi)$. Thus,

$$Nu = f(\Psi) \cdot Nu_{\mathrm{sp}} \tag{4.91}$$

and

$$Nu_{\mathrm{sp}} = 2 + (Nu_{\mathrm{l}}^2 + Nu_{\mathrm{t}}^2)^{1/2} \tag{4.92}$$

For laminar and turbulent heat transfer, the Nusselt numbers for both regimes can be expressed as:

$$Nu_{\mathrm{l}} = 0.664 \cdot Pr^{1/3} \cdot Re^{1/2} \tag{4.93a}$$

$$Nu_{\mathrm{t}} = \frac{0.037 \cdot Re^{0.8} Pr}{1 + 2.443 \cdot Re^{-0.1} \cdot (Pr^{2/3} - 1)} \tag{4.93b}$$

and the Prandtl number Pr [-]:

$$Pr = \frac{\nu_{\text{pa}}}{\zeta} \tag{4.94}$$

Where ν_{pa} [m^2/s] is the kinematic viscosity of fluid and ζ [m^2/s] denotes the thermal diffusivity.

The empirical arrangement factor $f(\Psi)$ for a void fractions in the range of $0.26 < \Psi < 0.935$ can be calculated as follows:

$$f(\Psi) = 1 + 1.5 \cdot (1 - \Psi) \tag{4.95}$$

The void fraction Ψ [-], which is the statistical quantity of randomly packed bed, is defined as [Achenbach, 1995]:

$$\Psi = 1 - \frac{V_s}{V_{\text{tot}}} \tag{4.96}$$

Here, V_{s} [m^3] is the volume of the solid particles and V_{t} [m^3] the total volume. For a porous bed with spherical particles of uniform diameter (see Figure 4.9).

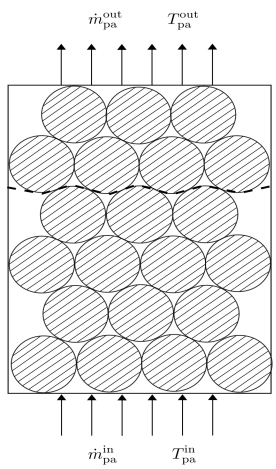

Figure 4.9: Convective heat transfer in a porous packed bed with uniform particles diameter d_p [m] and solid bed temperature T_s [K].

Finally, the physical properties of the fluid (air), such as the kinematic viscosity and the thermal diffusivity, needed for the calculation of the dimensionless numbers, are evaluated according to the mean temperature of the fluid given by [Stephan et al., 2010]:

$$T_{\text{m}} = \frac{T_{\text{pa}}^{\text{in}} + T_{\text{pa}}^{\text{out}}}{2} \tag{4.97}$$

4.4 Steam boiler

In biomass grate-firing power plant, the chemical bound energy contained in the solid fuel is released through combustion and transferred to boilers for steam generation, which can be exploited depending on the intended end-use, either for district

heating, or most certainly for electricity production by a turbine [Spliethoff, 2010].

In many power plants two boiler types can be distinguished, depending on the method in which steam-water mixture circulate through the evaporator tubes. These are [Kitto and Stultz, 1992]:

(a) natural circulation,

(b) forced circulation.

In natural circulation boilers the flow of the water through the banks of tubes is due to buoyancy effect caused by the density difference [Niessen, 2010], whereas in forced circulation boilers a pump is used to drive the water-steam mixture through the evaporator tubes [Ganapathy, 2002]. Therefore, it is important to identify the type of boilers being currently installed at the combustion power plant prior to the modeling task, as the dynamic behavior of these two types of boilers differs from one another.

Here, at the BMK Lünen power plant a boiler with natural circulation is installed, as a consequence, only this type of steam generators will be treated in this work. The boiler system design will include four main components, these are: the evaporator unit, the superheater unit, the economizer unit, and finally the air preheater unit. These units are primarily heat recovery surfaces, which operate at different heat flux densities depending on the firing and flue gases [Spliethoff, 2010], and aim at transferring the released thermal energy through combustion to the working mediums, here water/steam and air, via radiation and convection heat transfer mechanisms, whereas the convective heat transfer predominates in economizer and air preheating parts.

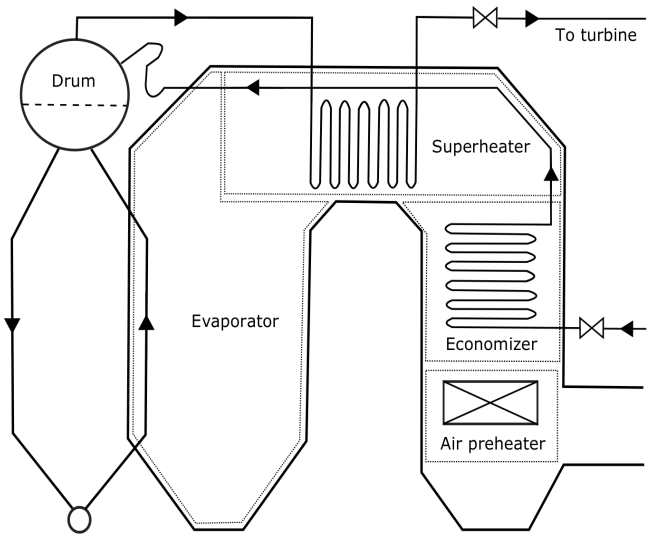

Figure 4.10: Steam generator unit and heat exchange surfaces in a biomass combustion power plant (adapted from [Effenberger, 2013]).

The superheater unit consists of more tube banks that are radiantly or convectively heated to produce dry steam with higher enthalpy than the saturated steam from the

drum [Niessen, 2010]. Hence, it has no influence on the amount of generated steam. The economizer is also a heat recovery surface convectively heated and placed at the region with lowest flue gas temperature. The intention of an economizer is to increase the feedwater temperature to the drum, and therefore, it has again no influence on the generated steam amount, unless the increase of temperature becomes considerably noticeable. However, as the heat transferred to this section is only a fraction compared to the drum and superheater sections, the impact of economizer dynamics on the generated steam is neglected [Van Kessel, 2003]. Therefore, the important part that has to be considered in the modeling discussion is the drum section, the crucial part in any power plant.

In literature, a significant amount of work has been dedicated to derive suitable dynamic models for the drum-boiler part with a natural circulation in a power plant. These models range from very complex and detailed models, to data-driven models based on measurements from the power plant. Among these works, there are models aiming at model-based plant control [Maffezzoni, 1997], [Adam and Marchetti, 1999], [TyssØ, 1981], [Casella and Leva, 2005], [Åström and Bell, 2000] just to name a few. The steam boiler model of [Åström and Bell, 2000] is being selected here. This is primarily due to its compactness and familiarity to control theorists, as it is derived from first-principles; moreover, this model is characterized by a small number of physical parameters.

Despite the fact that the design and the dynamic behavior of a steam boiler unit in a power plant is very complex in nature, [Åström and Bell, 2000] proved that the main dynamics of the process over a wide operating range and under different transient conditions can be well captured by a lumped-parameter modeling approach under some simplifying assumptions:

- The steam boiler is adiabatic.
- The vapor-liquid phases are in equilibrium.
- Pressure and temperature are uniform in both phases.

In [Åström and Bell, 2000], the drum pressure is given by the following differential equation:

$$e\frac{dp}{dt} = \dot{Q}_N - \dot{m}_{\mathrm{fw}}\left(h_{\mathrm{w}} - h_{\mathrm{fw}}\right) - \Phi_{st}(h_{\mathrm{st}} - h_{\mathrm{w}}) \tag{4.98}$$

with $\dot{m}_{\mathrm{fw}}$ [kg/s] feedwater flow rate, h_{fw} its enthalpy [J/kg], h_{w} the enthalpy of water inside the drum [J/kg], Φ_{st} the steam flow rate [kg/s].

The term e on the left hand-side of Eq. (4.98) results from the relation between internal energy and enthalpy, which can be well approximated as follows:

$$e \approx \rho_{\mathrm{w}} V_{\mathrm{w}} \frac{\partial h_{\mathrm{w}}}{\partial p} + m_m c_{p,m} \frac{\partial T_{\mathrm{st}}^{\mathrm{sat}}}{\partial p} \tag{4.99}$$

This indicates that the change in the drum pressure dynamics is dominated by the energy content of the water in the drum and the total mass of the system. With both terms appearing in the partial derivatives are determined from steam tables

and m_m [kg] denotes the total metal mass of the boiler unit.

Finally, as the interest is in the amount of generated steam, Eq. (4.98) has to be connected with a hydronamical relation for the steam flow Φ_{st} [kg/s] based on the sizing equations proposed in the Instrument Society of America (ISA) [Van Kessel, 2003]:

$$\Phi_{\text{st}} = Cp^{(1-\bar{\alpha})}\rho_{\text{st}}^{\bar{\alpha}} \tag{4.100}$$

According to [Leva et al., 1999], the parameter $\bar{\alpha}$ mentioned in Eq. (4.100) varies between 0 for saturated steam, which means that the steam flow is proportional to the pressure inside the drum, and 0.5 for high superheated steam, meaning that the steam behaves as an ideal gas. Their experiments revealed that a value of $\bar{\alpha} = 0.5$ is acceptable.

The linearization of Eq. (4.101) around the equilibrium value yields:

$$\Phi_{\text{st}} = C(1-\bar{\alpha})p_0^{(1-\bar{\alpha})}\rho_{st}^{\bar{\alpha}}(p - p_0) \tag{4.101}$$

Lumping all the constants in one model parameter A_{dr} [(J.s)/kg] and after the substitution of Eq. (4.101) into Eq. (4.98), a first-order ordinary differential equation for the steam production can be formulated as follows [Van Kessel, 2003]:

$$A_{dr}\frac{d\Phi_{\text{st}}}{dt} = \dot{Q}_N - \dot{m}_{\text{fw}}\left(h_{\text{w}} - h_{\text{fw}}\right) - \Phi_{\text{st}}h_c \tag{4.102}$$

with:

$$h_c = h_{\text{st}} - h_{\text{w}} \tag{4.103}$$

and

$$A_{dr} = e\frac{1}{C(1-\bar{\alpha})}\left(\frac{p_0}{\rho_{\text{st}}}\right)^{\bar{\alpha}} \tag{4.104}$$

The first term on the right-hand side of Eq. (4.102) represents the net thermal power, which will be further discussed in Chapter 5. The parameter A_{dr} in Eq. (4.102), when divided by the condensation enthalpy term h_c [J/kg], determines the time constant of the drum unit, which can be identified using step response experiments. If conducting such step response experiments is not possible, the parameter A_{dr} can be fitted to measured steam data from the plant using a quadratic cost function.

4.5 Model calibration

In most practical cases, it happens too often that the established mathematical model for a given process is incomplete, in the sense that a part of the parameter values for the corresponding equations set is not available. Such process models are usually termed "grey-box" models in the literature and they need to be calibrated. Therefore, from what has just been mentioned, it becomes apparent that the goal of model calibration, also referred to as model parameter estimation, is to get a suitable model's parameter set; this allows the chosen model structure to make a good mapping from the input space to the output space, and thereby, fulfilling the task of representing the dynamic behavior of the system.

In order to accomplish this objective, the unknown model parameters will be inferred from the experimental data gathered from the real process. For linear systems, the parameter values can be computed analytically from the measured data by applying linear algebra, whereas for nonlinear systems, the model parameters cannot be computed analytically, and the estimation task must be done using iterative nonlinear methods in the form of nonlinear optimization methods. In this case, the model calibration task is mapped to solving a nonlinear constrained optimization problem with the model parameters as free design variables that have to be iteratively tuned by a nonlinear optimizer, which minimizes the error difference between the measured output and the simulated model output. The set of parameters, which minimizes this error difference, generally known as the cost function, is considered to be the optimal parameter set that will calibrate the model response to its measured counterpart.

The conceptual approach used to calibrate the parameter values of a nonlinear dynamic model to the measured experimental data from the process will be shown in Section 4.5.1. The fundamental principles of the used optimization method for solving the constrained nonlinear optimization problem will be given in Section 4.5.2. Here, a derivative-free evolutionary algorithm termed Differential Evolution (DE) algorithm that combines both the advantages of the population-based algorithms (global optimization) and gradient-based optimization methods is being selected to update the model parameters according to the error function output. The update cycle is repeated until a stop criterion, which defines the fitness of the model to measurements, is achieved.

4.5.1 The calibration procedure

As it has been mentioned earlier, the problem of model parameter estimation has turned out to be in reality a nonlinear constrained optimization problem with the following ingredients for its solution [Cameron and Hangos, 2001]:

- a process model of the form:

$$y_M = \hat{f}_M(\mathbf{x}; \mathbf{p}) \tag{4.105}$$

  where $\mathbf{x} \in \mathbb{R}^{n_x}$ is the vector of dynamic states and $\mathbf{p} \in \mathbb{R}^{n_p}$ is the vector of model parameters.

- a set of measured data

$$D[0, k] = [x(i), y(i) | i = 0, ..., k] \tag{4.106}$$

- a cost function to be minimized. The most common measure of the discrepancy between measured output $y(t)$ and the predicted one $y_M(t)$ is the sum of squared errors [Suykens, 2003],

$$J(\mathbf{p}) = \frac{1}{2} \sum_{i=1}^{k} (y(i) - y_M(i, \mathbf{p}))^2 \tag{4.107}$$

Here, the notation $y_M(i, \mathbf{p})$ indicates that the model output is a function of the model parameter vector to be optimized. The optimization algorithm used to minimize the suggested cost function will be discussed separately in the following subsection. Consequently, the solution for model parameter estimation for the nonlinear dynamic model can be achieved by dividing the estimation task into two interrelated steps [Cameron and Hangos, 2001]:

1. Formulate a least square minimization problem.
2. Combine dynamic simulation and optimization according to the following sub-steps:
   (a) Initialize the set of estimated parameters $\mathbf{p}^{(0)}$.
   (b) Solve the model equations using previously estimated parameter to obtain the output $y_M(\tau; \mathbf{p}^{(k)})$ for $t = [0, 1, ...T]$.
   (c) Estimate $J(\mathbf{p})$ using Eq. (4.107).
   (d) Decide on whether the minimum is found.
   (e) If yes, then END with a vector of optimal parameter values estimate $\mathbf{p}_{\text{opt}}^{(k)}$, else generate a new estimate for the parameters $\mathbf{p}^{(k+1)}$.
   (f) Go to step (b) with $\mathbf{p}^{(k)} = \mathbf{p}^{(k+1)}$.

4.5.2 Optimization algorithm

Model parameters estimation begins by designing a cost function that can model the the problem's objective, i.e., minimizing the error between the model output and the measured one. This is done by tuning the model parameters, which are usually presented as a vector, until a minimum value for the cost function is obtained or a certain stop criterion is achieved. To this end, the central idea for generating variations of the parameter vector that reduces the objective function will be highlighted. A detailed description of the search strategy can be found in [Price et al., 2006].

Initialization

The Differential Evolution (DE) is a parallel direct search method which utilizes $\mathrm{N_P}$ D-dimensional parameter vectors

$$\mathbf{x}_{i,G} = \{x_{i,G}^1, ..., x_{i,G}^D\} \text{ with } i = 1, 2, ..., \mathrm{N_P} \tag{4.108}$$

as a population for each generation G. Then, before the population can be initialized, both upper and lower parameter bounds have to be specified for each element $x_{i,G} \in \mathbf{x}_{i,G}$. These two-dimensional values can be collected into two D-dimensional vectors $\mathbf{x}_{\min} = \{x_{\min}^1, ..., x_{\min}^D\}$ and $\mathbf{x}_{\max} = \{x_{\max}^1, ..., x_{\max}^D\}$. Consequently, the population can be randomly initialized to cover the entire search space bounded by $\mathbf{x}_{\min}$ and $\mathbf{x}_{\max}$. For example, the jth parameter of the ith vector at a generation $G = 0$ can be initialized as follows:

$$x_{i,0}^j = \text{rand}_j(0, 1) \cdot (x_{\max}^j - x_{\min}^j) + x_{\min}^j \tag{4.109}$$

with $\text{rand}_j(0, 1)$ is a random number generator which returns uniformly distributed random values within the range [0,1].

Mutation

After the initialization step is done, DE produces a population of $\mathrm{N_p}$ trial vectors $\mathbf{V}_{i,G} = \left\{v_{i,G}^1, v_{i,G}^2, ..., v_{i,G}^D\right\}$ for each $\mathbf{x}_{i,G}$ via a particular mutation and recombination strategy. The trial vector $\mathbf{V}_{i,G}$ is then generated as follows:

$$\mathbf{V}_{i,G} = \mathbf{x}_{r1,G} + \mathrm{F} \cdot (\mathbf{x}_{r_2,G} - \mathbf{x}_{r_3,G}) \tag{4.110}$$

with random indexes $r1, r2, r3 \in [1, 2, ..., \mathrm{N_p}]$ are integer and distinct from each other, which are also different from the index i. F is a scaling user-specified constant that scales the vectors difference in Eq. (4.110) and chosen in the range [0,1] to expand the search space.

Crossover

After the generation of the mutation vector $\mathbf{V}_{i,G}$ through mutation, and in order to enhance the potential diversity of the population, crossover is then applied to each pair of target vector $\mathbf{x}_{i,G}$ and its corresponding mutant vector $\mathbf{V}_{i,G}$ to form so called trial vector $\mathbf{U}_{i,G} = \{u_{i,G}^1, ..., u_{i,G}^D\}$. To this extent, DE algorithm can employ two forms of crossover methods: (a) exponential, or (b) binomial [Das and Suganthan, 2011]. Here, the latter is being selected, then:

$$u_{i,G}^j = \begin{cases} u_{i,G}^j & \text{if } \mathrm{rand}_j\,[0,1] \leq \mathrm{CR} \text{ or } j = j_{\mathrm{rand}} \\ x_{i,G}^j & \text{otherwise} \end{cases} \tag{4.111}$$

with $j_{\mathrm{rand}} \in [1, 2, ..., D]$, the value $\mathrm{CR} \in [0, 1]$ is a user-defined parameter that controls the fraction of parameter value that are copied from the mutant if $\mathrm{rand}_j\,[0,1] \leq \mathrm{CR}$ or $j = j_{\mathrm{rand}}$. Otherwise, the binomial crossover operator will copy the jth element of the target vector $\mathbf{x}_{i,G}$ to its corresponding part in the trial vector $\mathbf{U}_{i,G}$.

Selection

Once the the trial vector $\mathbf{U}_{i,G}$ has been computed, the objective function $J\,(\mathbf{U}_{i,G})$ evaluated at $\mathbf{U}_{i,G}$ will be compared to that of its target vector $J\,(\mathbf{x}_{i,G})$. To this extent, if the trial vector $\mathbf{U}_{i,G}$ has an equal or lower objective function value than the corresponding target vector $\mathbf{x}_{i,G}$, it will replace the target vector for the next generated population; otherwise, the target vector will retain its value for the next generation. This process can be summarized by Eq. (4.112) as follows

$$\mathbf{x}_{i,G+1} = \begin{cases} \mathbf{U}_{i,G} & \text{if } J\,(\mathbf{U}_{i,G}) \leq J\,(\mathbf{x}_{i,G}) \\ \mathbf{x}_{i,G} & \text{otherwise} \end{cases} \tag{4.112}$$

This process, i.e. mutation, crossover, and finally selection is repeated until an optimum is found, or a specified termination condition is reached. Table 4.4 shows the identified parameters for the grate-firing unit model by the optimization algorithm.

Table 4.4: Optimal model parameters found from the identification step and used for the validation.

Parameter	Dataset 1	Dataset 2	Dataset 3
a	0.0432	0.0457	0.0448
ν_{O_2}	1.1574	1.1071	1.0736
Δ'_{rec}	0.2766	0.2815	0.2743
$c_{p,\mathrm{ash}}$	1.9243	1.9018	1.9512
α_s	0.9585	0.9472	0.9510
α_w	0.8586	0.8501	0.8523
φ_{sw}	0.9785	0.9845	0.9797
d_p	9.885	10.104	9.901
Ψ	0.4857	0.4861	0.4842
$c_{p,m}$	0.4871	0.4848	0.4889
m_m	251×10^3	251×10^3	251×10^3
A_{dr}	3.761×10^{-3}	3.681×10^{-3}	3.741×10^{-3}

5 Biomass calorific value soft-sensing

Alike any large-scale industrial process, a biomass heat recovery plant requires a complex physical instrumentation and measuring network to be installed in order to run the process in a more efficient and reliable way. These measuring devices are mainly devoted to monitoring of a large set of process variables that are of economical and ecological relevance, and other tasks related to process control. Such present sophistication is therefore expected, since biomass heat recovery plants as in other industrial fields are day by day faced with stringent regulation laws, which impose further constraints on the process operability.

Addressing these constraints is a real challenge to control engineers and plant operators, as it requires a deeper knowledge of the process background, which is achieved by better understanding the physical and chemical mechanisms underlying the process, determining the process variables that have an influence on the output, which, if appropriately supervised and controlled, would improve the plant efficiency, while respecting the environmental aspects, and last but not least, determining the appropriate physical instrumentation and the apparatus design to meet the set objectives.

However, endowing the plant with more sophisticated physical instrumentation will increase not only the investment capital in the process, but also the maintenance planning and scheduling time burden, which the plant managers often try to prevent. Furthermore, some process dependent variables, which are key to efficient process operation, are hard to measure in real-time, simply due to the non-existing measurement technology or the infeasibility of the method used, such as off-line analyses, where samples are taken to the laboratory to determine the product quality, which introduces a considerable measurement delay. For the biomass combustion power plant case, this can be: the calorific value of biomass feedstock, the amount of fuel being fed to the furnace, as well as other process performance indicators such as: furnace and boiler efficiencies, just to name a few.

The rapid development of low-cost computer hardware and software facilities in the last few decades has enabled the emergence of the soft-sensing paradigm, which allowed for the establishment of more effective and appealing ways to overcome the existing problems of the data acquisition of critical process variables, or those which cannot be measured otherwise by the deployment of so called soft-sensors, also known as inferential model or virtual sensor [Warne et al., 2004]. This term is the conjunction of the words "software", since the models are usually computer programs, and "sensors", because the model are delivering similar information as their hardware counter parts [Kadlec et al., 2009].

Another concise explanation of the terminology is summerized by [Fortuna et al., 2007]:

> "*Soft sensors focus on the process of estimation of any system variable or product quality by using mathematical models, substituting some physical*

sensors and using data acquired from some other available ones."

Therefore, soft-sensing, in a broader sense, means the estimation of process variables using a pure mathematical description and existing process measurements. The mathematical model takes a direct feed of information from the process current physical instrumentation to estimate the process dependent variable of interest, which are hard to measure. Hence, different advantages can be offered by implementing a soft-sensor, these benefits can be summarized as follows [Fortuna et al., 2007]:

- a low-cost alternative to expensive hardware devices.
- can be run in parallel with existing hardware sensors for fault detection tasks. Therefore, realizing more reliable processes.
- can be directly integrated with existing hardware without any additional overhead.
- allow for real-time estimation of process variables. Hence, overcoming the time delays introduced by off-line sampling and/or slow hardware sensors.

According to [Warne et al., 2004], there are three main approaches to build a soft-sensor, these are:

1. Mechanistic modeling: this method describes the phenomenological knowledge underlying the process, i.e., based on physical and chemical laws such as mass and energy balance, reaction kinetics, etc.
2. Data-driven modeling: the method is based on collected measurements from the process and using statistical regression methods to estimate the process variable of interest.
3. Artificial intelligence modeling: this method is based on artificial neural networks (ANN), fuzzy inference system (FIS) and hybrid methods.

In this chapter, and in order to integrate the information about the main source of acting disturbance on the combustion process in the dynamic model of the grate-fired furnace developed in Chapter 4, which is the calorific value and the closely related moisture content of the biomass fuel, a mechanistic modeling approach is adopted here to design a soft-sensor that aims at estimating the fuel's calorific value. This value often fluctuates between the different batches delivered to the furnace, as a reason of mixing different fuels with different properties and moisture content together, and may even vary for the same type of biomass fuel due to harvesting, storing and transport conditions [Yin et al., 2008]. Consequently, the uncertainty introduced by the calorific value of the supplied fuel will cause severe disturbances inside the combustion furnace, which prevents a stable power output from the plant.

The soft-sensing of the moisture content and subsequently the estimation of calorific value of the biomass solid fuel will be based upon two interlinked main parts: the thermal power estimation and steam amount prediction, together with measurements in the flue gas. Here, the thermal power, i.e. the released power from the

reaction of solid fuel with the oxidant, includes the estimation of the amount fuel burned, the flue gas flow, the flame temperature and the furnace efficiency. The second part is predicting the steam amount with a dynamic steam-boiler model based on the transferred heat from the furnace side. The aforementioned concept of the soft-sensor for the biomass combustion plant is illustrated in Figure 5.1.

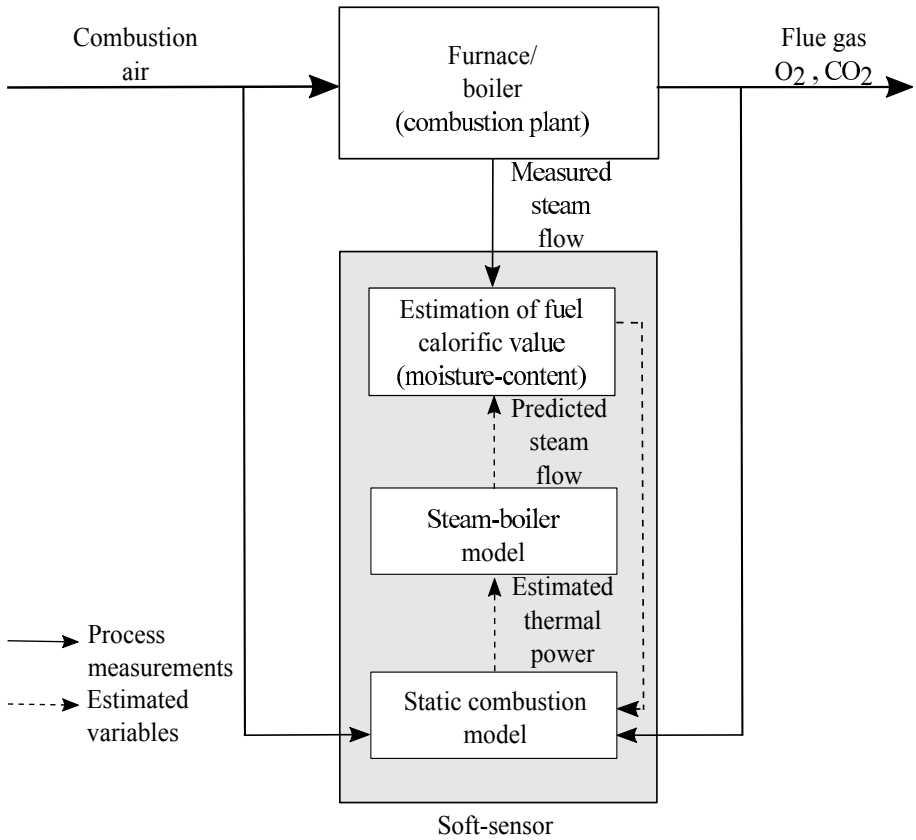

Figure 5.1: Calorific value soft-sensing concept in biomass combustion plant .

In the next section, different commercially available technologies, that deal with measuring in real-time the water fraction in biomass solid fuel are presented. This includes also the soft-sensing methodologies reported so far in literature. As it will be shown, the techniques will be classified into two main categories: direct or indirect, depending on how the fuel's water content is being determined, which will be elucidated next.

5.1 Existing techniques

In industries where the biomass fuels represent the main raw material to be exploited, such as in pulp and paper as well as in power generation sectors, there has often been a shared keen interest among these industries in finding fast and reliable non-destructive ways for determining the energy content of the delivered bio-fuel. This is due primarily to the following main reasons [Dahlquist, 2013b]:

- Price settlement at the delivery between sellers and end-users.
- Efficient control of combustion/kraft pulping processes.

The aim of this section is to give a "bird's-eye" view of the current state-of-the art technologies and to refer also to relevant and previously published works, that deal with soft-sensing methodologies for moisture content determination in biomass fuel. Here, a review of all publications in the area of direct moisture content determination will not be conducted, since any attempt to give a detailed description of such huge literature will be unsuccessful. Furthermore, the reported publications just represent a small variation in some part of the technique but the overall concept is still the same, while an emphasis will be put on reported works using indirect methods.

As mentioned previously, the existing techniques, including soft-sensing, for moisture content determination of solid biomass for power generation, can be classified into just two categories, these are: (a) direct or (b) indirect. Such classification is based on whether the water content is determined from direct measurements carried out on either the entering fuel flow or the fuel bulk, or it is inferred from some measurements in the flue gas. Therefore, such direct/indirect notation helps in making a clear distinction between hardware-based methods and other techniques, which most of them use the soft-sensing methodology based on measurements in the flue gas for determining the moisture content.

The different techniques for moisture determination in bio-fuels for power generation and their classification are illustrated in Figure 5.2.

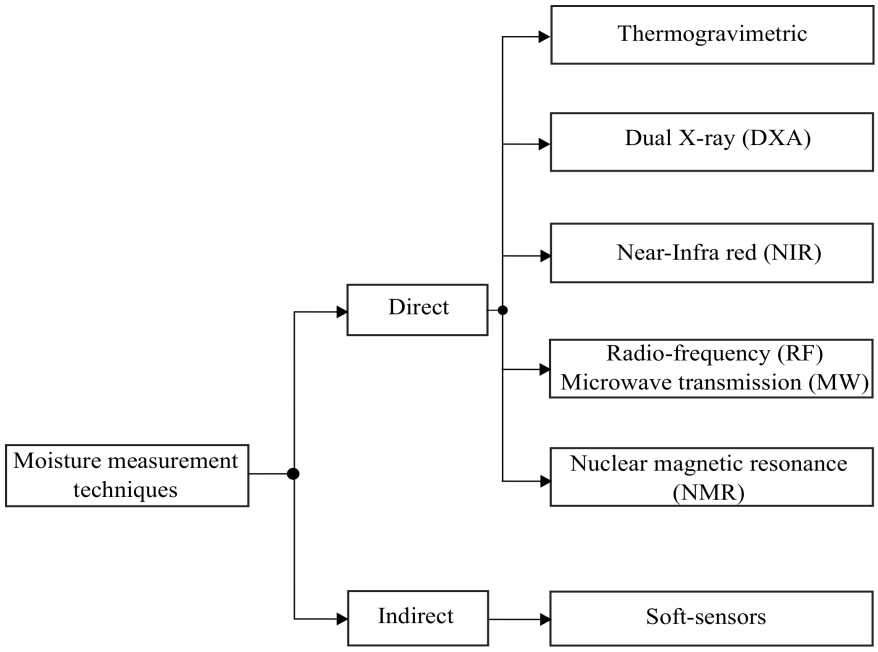

Figure 5.2: Classification of the different existing techniques for determining moisture content in biomass fuels for power generation according to [Nyström and Dahlquist, 2004].

In what follows, these methods will be shortly described and according to their corresponding classification except for the thermogravimetric technique, which has been already elucidated in Subsection 2.1.2.

5.1.1 Direct techniques

Dual X-ray absorptiometry (DXA)

Even though the Dual X-ray absorptiometry is a well known method in the medicine field for measuring bone and soft-tissue composition in vivo [Sartoris and Resnick, 1989], [Mazess et al., 1990]. Only recently, other applications of this technique have been emerging in wood science to provide useful information in wood industry, such as distinguishing between different types of constituents in wood, and giving a relative estimation for the amounts of moisture and ash content in the biological material, for this case wood chips [Ullberg et al., 2010].

In X-ray photon absorptiometry method, a sample or a plurality of wood chips samples are scanned at two different X-ray photon energy levels emitted from an X-ray tube, and the transmission of the electromagnetic radiation, i.e., the amount of absorbed radiation for each wavelength by the sample, is observed using a detector placed at the front-end of the X-ray source. The detector consists of a semiconductor array detector, and it registers the attenuation in the intensities of the two absorption energy levels. The values of the attenuated intensities detected are used to calculate the so called "k-value" [Kullenberg et al., 2010]. The ratio is neither dependent on thickness of the object nor on its density, but it depends on the linear attenuation coefficient of the material, which is further related to the photon energies and the atomic number of the material [Akkurt et al., 2005]. According to [Kullenberg et al., 2010], the atomic number of the wood chips mixture will be dependent on the amount of moisture in the scanned sample. When the moisture content varies, the effective atomic number varies as well. Hence, the linear attenuation coefficient will also vary.

Therefore, by associating the calculated k-values with the different moisture content of plurality of wood chip samples, a reference database or a calibration model can be created [Ullberg et al., 2010], which consists of a static linear regression equation, that relates the computed k-value from the scanning step to the moisture content of the biomass fuel determined by the conventional gravimetric methods. Consequently, when a new biomass fuel is to be measured for its moisture content, the sample is scanned and a material type from the reference database most resembling to the current sample, based on the so called T-value, is automatically identified. Subsequently, the moisture content is calculated based on the calibration model in the identified database [Kullenberg et al., 2010], [Hultnäs and Fernandez-Cano, 2012], [Kim et al., 2015]. Similar method using the same Dual X-ray absorptiometry technology for measuring moisture content of wood, but instead of computing the k-value, the regression model is obtained by finding a relationship between brightness of the obtained two X-ray radiographs and moisture content [Tanaka and Kawai, 2013].

Near-Infrared spectroscopy (NIR)

An emerging paradigm in wood science for real-time monitoring of moisture content and other chemical and physical related properties of the biofuel is using near-infrared spectroscopy in the context of chemometrics, a term borrowed from analyt-

ical chemistry, which indicates the extraction of useful information from collected data of a sample by applying numerical techniques, namely the multivariate analysis methods, to yield statistical calibration models that aim at determining the solid fuel properties. [Naes et al., 2002] defines chemometrics as follows:

> "*Chemometrics, in the most general sense, is the art of processing data with various numerical techniques in order to extract useful information.*"

Therefore, chemometrics is a symbiosis of different interdisciplinary areas in engineering ranging from multivariate analysis to applied mathematics and computer science, in order to address problems in chemistry, wood science and other fields. The information extraction of the property of interest is based on acquired spectral data from NIR spectroscopy reading device. In NIR spectroscopy technique, the incident radiation energy upon a solid, liquid or gaseous sample will be diffusely reflected, transmitted and part of it will be absorbed [Ayalew and Ward, 2000]. However, for the most application dealing with solid biomass, only the reflected NIR spectra are detected using either a silicon photodiode detector (below 1100 nm) or a photoresist cooled or uncooled lead sulfide detector (above 850 nm)[Burns and Ciurczak, 2007]. These spectra are the result of dominating overtone absorbances and combination bands of $C-H$, $O-H$ and $N-H$ [Leblon et al., 2013]. The NIR region of the electromagnetic spectrum ranges from 780 nm to 2500 nm (12800 cm^{-1}- 4000 cm^{-1}) [Burns and Ciurczak, 2007].

The measured data, which consist of absorbance spectra of a number of samples with known composition in a first step, are collected. The obtained data from the instrument response at different selected wavelengths are then assembled into a matrix called the "*absorbance matrix*". Similarly, a matrix, referred to as "*concentration matrix*", is formed. The concentration matrix contains the independent variables of interest, which for the most situations are hard to measure online. The elements in the concentration matrix are obtained using a reference method such as the conventional gravimetric (oven-drying) method for the case of determining the moisture content in biomass solid fuel [Beebe and Kowalski, 1987]. The pair of these two matrices will define the training set, which will be employed to develop a calibration model based on the available multivariate analysis techniques. An important prerequisite for the training set used to develop the calibration model is that it has to span a wide concentration range of interest [Kramer, 1998]. This statement sounds intuitive, because a data set that does only span a narrow range cannot be used to develop calibration model for the variable to be predicted that lies outside the range of calibrating samples.

Once the training set is appropriately prepared, multivariate calibration techniques can be applied to the data set. In the realm of multivariate analysis three main methods are usually employed by a "calibrationist", these are: multiple linear regression (MLR), partial least square (PLS), and principle component analysis (PCA). The application of these techniques on the data in the training set will yield to statistical calibration regression models. The prime goal of the calibration model is to relate the measured spectral data from the unknown sample to estimate the dependent variables that are hard to measure from those samples. Usually, before the regression model is put into practice, it has to be validated with another set of data that

is independent of the one used when generating the model. The validation data set aims at assessing the prediction capabilities of the calibration model to predict the independent variables of interest. In literature, there exists a considerable amount of books that cover the multivariate analysis in much greater detail. Therefore, the interested reader is directed to [Kramer, 1998] and [Naes et al., 2002].

Microwave and Radio frequency

Radio frequency and the microwave transmission methods are both non-destructive, and free-space techniques for measuring the water content as well as other physical-related properties of biomass. The concept underlying these two applications is quite similar and starts from the fact that biomass solid fuels are classified as anisotropic dielectrics, and based on electric field changes due to the dielectric properties of the material upon radiation with an electromagnetic wave [Jensen et al., 2006]. Hence, these two techniques will be discussed in parallel due to the existing similarity in theory and setup [Nyström and Dahlquist, 2004].

As mentioned previously, bio-fuels are polar dielectrics and characterized by their intrinsic ability to polarize under the influence of an alternating electromagnetic field. This defines the electric properties of material, and determines the way how the molecules of biomass will interact with the externally applied electric field. It is under such an external influence that the solid biomass reveals its dielectric properties [Torgovnikov, 1993]. As a consequence, the interaction between the electromagnetic energy and the material will be quantified by the complex physical quantity, the relative permittivity of the dielectric, which is composed of two parts: a real part that constitutes the dielectric constant, and an imaginary part that represents the dielectric loss factor. These two parameters are of particular interest [Nelson, 2015]. The dielectric properties are influenced by several factors, with biomass being a hygroscopic material in nature, the most dominating one will be the moisture content. Other influencing factors are the frequency of the electromagnetic wave of the applied electrical field, the temperature of the bio-fuel, and its density [Skaar et al., 1988].

When the flow or bulky biomass is irradiated by an electromagnetic wave, the wave will be propagated through the matter and there will most likely be a retardation in speed of propagation, such a retardation is proportional to the dielectric constant and it is related to the moisture content of biomass fuel under investigation. Additionally, the retardation of speed of propagation will give an indication about the biomass density which correlates with the moisture content due to biomass hygroscopicity. Such retardation is measurable as a phase change of the electromagnetic wave transmitted through the fuel. The wave will be also attenuated in intensity as a reason of the energy absorption and the scattering effect. The intensity of loss depends on the thickness of the solid fuel and is quantified by the loss factor of the dielectric [James et al., 1985], [Kraszewski, 1991].

It is therefore apparent that the prime interest in designing a measurement apparatus based on both techniques is to measure with a good accuracy the aforementioned dielectric properties of the fuel and adequately model the circuit for reliable calculation of the relative permittivity [Nelson, 2015]. According to [Kraszewski, 1991],

when using the microwave method for measuring the dielectric properties of materials, the measurement technique can be done in either transmissive or reflective measuring modes using resonant or aperiodic systems, with opened or closed topologies for sensing the dielectric parameters [Nelson, 2015]. Here, open-structure is of interest since a transmission sensor can be designed, which measures the attenuation in the energy of the penetrating wave through the wet biomass carried on the conveyor belt.

For the case where moisture measurement in a bulk of biofuel is required, then radio-frequency is considered to be a suitable option due to its large penetration depth in comparison to microwaves. Here, the apparatus is comprised of two horn antennas and a simple holder in between these antennas for the case where a transmissive measuring mode is selected, a personal computer for data acquisition and analysis (PC), and a network analyzer that emits the electromagnetic waves in radio frequent region. Then, phase shift and attenuation are calculated from the real and imaginary part of the relative permittivity based on the registered signals from the antennas. Consequently, these will allow for the estimation of moisture content in the bio-fuel [Nyström and Dahlquist, 2004].

Nuclear magnetic resonance (NMR)

Since the early 70's, Nuclear magnetic resonance (NMR) technique has been applied to measure moisture content in wood. Such technique is based on the fact that the nucleus of each hydrogen atom in water behaves like a magnet due to its characteristic spin. When subjected to an external static magnetic field of intensity I_0, the magnetic dipole precesses about the direction of I_0 with a frequency f[1] [Skaar et al., 1988].

According to [Sharp et al., 1978], there are two techniques when using NMR to measure the moisture content in wood: one steady state and the other unsteady state. In the former one, a homogeneous electromagnetic field with a frequency f, in the MHz range, is applied to a small wood specimen. A magnetic field of a slow varying intensity I is also applied. As a consequence, the nuclei will absorb energy from the oscillating magnetic field at a frequency equal to the resonance condition. The absorbed power is plotted as a function of I and at a constant frequency f. The curve and its derivative give information on the amount of water in the wood [Skaar et al., 1988]. In the second technique, the pulsed NMR method, and according to [Skaar et al., 1988], an initial equilibrium magnetization is applied to the sample parallel to the external magnetic field I_0, along with a sinusoidally alternating magnetic field of a frequency f. Next, a short intense burst of a magnetic field oscillating in resonance with the spin precession frequency is applied at the right angle to I_0. By proper choice of the intensity and duration of this pulse, a net magnetization is induced perpendicular to I_0 and a voltage is induced in a coil surrounding the sample, known as the free induction decay (FID), which increases linearly with the moisture content [Sharp et al., 1978]. Therefore, based on the aforementioned principles, an online NMR moisture measurement device that consists of the following components can be built. These components are comprised

[1] The units of I_0 and f are in Gauss and kHz respectively.

of: a permanent magnet, a magnet coil and an enclosure, a pot for carrying the sample to be measured, and a Radio-frequency (RF) coil that sends and receives the RF pulses for making the NMR measurements, an RF pulse generator, an RF receiver and a computer that analyzes the spectral information and analyzes the data [Barale et al., 2001].

5.1.2 Indirect techniques

[Ruusunen, 2008] presented an indirect, combustion temperature-based procedure for in-situ determination of moisture content of the solid biomass (wood chips) in a grate combustion unit. The method is based on assumption that the flame temperature changes at least partially related to changes in fuel moisture content. Therefore, a data analysis step is carried out on the information collected from multiple temperature sensors in the combustion chamber in order to find the most relevant sensors for moisture monitoring. This step consists of evaluating a criterion which is finding the mean maximum difference between temperature values for each sensor and at two different moisture level of the biomass fuel. Consequently, the largest mean values indicate the most relevant sensors for moisture monitoring.

The second step of the proposed estimation framework consists of testing feature prototypes that are extracted from the selected temperature data using a data mining algorithm. Within this context, feature prototypes are variables that are subject to transformations or calculations with other variables. Preferred properties for features according to the method are: the monotonically increasing values with respect to moisture level, and the degree of mutual independence of model inputs if used with other features. Regression was then used to obtain an identified calibration model which maps the selected features into absolute moisture content values. As stated previously, the method requires two moisture level data sets to be available, which can be a limitation when considering a large-scale combustion power plant. Additionally, another disadvantage is that the measurements obtained from the temperature sensors may not be sensitive enough to monitor the variation of the moisture levels in the biomass solid fuel.

Another indirect method based on measurements in the flue gas was proposed in [Hermansson et al., 2011]. Here, the central idea is to measure first the moisture content of the flue gas before determining indirectly the moisture content of the fuel by a mass balance calculation, including the moisture content of the combustion air. The Fourier-transform Infrared Technology (FT-IR) is one method among other methods to determine the moisture content with enough accuracy in a combustion unit; however, the accuracy of the FT-IR has been reported to be sensitive to the absolute temperature level, pressure, temperature gradients and particles carried with the gas.

As an alternative, [Hermansson et al., 2011] used a sensor for measuring relative humidity (RH) together with temperature measurement in flue gas to estimate the moisture fraction. Such RH-sensors have been developed for measurements in gases up to 200 °C and use chemically modified polymer as a detector material that responds by capacitance to the RH of the surrounding gas, and have shown their resistance in environments that are contaminated with different organic compounds

[Ikonen et al., 2006]. However, when using RH-sensor at high flue gas temperature, which is typical in a biomass combustion unit, the accuracy of the sensor is degraded. As consequence, it cannot be used for indirect determination of the flue gas moisture content due to the low RH level (< 0.01). Hence, in the proposed work, a method to increase the sensor accuracy into acceptable level was developed, which consists of designing a measurement setup that extracts a part of the flue gas from the duct and filtering it, before it gets cooled to a target temperature in a tube that passes through a temperature-controlled oil bath to elevate the RH of the flue gas. Even though the results obtained from this measurement setup indicated that the method was able to monitor the moisture variation in fuel in a grate furnace burning saw dust and CFB-boiler burning wood chips, an application of the proposed method is limited by the fact that new devices as well as the calibration issue of the apparatus are needed.

In [Van Kessel et al., 2004a], a method was presented for estimating the calorific value of municipal solid waste in a grate firing unit by means of a soft-sensor which was developed using a mechanistic modeling approach. The main characteristic of the developed calorific value sensor (CVS) is that it is based upon stationary mass balances over the gas phase together with concentration measurements in the flue gas. In a first step, the composition of combustible part, described by CH_aO_b, of the waste layer on the grate is modeled. While the stoichiometric coefficient (a) in the previous chemical formula is fixed to 1.72 based on the analysis of different waste fuels, the coefficient (b) is derived from mass balances for O_2, CO_2 and N_2 along with measurement concentrations of the following components in the flue gas O_2,H_2O, and N_2. The second step of CVS is to compute the calorific value of the waste from the identified chemical composition of the fuel using a well-known formula of Michel [Klose et al., 1989]. Even though the experiments showed that sensor was capable of continuously monitoring the calorific value of the waste being converted, a drawback that counts here is that more measurements in the flue gas are needed, which implies that additional hardware sensors have to be installed in the combustion site.

In [Kortela and Jämsä-Jounela, 2013], another soft-sensor was introduced for estimating the fuel quality based on a nonlinear dynamic model of a secondary superheater in the steam-boiler part. The method assumes that water evaporation affects the enthalpy of the secondary superheater, and the effective heat value of the fuel depends linearly on the fuel moisture content. Furthermore, the heat transferred to the secondary superheater requires a direct measurement of the thermal decomposition rate of the dry fuel, which cannot be directly measured; however, it can be calculated by utilizing the method presented in [Kortela and Marttinen, 1985] for estimating the released thermal power. From this it follows that the unknown moisture content is estimated based on minimizing difference between the estimated steam enthalpy by the superheater model and its measured counter part. In contrast to the discussed method, here, the calorific value of the fuel will be inferred from the generated steam amount by deploying a simpler steam-boiler dynamic model that is characterized by the less parameters to be fitted than in the superheater model, which involves the identification of many unknown dimensionless parameters used to model the nonlinear transfer coefficients. Moreover, steam measurements are often reliable and accurate in a combustion power plant [Van Kessel et al., 2004a].

5.2 Thermal power estimation

Up until now, the term "biomass fuel" has been always indicating the kind of potential energy stored in chemical bonds of the carbohydrate. In combustion, the chemical internal energy, which is associated with the destruction of chemical bonds between atoms, will be converted into a thermal energy, in which the combustible substances of the chemical fuel (either solid, liquid or gas) react with an oxidizer during an exothermic chemical reaction, where the exchange and/or the rearrangement of atoms between colliding molecules takes place, with a simultaneous release of energy in the form of heat [Warnatz et al., 2001].

To better understand the modeling approach for the first part of the sensor, some combustion fundamentals and definitions will be described in the next subsections. This includes the definition of the combustion stoichiometry that represents a key building block for estimating the total released thermal power from burning the fuel, and further entails the calculation of the minimum oxygen and the total air required to achieve a complete combustion of the fuel fed to the chamber.

5.2.1 Combustion stoichiometry

As mentioned previously, combustion processes are chemical reactions during which the fuel compounds are oxidized in order to release heat and other combustion products. When using biomass as a fuel, the main constituents are carbon C, hydrogen H_2 and sulfur S. The most commonly used oxidizer is the oxygen carried in the atmospheric air that contains approximately 21% oxygen (O_2) and 79% nitrogen (N_2) by volume [Watter, 2009].

The result of this step is the combustion flue gas together with the inert gas stemming from the nitrogen contained in the air, which does not react with other fuel elements. If some minerals and incombustible materials should be present in the biomass solid fuel, these will manifest themselves in the bottom ash residues, as shown in Figure 5.3.

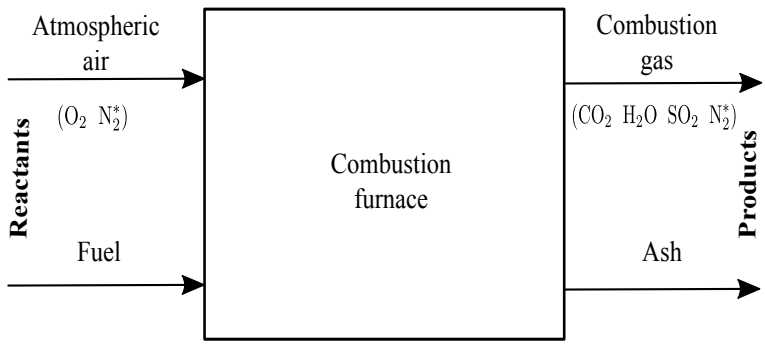

Figure 5.3: Combustion system.

It should be noted that bringing the solid fuel to an intimate contact with the oxygen is not sufficient to start the combustion process. The biomass solid fuel must be brought above its ignition temperature to start combustion, which can occur at temperatures between 300-365 °C for woody biomass [Babrauskas, 2002], [Dahlquist,

2013a]. Once the ignition temperature is reached, the hydrocarbon starts to decompose thermally releasing the volatile compounds that will be oxidized in a second step [Cengel et al., 2002].

Moreover, a combustion is said to be complete if the oxidized species from this step are: carbon dioxide CO_2, water H_2O, and sulfur dioxide SO_2. On the contrary, a flue gas that contains incombustible volatiles in its composition such as: carbon monoxide CO, is said to be incomplete; this can be either due to the few amount of air provided which will lead to an oxygen depletion in the furnace, or a part of the furnace where the air has no sufficient access to it [Baehr and Kabelac, 2012],[Karl, 2012].

Another cause of incomplete combustion is dissociation, which becomes important at high temperatures [Cengel et al., 2002]. Therefore, the combustion stoichiometry aims at determining the amount of air needed to oxidize completely the combustible elements of the fuel, the amount of the exhaust gas and its composition.

5.2.2 Chemical reactions

A complete combustion of biomass fuel means the total oxidation of its compounds C, H_2 and S, as described in the following reaction equations [Langeheinecke et al., 1993]:

$$\mathrm{C} + \mathrm{O_2} \longrightarrow \mathrm{CO_2} \qquad +\,393{,}5 \quad \mathrm{MJ/mol} \tag{5.1a}$$

$$\mathrm{H_2} + \frac{1}{2}\mathrm{O_2} \longrightarrow \mathrm{H_2O} \qquad +\,241{,}8 \quad \mathrm{MJ/mol} \tag{5.1b}$$

$$\mathrm{S} + \mathrm{O_2} \longrightarrow \mathrm{SO_2} \qquad +\,296{,}9 \quad \mathrm{MJ/mol} \tag{5.1c}$$

Here, the atoms are conserved, meaning that they are not created nor destroyed, on the other hand the molecules are not conserved. As an example, in the above chemical reaction (see Eq. (5.1a)), C and O are conserved atoms while the product molecule CO_2 is not. Furthermore, this reaction is exothermic, since heat is being released.

Additionally, from the stoichiometric coefficients of this equation, it can be seen that 1 mol of C reacts with 1 mol O_2 to produce 1 mol CO_2, which is referred to as: "*the mole ratio*". Hence, the molar ratio can be defined as the stoichiometric ratio of reactants and products, which can be easily deduced from the aforementioned balanced chemical equations as follows [Joos, 2006]:

$$n_{\mathrm{C}} : n_{\mathrm{O_2}}^{\mathrm{C}\longrightarrow\mathrm{CO_2}} : n_{\mathrm{CO_2}} \quad = 1 : 1 : 1 \tag{5.2a}$$

$$n_{\mathrm{H_2}} : n_{\mathrm{O_2}}^{\mathrm{H_2}\longrightarrow\mathrm{H_2O}} : n_{\mathrm{H_2O}} \quad = 1 : \frac{1}{2} : 1 \tag{5.2b}$$

$$n_{\mathrm{S}} : n_{\mathrm{O_2}}^{\mathrm{S}\longrightarrow\mathrm{S_2O}} : n_{\mathrm{SO_2}} \quad = 1 : 1 : 1 \tag{5.2c}$$

Stoichiometric oxygen and air requirements

The stoichiometric oxygen is the exact amount of oxygen needed to oxidize the biomass compounds, i.e., the carbon to carbon dioxide, the hydrogen to water and finally the sulfur to sulfur dioxide (see Eqs. (5.1a) - (5.1c)). Furthermore, no trace of oxygen will be found in the exhaust gas, which is the equivalent of a perfect combustion.

The minimum oxygen amount needed is straightforwardly obtained from the mole ratio Eqs. (5.2a) - (5.2c) and the biomass fuel composition. This part was already discussed in Chapter 2, where a chemical formula for the solid fuel was derived in order to carry out the combustion calculations.

Therefore, the oxygen required to oxidize each component of biomass fuel can be easily given by:

$$n_{\mathrm{O_2}}^{\mathrm{C}\longrightarrow\mathrm{CO_2}} = n_{\mathrm{C}} = \frac{\gamma_{\mathrm{C}}(1-\gamma_{\mathrm{w}})}{M_C} m_{\mathrm{B}} \tag{5.3a}$$

$$n_{\mathrm{O_2}}^{\mathrm{H_2}\longrightarrow\mathrm{H_2O}} = \frac{1}{2} n_{\mathrm{H_2}} = \frac{\gamma_{\mathrm{H_2}}(1-\gamma_{\mathrm{w}})}{M_{H_2}} m_{\mathrm{B}} \tag{5.3b}$$

$$n_{\mathrm{O_2}}^{\mathrm{S}\longrightarrow\mathrm{SO_2}} = n_{\mathrm{S}} = \frac{\gamma_{\mathrm{S}}(1-\gamma_{\mathrm{w}})}{M_S} m_{\mathrm{B}} \tag{5.3c}$$

with m_B is the fuel mass in [kg], and M_i represents the molar mass of component i in [kg/mol].

By taking into account the oxygen fraction present in the biomass fuel itself before combustion $n_{\mathrm{O_2}}^{B}$, the minimum oxygen required for complete combustion $n_{\mathrm{O_2}}^{+}$ [mol $\mathrm{O_2}$] can be calculated as shown in Eq. (5.4):

$$n_{\mathrm{O_2}}^{+} = n_{\mathrm{O_2}}^{\mathrm{C}\longrightarrow\mathrm{CO_2}} + n_{\mathrm{O_2}}^{\mathrm{H_2}\longrightarrow\mathrm{H_2O}} + n_{\mathrm{O_2}}^{\mathrm{S}\longrightarrow\mathrm{SO_2}} - \frac{1}{2} n_{\mathrm{O_2}}^{B} \tag{5.4a}$$

$$n_{\mathrm{O_2}}^{+} = n_{\mathrm{C}} + \frac{1}{2} n_{H_2} + n_{\mathrm{S}} - \frac{1}{2} n_{\mathrm{O_2}}^{B} \tag{5.4b}$$

Under the consideration of the oxygen molar mass $M_{\mathrm{O_2}}$, the required oxygen amount $L_{\mathrm{O_2}}^{+}$ [$\mathrm{kg_{O_2}/kg_B}$] is given by:

$$L_{\mathrm{O_2}}^{+} = M_{\mathrm{O_2}} \cdot \left(\frac{n_{\mathrm{O_2}}^{+}}{m_B}\right) = M_{\mathrm{O_2}} \cdot \mathrm{O_2^{+}} \tag{5.5}$$

Similar to the previously given definition of the stoichiometric oxygen, the theoretical air L_{A}^{+} [$\mathrm{kg_A/kg_B}$] is the amount of required air that contains the minimum oxygen needed to oxidize the fuel compounds, and no trace of oxygen will be found in the exhaust gas, since it will be fully consumed. Consequently, the theoretical air requirement to burn 1 kg of fuel can be directly obtained, by taking into account Eq. (5.5) as follows [Langeheinecke et al., 1993]:

$$L_{\mathrm{A}}^{+} = \frac{m_{\mathrm{A}}^{+}}{m_{\mathrm{B}}} = \frac{L_{\mathrm{O_2}}^{+}}{\xi_{\mathrm{O_2}}^{A}} = \frac{L_{\mathrm{O_2}}^{+}}{0.2314} \tag{5.6}$$

Here $\xi_{\mathrm{O_2}}^{A}$ is the mass fraction of oxygen in air [-].

Excess air

In almost all technical combustion systems, the minimum required air is seldomly supplied to the furnace in order to operate the process. Therefore, more air beyond the minimum required must be added to achieve a complete fuel burnout, which is referred to as "excess air", one of the most important parameters in operating the combustion process efficiently [Koppejan and Van Loo, 2012],[Nuusbaumer, 2002].

At this stage, it is quite intuitive to ask why more air is being added than needed if the theoretical air amount would achieve that?. The first and quite obvious reason for this is that reality is far away from theory, since the solid fuel is a blend of different biomass fuels and only a rough approximation of the fuel's composition is possible. Therefore, the required theoretical air value cannot be known exactly, and only an approximation of it will be available.

A second possible reason is due to the poor mixing conditions of the burning bed on the moving grate, giving rise to zones with a rich air supply and zones with a poor air supply [Karl, 2012]. Consequently, the ratio of the real supplied air $\dot{m}_{\mathrm{A}}$, which will be treated separately in Section 5.2.3, over the required air amount $\dot{m}_{\mathrm{A}}^{+}$ needed to burn the solid fuel of a mass flow rate $\dot{m}_{\mathrm{B}}$[2], is indicated by the excess air factor λ [-] given by [Baehr and Kabelac, 2012]:

$$\lambda = \frac{\text{amount of air supplied}}{\text{minimum of air required}} = \frac{\dot{m}_{\mathrm{A}}}{\dot{m}_{\mathrm{A}}^{+}} \tag{5.7}$$

Substituting Eq. (5.6) in Eq. (5.7), the excess air λ can be rewritten as:

$$\lambda = \frac{\dot{m}_A}{L_{\mathrm{A}}^{+} \cdot \dot{m}_B} \tag{5.8}$$

Depending on the excess air ratio value, the combustion can proceed under three main conditions; these are [McAllister et al., 2011]:

- The combustion proceed under the fuel-lean regime regime ($\lambda > 1$), if there will be more air than theoretically needed.
- The combustion proceeds under the fuel-rich regime ($\lambda < 1$), if the fuel is supplied in excess.
- Finally, the combustion is said to be stoichiometric ($\lambda = 1$), if the exact amount of air is supplied to burn completely the solid fuel.

5.2.3 Combustion air

The most frequently used oxidizer for almost all combustion applications, as stated in Subsection 5.2.1, is air [Baukal Jr, 2012], which is a mixture of oxygen, nitrogen and other inert gases which do not undergo a chemical reaction with the biomass solid fuel such as: argon Ar, neon Ne, and carbon dioxide CO_2. Air in the atmosphere contains also water vapor (or moisture), and it is referred to as atmospheric or combustion air. In contrast, air that contains no water vapor is called dry air

[2] ash-free

[Cengel et al., 2002].

Therefore, the mass of the atmospheric air m_{A} [kg] can be written as the sum of the mass that contains only dry air m_{A}^{dry} and a second part that contains water vapor mass m_{A}^{wet} [Baehr and Kabelac, 2012]:

$$m_{\mathrm{A}} = m_{\mathrm{A}}^{dry} + m_{\mathrm{A}}^{wet} \tag{5.9}$$

Specific humidity

According to [Cengel et al., 2002], the amount of water vapor in air can be specified in different ways. However, the most simple way is to specify the mass of water vapor present in a unit mass of dry air, which is denoted as the specific humidity X [-], that is the ratio of the moisture in air m_{A}^{wet} relative to dry air amount m_{A}^{dry}, which can be given by [Baehr and Kabelac, 2012]:

$$X = \frac{m_{\mathrm{A}}^{wet}}{m_{\mathrm{A}}^{dry}} = 0.622 \cdot \frac{\varphi \cdot p_{\mathrm{w}}^{sat}(T)}{p - \varphi \cdot p_{\mathrm{w}}^{sat}(T)} \tag{5.10}$$

where p [Pa] is the total pressure, p_{w}^{sat} [Pa] stands for the saturation water vapor pressure at specific temperature, and φ [-] is the relative humidity, respectively.

Relative humidity

By definition the relative humidity φ [-] is the ratio of the partial pressure of water vapor p_{w} in the mixture to the saturation pressure p_{w}^{sat} [Baehr and Kabelac, 2012]:

$$\varphi = \frac{p_{\mathrm{w}}}{p_{\mathrm{w}}^{sat}(T)} \tag{5.11}$$

For a temperature from 0,01 °C to 60 °C and triple point pressure $p_{tr} = 611,657\,\mathrm{Pa}$ in this range, the saturation vapor pressure shown in Eq. (5.11) can be given by Antoine equation [Baehr and Kabelac, 2012]:

$$\ln\frac{p_{\mathrm{w}}^{sat}}{p_{tr}} = 17,27 - \frac{4102,99}{T + 237,43} \tag{5.12}$$

Finally, Eq. (5.9) can be reformulated as follows:

$$m_{\mathrm{A}} = m_{\mathrm{A}}^{dry} \cdot (1 + X) \tag{5.13}$$

5.3 Static combustion model

After laying the first foundations on the quest to estimate the thermal power released from the combustion of biomass solid fuel, the gained knowledge from what was previously discussed in Section 5.2 will be used in developing a static combustion model for the furnace, which is a pre-requisite for building the soft-sensor. Here, a first problem to be solved is that some fundamental dependent variables needed cannot be measured, these are: the biomass flow rate and other process performance

indicators such as: the furnace and the boiler efficiencies.

In this section, a static combustion model will be thoroughly developed and discussed. The inferential model will be based on fundamental laws of physics applied on the fundamental quantities, i.e. the total mass and the total energy and by using the existing measurements to estimate the process variables that cannot currently be measured at the power plant.

5.3.1 Mass balance

In every real-world process, the phenomena underlying the dynamics are obeying the laws of thermodynamics and the conservation principles. In combustion engineering, as well as other fields, the conservation of mass and energy is the basis for any consideration, and depending on the interpretation of these laws as they apply to different processes, as well as the boundary of the control volume that defines how the system interacts with its surrounding and for which the law of conservation of mass and energy will be applied, will lead to different forms of equations describing the process dynamics [Thomas, 1999].

The basic principle to obtain a rigorous model by balancing of conserved quantities (S) within the defined system boundary such as the total mass, the total energy and the momentum is based on the following concept [Stephanopoulos, 1984]:

$$\frac{\begin{bmatrix}\text{accumulation of S}\\ \text{within a system}\end{bmatrix}}{\text{time period}} = \frac{\begin{bmatrix}\text{flow of S in}\\ \text{the system}\end{bmatrix}}{\text{time period}} - \frac{\begin{bmatrix}\text{flow of S out}\\ \text{of the system}\end{bmatrix}}{\text{time period}} \tag{5.14}$$

Since the word "static" was mentioned before, this means that the accumulation term in Eq. (5.14) is zero. The reason of such assumption in developing the static combustion model under steady state conditions is to calculate the incoming and outgoing mass flows of interest, these are: the gas mass flow and the fuel mass flow in the furnace (see Figure 5.4).

Flue gas estimation

Recall from Subsection 5.2.2, that a combustion gas with nothing but carbon dioxide CO_2, water H_2O, sulfur dioxide SO_2 and nitrogen N_2^*, is known as the stoichiometric combustion gas with its mass flow rate $\dot{m}_g^+$ [kg/s], which is achieved if only the exact amount of air L_A^+ [kg_A/kg_B] required to burn the fuel completely is known, but in many technical combustion processes the value of it is seldom known. Hence, more amount of combustion air is required to achieve a complete fuel burnout. Consequently, this will lead to an excess air λ [-] in the gas phase. Also, if some minerals fraction γ_{Ash} [kg_{Ash}/kg_B] contained in the biomass fuel, these will leave the furnace with a mass flow rate $\gamma_{Ash}\dot{m}_B^{Ash}$ [kg/s].

The calculation of the variables of interest is based on mass balance. According to Figure 5.4, the stoichiometric flue gas $\dot{m}_g^+$ can be given by [Baehr and Kabelac, 2012]:

$$\dot{m}_g^+ = \dot{m}_B + \dot{m}_A^+ \tag{5.15}$$

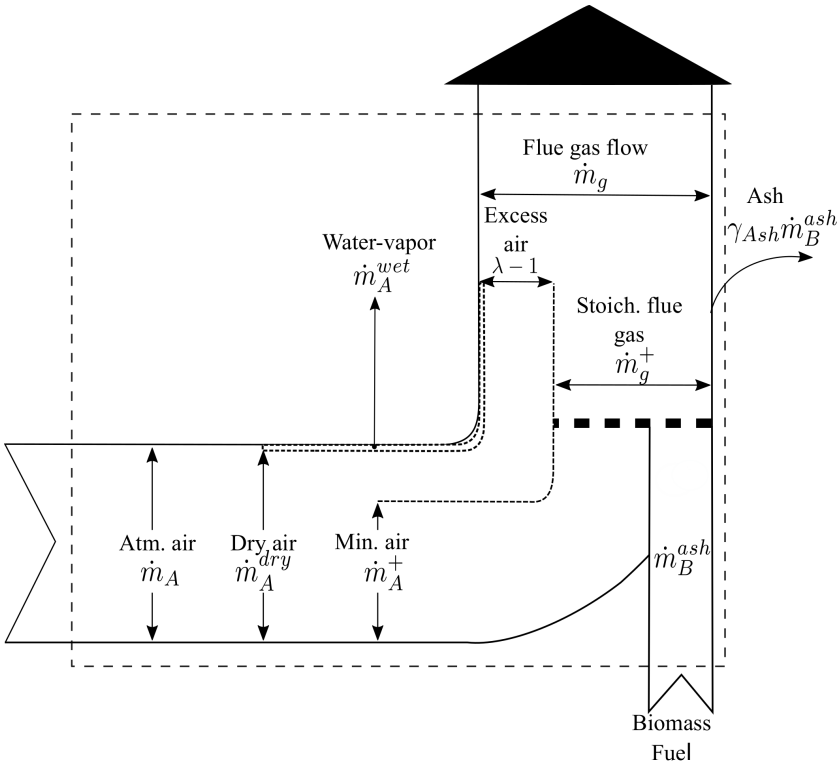

Figure 5.4: Different mass flows entering and leaving the combustion chamber control volume boundary (dashed-line) [Baehr and Kabelac, 2012].

with

$$\dot{m}_B = (1 - \gamma_{Ash}) \cdot \dot{m}_B^{Ash} \tag{5.16}$$

and

$$\dot{m}_g = \dot{m}_g^+ + (\lambda - 1) \cdot \dot{m}_A^+ \tag{5.17}$$

Substituting Eq. (5.15) into Eq. (5.17), this gives:

$$\dot{m}_g = \dot{m}_B + \dot{m}_A^+ + (\lambda - 1) \cdot \dot{m}_A^+ \tag{5.18}$$

with the minimum required air $\dot{m}_A^+$ is given by Eq. (5.18):

$$\dot{m}_A^+ = L_A^+ \cdot \dot{m}_B \tag{5.19}$$

Thus, Eq. (5.17) becomes:

$$\dot{m}_g = (1 + \lambda L_A^+) \cdot \dot{m}_B \tag{5.20}$$

Fuel flow estimation

Recall from Subsection 5.2.1, that the biomass flow rate $\dot{m}_B$ can be given by:

$$\dot{m}_B = \frac{\dot{m}_A}{\lambda \cdot L_{\mathrm{A}}^+} \tag{5.21}$$

Here, the fuel flow rate $\dot{m}_B$ [kg/s] is still unknown, which calls for an additional equation to compute the excess air λ [-] as a function of the oxygen concentration in the gas phase.

The oxygen mass balance can easily be deduced from the control volume of the system (see again Figure 5.4):

$$\xi^g_{O_2}\ (\dot{m}_B + \dot{m}_A) = \xi^A_{O_2}\ \dot{m}_A - L^+_{O_2}\ \dot{m}_B \tag{5.22}$$

The substitution of Eq. (5.21) into Eq. (5.22) leads to:

$$\xi^g_{O_2} + L^+_{O_2} = \lambda\ L^+_A\ (\xi^A_{O_2} - \xi^g_{O_2}) \tag{5.23}$$

Hence,

$$\lambda = \frac{\xi^g_{O_2} + L^+_A \xi^A_{O_2}}{L^+_{O_2} - \frac{\xi^g_{O_2}}{\xi^A_{O_2}}\ L^+_{O_2}} = \frac{\xi^g_{O_2} + L^+_A \cdot \xi^A_{O_2}}{L^+_{O_2}\ \left(1 - \frac{\xi^g_{O_2}}{\xi^A_{O_2}}\right)} \tag{5.24}$$

Finally, the substitution of Eq. (5.24) into Eq. (5.21) allows for the computation of the unknown biomass mass flow rate $\dot{m}_B$ [kg/s] under its final form, which is given by Eq. (5.25) [Belkhir and Frey, 2016a]:

$$\dot{m}_B = \frac{\dot{m}_A}{\frac{1}{\xi^A_{O_2}}\ \left(\frac{\xi^g_{O_2} + L^+_{O_2}}{1 - \frac{\xi^g_{O_2}}{\xi^A_{O_2}}}\right)} = \frac{\xi^A_{O_2} - \xi^g_{O_2}}{L^M_{O_2} + \xi^g_{O_2}} \cdot \dot{m}_A \tag{5.25}$$

Thus, it turns out to be that the unmeasured fuel mass flow rate can be estimated from the oxygen content in the exhaust gas $\xi^g_{O_2}$ together with the conducted amount of the air inside the combustion chamber $\dot{m}_A$ with its oxygen mass fraction $\xi^A_{O_2} = 0.23$ [Kortela and Marttinen, 1985].

5.3.2 Energy balance

In combustion, as well as in other thermodynamics processes, the chemical bonds in the reactants are rearranged, which results in the formation of products and energy being liberated during an exothermic reaction or being absorbed during an endothermic reaction [McAllister et al., 2011]. Similar to the mass balance, the energy balance deals with energy flows entering and leaving the control volume that defines the furnace boundary (see Figure 5.5).

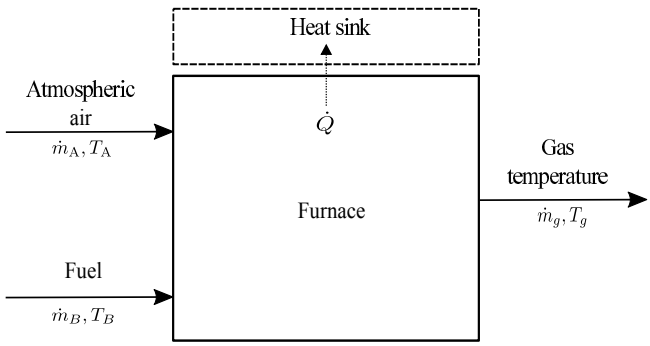

Figure 5.5: Energy flows enetering and leaving the combustion furnace [Langeheinecke et al., 1993].

Here, before the application of the first law of thermodynamics, which states that the net change (increase or decrease) in the total energy of the system during a process is equal to the difference between the total energy entering and the total energy leaving the system during that process [Cengel et al., 2002], some simplifying hypotheses should be made in order to carry out the energy balance calculations; these are [Turns et al., 1996]:

- The control volume is fixed relative to the coordinate system. Herewith, both the kinetic and potential energies of the system are not considered and only the internal energy is taken into account.
- The property of the mixture at each point within the control volume, or control surface does not vary with time. Thus, the process is treated as steady.
- The combustion is assumed to be complete, i.e., all the carbon C is converted to carbon monoxide CO_2 and the hydrogen to water H_2O.
- The combustion is isobaric, i.e., the pressure inside the combustion furnace is constant. This allows for the treatment of the combustion gas as an ideal gas.
- The dissociation effect is not taken into account, since it must be considered only at very elevated furnace temperatures ($> 1500\,°\mathrm{C}$).
- The temperature and pressure at the standard conditions are $T_0 = 25\,°\mathrm{C}$ and $p_0 = 101,325\,\mathrm{Pa}$ respectively.

Referring to Eq. (5.14) and from Figure 5.5, the energy balance of the stationary combustion process reads [Baehr and Kabelac, 2012]:

$$\dot{Q} = \dot{m}_g\, h_g(T_g) - \dot{m}_B\, h_B(T_B) - \dot{m}_A\, h_A(T_A) \tag{5.26}$$

Dividing Eq. (5.26) by the biomass flow rate $\dot{m}_\mathrm{B}$ and taking Eq. (5.21) into account, Eq. (5.26) can be rewritten as:

$$q = \frac{\dot{Q}}{\dot{m}_B} = \frac{\dot{m}_g}{\dot{m}_B}\, h_g(T_g) - \; h_B(T_B) - \lambda\, L_A^+\, h_A(T_A) \tag{5.27}$$

Heat of reaction and fuel calorific value

A maximum heat amount will be extracted from the combustion chamber if the exhaust gas temperature is cooled down in a such way that it is equal to the standard temperature $T_0 = 25\,°\mathrm{C}$ [McAllister et al., 2011]. Consequently, this will lead to the definition of the enthalpy of reaction given by Eq. (5.28):

$$-\Delta h_\mathrm{R}(T_0) = \frac{\dot{m}_g}{\dot{m}_B}\, h_g(T_0) - \; h_B(T_0) - \lambda\, L_A^+\, h_A(T_0) \tag{5.28}$$

Here, the value of the enthalpy of reaction $\Delta h_\mathrm{R}\,(T_0) < 0$, because all combustion processes are exothermic reactions, which means that the energy is being released to the environment. From another side, the heat of combustion (known as heating value) is equal to the enthalpy of reaction but with opposite sign [Turns et al., 1996]:

$$-\Delta h_\mathrm{R}(T_0) = H_L(T_0) \tag{5.29}$$

Assuming the case where none of the water in the solid fuel is assumed to condense, the lower heating value of a wet biomass solid fuel can be given by [Karl, 2012]:

$$H_L = H_{U,\mathrm{wf}}\,(1-\gamma_\mathrm{w}) - \mu_\mathrm{w}^\mathrm{g}\,\Delta h_v^\mathrm{w} \tag{5.30}$$

where $H_{U,\mathrm{wf}}$ is the higher heating value (water-free) in [kJ/kg] and $\Delta h_v^\mathrm{w} = 2441,7$ in [kJ/kg] is the enthalpy of vaporization of water. With the water fraction $\mu_\mathrm{w}^\mathrm{g}$ in the gas phase given by:

$$\mu_\mathrm{w}^\mathrm{g} = \frac{m_{\mathrm{H_2O}}^\mathrm{g}}{m_\mathrm{B}} = \gamma_{H_2}\,\frac{M_{\mathrm{H_2O}}}{M_{\mathrm{H_2}}}\,(1-\gamma_\mathrm{w}) + \gamma_\mathrm{w} \tag{5.31}$$

The higher calorific value (water-free) $H_{U,\mathrm{wf}}$ in [kJ/kg] of the solid fuel can be approximated by the following empirical equation [Döring, 2010]:

$$H_{U,\mathrm{wf}} = 1.87\,\gamma_\mathrm{C}^2 - 144\,\gamma_\mathrm{C} + 2802\,\gamma_\mathrm{H} + 36.8\,\gamma_\mathrm{C}\gamma_\mathrm{H} + 129\gamma_\mathrm{N} + 20147 \tag{5.32}$$

Here, it should be noted that the lower calorific value and the upper calorific value of solid fuel are both characteristic properties of the solid fuel and do not depend on whether the oxidizer used is oxygen in air, or the combustion is accomplished with an excess of air [Langeheinecke et al., 1993].

The substraction of Eq. (5.27) from Eq. (5.28) gives [Baehr and Kabelac, 2012]:

$$-q = h'(T,\lambda) + h''(T,\lambda) \tag{5.33}$$

with

$$h'(T,\lambda) = H_L(T_0) + \lambda\,L_\mathrm{A}^+\,[h_\mathrm{A}(T_\mathrm{A}) - h_\mathrm{A}(T_0)] + [h_\mathrm{B}(T_B) - h_\mathrm{B}(T_0)] \tag{5.34}$$

$$h''(T,\lambda) = \frac{\dot m_\mathrm{g}}{\dot m_\mathrm{B}}\,[h_\mathrm{g}(T_\mathrm{g}) - h_\mathrm{g}(T_0)] \tag{5.35}$$

The enthalpy difference between two states and at the same pressure can be defined as [Windisch, 2014]:

$$h(T_1) - h(T_2) = \int_{T_1}^{T_2} c_p(T)dT = \bar c_p\,(T_2 - T_1) \tag{5.36}$$

Hence, Eq. (5.34) and Eq. (5.35) can be reformulated as follows:

$$h'(T,\lambda) = H_L(T_0) + \lambda\,L_\mathrm{A}^+\,\bar c_{p,A}(T_\mathrm{A} - T_0) + \bar c_{p,\mathrm{B}}(T_B - T_0) \tag{5.37}$$

$$h''(T,\lambda) = \frac{\dot m_\mathrm{g}}{\dot m_\mathrm{B}}\,[\bar c_{p,\mathrm{g}}(T_\mathrm{g} - T_0)] \tag{5.38}$$

Adiabatic gas temperature

The adiabatic gas temperature is an idealistic situation where there will be no heat dissipation to the surrounding and all the energy released from the combustion is used to heat the gas products [McAllister et al., 2011],[Baukal Jr, 2012]. Therewith, the heat flow $q = 0$ and Eq. (5.33) can be given by:

$$h'(T,\lambda) = h''(T,\lambda) \tag{5.39}$$

Replacing Eqs. (5.37) and (5.38) in Eq. (5.39), and taking into account Eq. (5.20), derived in Subsection 5.3.1 for the flue gas mass flow, the adiabatic gas temperature T_g^{ad} [K] can be given by:

$$T_g^{ad} = T_0 + \frac{1}{\bar{c}_{p,g}} \left[\frac{\dot{m}_\mathrm{B} H_L + \lambda\, L_\mathrm{A}^+ \dot{m}_\mathrm{B} \bar{c}_{p,A} (T_\mathrm{A} - T_0) + \dot{m}_\mathrm{B} \bar{c}_{p,\mathrm{B}} (T_\mathrm{B} - T_0)}{(1 + \lambda L_A^+)\, \dot{m}_\mathrm{B}} \right] \tag{5.40}$$

Usually, the solid fuel inlet temperature is assumed to be equal to the standard temperature $T_0 = 25$ °C. Therefore, Eq. (5.40) can be further simplified to:

$$T_g^{ad} = T_0 + \frac{1}{\bar{c}_{p,g}} \left[\frac{H_L + \lambda\, L_\mathrm{A}^+ \bar{c}_{p,A} (T_\mathrm{A} - T_0)}{(1 + \lambda L_A^+)} \right] \tag{5.41}$$

As it can be seen from Eq. (5.41), the adiabatic temperature depends on the lower calorific value of the fuel H_L, the excess air λ and the air temperature T_A. Table 5.1 illustrates the value of the adiabatic temperature for different fuel types and under a stoichiometric combustion regime.

Table 5.1: Example of adiabatic temperature and minimum required air for different fuel types ($\lambda = 1$ and $T_0 = 0$ °C) [Karl, 2012].

Fuel type	Calorific value H_L in [kJ/kg]	Minimum air requirement L_A^+ in [$\mathrm{kg_A/kg_B}$]	Specific heat capacity $\bar{c}_{p,g}$ in [kJ/kg.K]	adiabatic temperature T_g^{ad} in [°C]
Methan (with air)	50015	17.19	1.35	2041
Bituminous coal	31.3-33.7	10.6-11.2	1.24-1.28	2120-2220
Lignite (dry)	25.7-28.7	8.6-9.5	1.28-1.29	2080-2180
Lignite ($\gamma_\mathrm{w} = 50\%$)	12.8-14.3	4.3-4.8	1.32-1.35	1630-1720
Wood chips ($\gamma_\mathrm{w} = 15\%$)	15535	5.1	1.32	1941
Wood chips ($\gamma_\mathrm{w} = 30\%$)	12370	4.2	1.34	1772
Wood chips ($\gamma_\mathrm{w} = 50\%$)	8150	3.0	1.37	1479

Additionally, the influence of both air temperature and excess air on combustion temperature in a furnace is shown in the so called h-t diagram (see Figure 5.6b). If the excess air inside the combustion furnace is increased to the value λ_2, this will lead to a decrease in the value of the adiabatic temperature T_{ad_2}, in comparison to the reference case where the furnace is fired with an excess air λ_1. The reason of such decrease is clearly the extra amount of air, which will introduce a cooling effect inside the combustion furnace. Also, by increasing the primary air temperature, the adiabatic temperature can be increased.

Non-adiabatic gas temperature

As it can clearly be seen from Figure 5.6a, adiabatic temperature is only attained if there is no heat flow to the surrounding, i.e. $-q = 0$, but such idealistic case is not realizable, as there will be present energy losses out of the combustion chamber, which will be thoroughly treated in Subsection 5.3.3. Therefore, only the gas

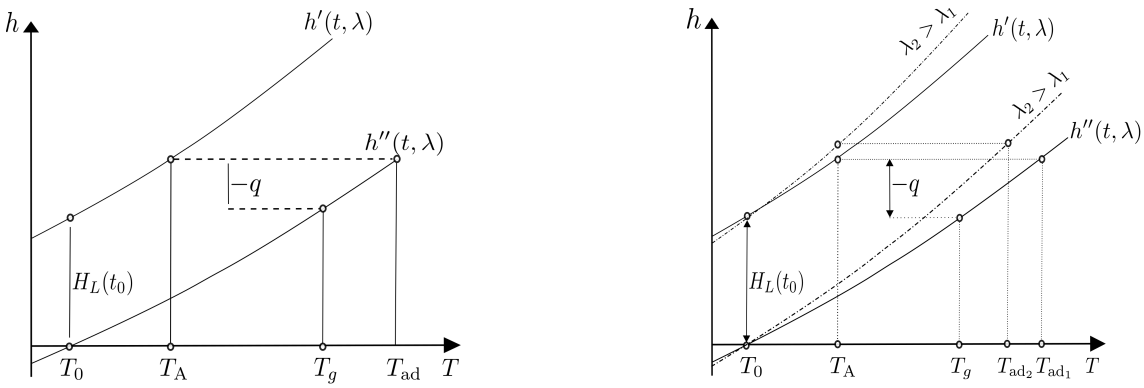

(a) fixed excess air λ_1. **(b)** $\lambda_2 > \lambda_1$.

Figure 5.6: h,T-Diagram for combustion process [Baehr and Kabelac, 2012].

temperature T_g will be achieved in reality, and the inclusion of energy loss term $\dot{Q}^{\mathcal{L}}$ in Eq. (5.41) is straightforward and leads to:

$$T_{\mathrm{g}} = T_0 + \frac{1}{\bar{c}_{p,g}} \left[\frac{H_L + \lambda\, L_{\mathrm{A}}^{+} \bar{c}_{p,A}(T_{\mathrm{A}} - T_0) - \dfrac{\dot{Q}^{\mathcal{L}}}{\dot{m}_{\mathrm{B}}}}{(1 + \lambda L_A^{+})} \right] \tag{5.42}$$

Here, the energy loss $\dot{Q}^{\mathcal{L}}$ out of the system, which is defined as the unused part of the fuel input energy and includes also other heat transfer losses to the surroundings, is hard to measure in reality and it will be estimated based on the definition of furnace and boiler efficiencies using so called direct/indirect methods for this purpose [Vakkilainen and Ahtila, 2011],[Karl, 2012].

5.3.3 Combustion and boiler efficiencies

The exploitation of the chemical latent energy in the combustion process leads to the release of a considerable amount of energy in the form of heat. A maximum heat flow will be achieved, if there is no heat exchange with the environment, and the furnace is assumed perfectly isolated. As a consequence, the maximum temperature of the reactants is achieved, which was referred to as the adiabatic temperature, and the largest amount of useful thermal heat flow is captured, if the flue gas temperature at the exit is cooled down to the ambient temperature. Unfortunately, such a case is impossible, since all industrial combustion processes are notoriously leaky for many reasons [Baukal Jr, 2012].

One of these reason was already mentioned in Subsection 5.3.2, namely the intimate effect of excess air on the adiabatic temperature. Ideally, the combustion furnace should be supplied only with the right amount of combustion air, but due to the imperfect mixing between the oxidizer and the solid fuel, an extra amount of air is added to achieve complete burnout of the solid fuel. The excess air will cool down the temperature inside the combustion chamber, because a part of the thermal energy released will be used to heat this extra amount of air from its initial temperature to the combustion gas temperature. Therefore, the right amount of excess air should be selected in order not to compromise the thermal efficiency of the furnace.

Another cause of heat leakage in the combustion system is the energy loss at the stack, referred to as "the flue gas heat loss", which is typically the largest source of energy waste [Dolezal, 1985],[Morvay and Gvozdenac, 2008],[Niessen, 2010]. This type of loss stems from the combustion gas that escapes the furnace with a considerably high exit temperature, that can range from 120 up to 160 °C for large-scale firing units [Baehr and Kabelac, 2012], which is clearly higher than the ambient temperature. Hence, the heat contained in the exhaust gas is a wasted energy [Morvay and Gvozdenac, 2008]. The loss can range from 4-10% [Dolezal, 1985] or 5-15% of the fuel input energy according to Baehr and Kabelac [Baehr and Kabelac, 2012].

Moreover, the heat loss can stem from the incomplete combustion of gaseous species in the stack gas such as: CO, H_2, which appears as a result of low temperatures in the different combustion zones on the grate-firing unit, as well as the improper oxidation and mixing conditions. Therefore, for combustion to proceed to completion, high temperatures and high oxidation reaction is necessary [Niessen, 2010]. Together with the rest of carbon that exits the furnace with ash without being burned, these two ways of heat loss make 1% from the total fuel calorific value as reported in Baehr and Kabelac [Baehr and Kabelac, 2012]. [Morvay and Gvozdenac, 2008] presume that the unburned carbon loss is expected to be less than 0.5% of the total fuel input energy .

The last category of heat loss in a furnace is the radiation loss, including other heat transfer related losses, namely via convection and conduction mechanisms. Such losses occur as result of the heat transfer from the internal areas of the furnace to the environment, or due to the present opening in the furnace enclosure [Niessen, 2010], and are strongly interrelated to the physical design of the furnace, as well as its insulation. This type of loss is hard to measure in reality but it can be deduced from empirical values and tables [Morvay and Gvozdenac, 2008]. Fortunately, for large-scale power plants this loss is minimal and a value of 0.5% is considered to be a good approximation of its value according to EN 12953-11 standards [EN 12953-11, 2003],[Baehr and Kabelac, 2012], since most of the state-of-the-art grate-firing plants have refractory lining with water-cooled walls, which allows for an efficient heat recovery. A summary of all energy flows entering and leaving the furnace is shown in Figure 5.7.

Combustion efficiency

It has been already mentioned that in order to extract a maximum amount of energy from burning the solid biomass fuel, the flue gas outlet temperature has to be cooled down to the standard temperature. In reality, the flue gas escapes at a very elevated temperature, meaning that a fraction of the fuel's total input energy will remain unused. Consequently, the arising energy leakage was called the flue gas loss, which is the major energy leakage in a power plant [Morvay and Gvozdenac, 2008],[Spliethoff, 2010],[Vakkilainen and Ahtila, 2011].

Therefore, the flue gas loss, according to the above description and assuming that the energy carried with combustion air is negligible in comparison to the energy

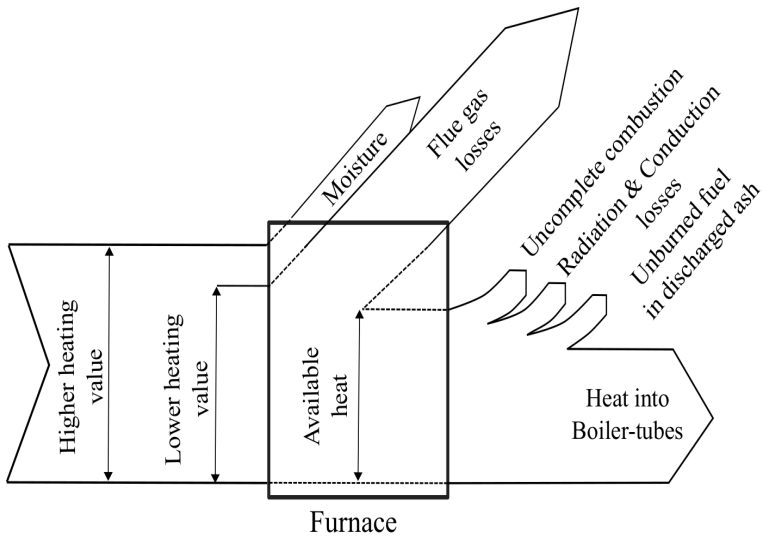

Figure 5.7: Sankey diagram of energy flows entering and leaving the system (adapted from [Baukal Jr, 2012]).

released from burning the solid fuel, can be analytically given by Eq. (5.43):

$$q_{\mathrm{fg}}^{\mathcal{L}} = H_L(T_0) - (-q) = h''(T_{\mathrm{fg}}, \lambda) \tag{5.43}$$

The combustion efficiency η_F [-], defined as the ratio of the extracted heat from burning the solid fuel over the lower calorific value of the fuel, leads to the evaluation of the combustion efficiency, which is given by [Baehr and Kabelac, 2012]:

$$\eta_F = \frac{-q}{H_L(T_0)} = 1 - \frac{q_{\mathrm{fg}}^{\mathcal{L}}}{H_L(T_0)} \simeq 1 - \frac{h''(T_{\mathrm{fg}}, \lambda)}{H_L(T_0)} \tag{5.44}$$

Boiler efficiency

On the contrary to the combustion (furnace) efficiency, that takes into account only the flue gas loss in its computation, the boiler efficiency includes other losses such as: chemical loss from the incomplete combustion, radiation (including convection and thermal conduction) loss, and unburned fuel fraction in the ash.

Similar to the definition of combustion efficiency, the boiler efficiency is defined as the ratio between the effective (net) energy $\dot{Q}_N$ in [W] that will go to the heat sink, here the boiler water-tubes for steam generation, and the total energy carried with the the solid fuel, i.e., the calorific value of the biomass solid fuel. Therefore, the boiler efficiency can be described as follows [Baehr and Kabelac, 2012]:

$$\eta_B = \frac{\dot{Q}_N}{\dot{m}_{\mathrm{B}} \cdot H_L(T_0)} = \frac{|\dot{Q}| - |\dot{Q}^{\mathcal{L}}|}{\dot{m}_{\mathrm{B}} \cdot H_L(T_0)} \tag{5.45}$$

with

$$|\dot{Q}| = \dot{m}_{\mathrm{B}}\,(-q) \tag{5.46a}$$

$$|\dot{Q}^{\mathrm{L}}| = \dot{m}_{\mathrm{B}}\,|q_{\mathrm{Rest}}^{\mathcal{L}}| \tag{5.46b}$$

By taking into account Eq. (5.43), and substituting Eqs. (5.46a)-(5.46b) into Eq. (5.45), the boiler efficiency can be re-formulated as follows:

$$\eta_B = 1 - \frac{q_{\text{fg}}^{\mathcal{L}}}{H_L(T_0)} - \frac{|q_{\text{Rest}}^{\mathcal{L}}|}{H_L(T_0)} = \eta_F - \frac{|q_{\text{Rest}}^{\mathcal{L}}|}{H_L(T_0)} \tag{5.47}$$

As it can be concluded from Eq. (5.47), the boiler efficiency is less than the combustion efficiency. With a good furnace insulation and complete combustion, in such a way that no carbon will remain in the ash, the boiler efficiency value will be very close to the value reported for the combustion efficiency, i.e., $\eta_B \simeq \eta_F$ [Kaltschmitt et al., 2009].

Efficiencies estimation using indirect method

In literature, two practical procedures for estimating and evaluating the efficiency in a combustion power plant are reported as per ASME performance test code PTC 4-2008 standard [ASME PTC 4-2008 , 2009]:

- Direct (input/output) method.
- Indirect (energy balance) method.

Efficiency evaluation by direct method requires the measurement of the input energy, that is the biomass flow rate, its calorific value, and the useful energy absorbed by the working fluid (water) for steam generation. Usually, the useful energy, when using direct method, is quantified in terms of the steam mass flow rate leaving the unit times the enthalpy difference between steam leaving the unit and the feedwater enthalpy [Abbi, 2012].

Consequently, necessary measurements have to be made such as: temperature and pressure and flow rate of steam as well as the boiler feedwater. As a consequence, significant errors will be introduced due to the instrumentation and fuel flow determination uncertainties, which limit its applicability [Petrecca, 2012], as it will be shown subsequently.

The indirect method, sometimes also referred to as heat-losses method, consists of the determination of all type of individual losses, which occur out of the furnace control volume, and contribute to efficiency degradation. These losses are relative to the total fuel input energy, and therefore their values are usually expressed in percentage. The major types of energy leakage in a power plant have already been reassessed in Subsection 5.3.3, with the dominant loss being associated with the flue gas leaving the stack. By adding the value of each individual loss and subtracting total losses from the the total fuel energy input, the efficiency (boiler) can be evaluated [Morvay and Gvozdenac, 2008].

The indirect method is considered to be more preferable and more accurate method when estimating both the furnace and boiler efficiencies, because primary measurements in flue gas and its temperature can be made accurately, in comparison to the direct method, where the uncertainty in efficiency calculation is proportional to the

measurements error and the associated uncertainties in the determination of variables of interest, such as for instance the fuel mass flow rate [Abbi, 2012]. For example, if the total loss, when using indirect method, is 10% of the total input energy, a 1% measurement error will results in 0.1% error in efficiency, whereas 1% error in fuel flow measurement results in 1% error in efficiency calculation [ASME PTC 4-2008 , 2009].

Table 5.2 shows different values of uncertainty when using direct and the indirect method to determine the boiler efficiency for different combustion systems for steam generation.

Table 5.2: Uncertainties in efficiency for different firing systems according to ASME performance test [ASME PTC 4-2008 , 2009].

Type of firing system	Indirect method [%]	direct method [%]
Utility/Large Industrial		
Coal fired	0.4-0.8	3.0-6.0
Oil fired	0.2-0.4	1.0
Gas fired	0.2-0.4	1.0
Fluidized bed	0.9-1.3	3.0-6.0

As it can be deduced from Table 5.2, the uncertainty is higher when using the direct method than in the indirect case. Another striking fact is that the uncertainties in efficiency computation are higher in both coal-fired and fluidized-bed in comparison to other firing systems for direct method, because of large uncertainties in the solid fuel mass flow rate measurements. This is due to the bulk density and the volumetric feeding of the fuel, that vary between the different batches fed into the furnace [Abbi, 2012], which is clearly the same case when using a biomass grate-firing system for power generation. Therefore, using the direct method is not recommended when estimating the boiler efficiency. Hence, it is wise to use an indirect method for this purpose.

In [Nussbaumer and Good, 1994], a simple, yet, accurate indirect method was proposed, for the determination of the efficiencies of biomass combustion plants and for different operation modes. The method is claimed to deliver the same result as the one defined in DIN 4702 standard [Kaltschmitt et al., 2009].

To this extent, the method requires the following measurements to be made:

- Percentage of O_2, CO_2, and CO concentrations in the flue gas.
- Flue gas temperature at the boiler exit (T_{fg}).
- Ambient air temperature (T_0).

For consistency reasons, the losses due to incomplete combustion will be included in the computation of the furnace (combustion) efficiency. This is in contrast to Eq.

(5.44), where only flue gas losses are taken into account. In the range of [CO] < 0.5 Vol.-%, [CO_2] > 5 Vol.-%, and flue gas temperature 400°C, the furnace efficiency of a biomass combustion plant is determined as follows [Nussbaumer and Good, 1994]:

$$\eta_F = 1 - \frac{q_{\text{fg}}^{\mathcal{L}}}{H_L(T_0)} - \frac{q_{\text{ch}}^{\mathcal{L}}}{H_L(T_0)} = 1 - \mathcal{L}_{\text{fg}} - \mathcal{L}_{\text{ch}} \tag{5.48}$$

With the thermal loss due to the escaped heat with flue gas is given by:

$$\mathcal{L}_{\text{fg}} = \frac{q_{\text{fg}}^{\mathcal{L}}}{H_L(T_0)} = 0.01 \frac{(T_{\text{fg}} - T_0)\left[1.39 + \dfrac{122}{[\text{CO}_2] + [\text{CO}]}\right] + 0.02\, y}{\dfrac{H_L}{100} - 0.2442\, y} \tag{5.49}$$

The humidity of the fuel y [-] is interrelated to the water content of the biomass fuel as follows [Karl, 2012]:

$$y = \frac{\gamma_{\text{w}}}{1 - \gamma_{\text{w}}} \tag{5.50}$$

Similarly, in the range of [CO] < 0.5 Vol.-%, [CO_2] > 5 Vol.-%, and flue gas temperature 400°C, the chemical losses by incomplete combustion is given by Eq (5.51):

$$\mathcal{L}_{\text{ch}} = \frac{[\text{CO}]}{[\text{CO}_2] + [\text{CO}]} \frac{11800}{\dfrac{H_L}{100} - 0.25\, y} \tag{5.51}$$

In case only the O_2-concentration is measured instead of CO_2-concentration in the flue gas, the latter can be computed by the following equation :

$$[\text{CO}_2] = 0.98\,(21 - [\text{O}_2]) - 0.61\,[\text{CO}] \tag{5.52}$$

Consequently, the boiler efficiency can be estimated by Eq. (5.53):

$$\eta_B = \eta_F - \mathcal{L}_{\text{rest}} \tag{5.53}$$

with

$$\mathcal{L}_{\text{Rest}} = \frac{|q_{\text{Rest}}^{\mathcal{L}}|}{H_L} = \mathcal{L}_{\text{rad}} + \mathcal{L}_{unburned} \tag{5.54}$$

Finally, the estimated useful thermal energy released from burning the biomass fuel $\dot{Q}_N$ in [W], can be given by:

$$\dot{Q}_N = \eta_B \cdot \dot{m}_{\text{B}} \cdot H_L(T_0) \tag{5.55}$$

Eq. (5.55) connects the static combustion model with the steam-boiler model, since the released thermal power will go to the boiler-tubes for an efficient heat transfer to produce steam.

This concludes the discussion of the static combustion model part, and calls for the treatment of the second building block of the soft-sensor (see Figure 5.1), that is the concept of estimating the biomass fuel calorific value, which will be the main focus of Section 5.4, using the dynamic model of steam-boiler discussed in Section 4.4.

5.4 Fuel calorific value monitoring

As mentioned earlier in this chapter, a decisive variable, when operating the biomass heat recovery power plant, is the biomass calorific value, which often fluctuates between the different batches delivered to the furnace, due to harvesting, storing and transport conditions [Yin et al., 2008]. Consequently, the operation of the grate-firing unit will be complicated as a result of the uncertainty introduced by the solid fuel moisture content and its quality, which could compromise the plant's lifetime and may result in a degraded overall conversion efficiency of the biomass solid fuel.

Hence, it will be advantageous, from a control point of view, to monitor online this value and at high frequent resolution (seconds or minutes) to effectively control the combustion-air system and the biomass feed rate into the furnace. Hence, maximizing and stabilizing the combustion process, leading to a better energy conversion performance [Ruusunen, 2008],[Hermansson et al., 2011].

In this section, a new developed sensor, that aims at estimating the energetic value and the moisture content of the solid fuel in a biomass combustion power plant, will be presented. At the core of the concept lies a dynamic steam-boiler model for steam prediction based on the released thermal power from the furnace side, which is strongly impacted by the moisture content of the wet solid fuel. By considering both measured and predicted steam values, the fuel moisture content is estimated using an optimization-based scheme. As it will be shown, the obtained result from this step will allow for the approximation of the fuel calorific value of the wet solid fuel in the biomass-fired power plant, inasmuch as both water content and the calorific value are linearly interrelated with each other, i.e., if the value of one variable is known the other can be inferred from it.

5.4.1 The monitoring approach

Depending on the water fraction, the exsiccation phase of the wet biomass fuel will have a strong influence on the amount of released thermal energy during the combustion of biomass on the moving grate, as a result of the linear dependency of the calorific value on the extrinsic moisture content of the fuel. Increasing the moisture content will reduce the maximum possible combustion temperature, and will limit the radiative and convective heat transfer to the boiler-tubes. As consequence, the generated steam amount will be reduced.

Referring to the molecular formula $CH_{1.44}O_{0.6}$ of wood biomass, which is equivalent to a fuel composition with 50% C, 44% O, and 6% H, and for $H_{U,\mathrm{wf}} = 19.935$ MJ/kg [Dahlquist, 2013a], the Eq. (5.30), which relates the usable heating energy (calorific value) to the moisture content of the fuel, can be further simplified to:

$$H_L = (18.7 - 21.1 \cdot \gamma_{\mathrm{w}}).10^3 \tag{5.56}$$

where H_L is the lower heating value of the fuel in [kJ/kg], and γ_{w} is the moisture fraction in the fuel in [$\mathrm{kg_{H_2O}/kg_B}$].

Therefore, if the moisture fraction is monitored on-line, the calorific value of the solid biomass can be well approximated by using this equation.

Figure 5.8 illustrates the linear dependency between these two variables and for different types of biofuels compared to woody biomass. An increase in the moisture content, due to for example the transport conditions, will decrease the energy content of the fuel, and vice versa. Hence, it will be suitable if the fuel is dried prior to its dosage into the furnace in order to increase its calorific value [Koppejan and Van Loo, 2012].

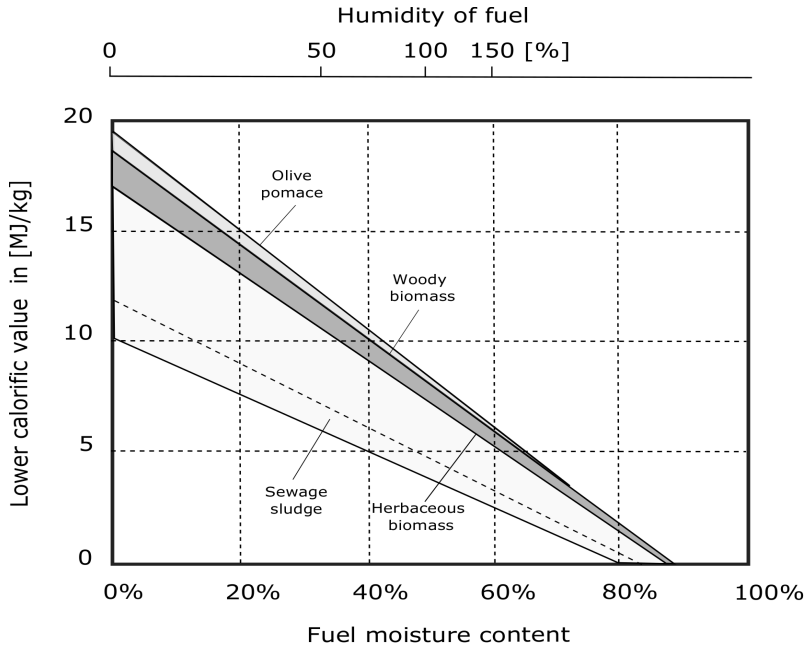

Figure 5.8: Dependency of calorific value on the moisture content (adapted from [Karl, 2012]).

Since the released thermal energy is interrelated to the calorific value of the fuel, as can be shown by Eq. (5.55), a decrease or increase in the value of the latter will be followed also by a decrease or increase in the value of the former. As a consequence, the convective heat transfer to the boiler-tubes, which is quantitatively represented by the net released thermal power, will be impacted by the moisture content in the fuel.

The last statement is true, since a part of the released thermal power by burning the solid fuel will be consumed to dry the fresh biomass on the moving grate, which will lead to a decrease in the maximum achievable gas temperature in the furnace and degraded efficiency of the combustion system. Thus, the amount of generated steam will be decreased in proportion to the amount of energy taken to dry the fuel.

Consequently, the last statement in previous paragraph leads to consider both values of measured and predicted steam amount by a dynamic steam-boiler model in order to approximate the water fraction in the biomass solid fuel. This achieved by minimizing the error between the measured steam value from the plant and the predicted one by the steam-boiler dynamic model using a quadratic cost function,

as shown in Eq. (5.57):

$$\min_{\gamma_{\mathrm{w}}} J = |y_{k|k} - \hat{y}_{k|k-1}| \tag{5.57}$$

According to Eq. (5.57), if a new measurement of steam is available $y_{k|k}$ at time instant k, the physical model of the boiler will predict the steam value for the same time instant, i.e., $\hat{y}_{k|k-1}$, using the value of fuel moisture content already computed from the previous step as a warm-start for the current optimization run. When a new process measurement is available at time step $k+1$, the procedure is repeated. The value that minimizes the difference between measured and predicted steam value is assumed to correspond to the fuel moisture content γ_{w}. Hence, the value of the fuel energy content can be approximated by using Eq.(5.56). This concept can be well illustrated by Figure 5.9.

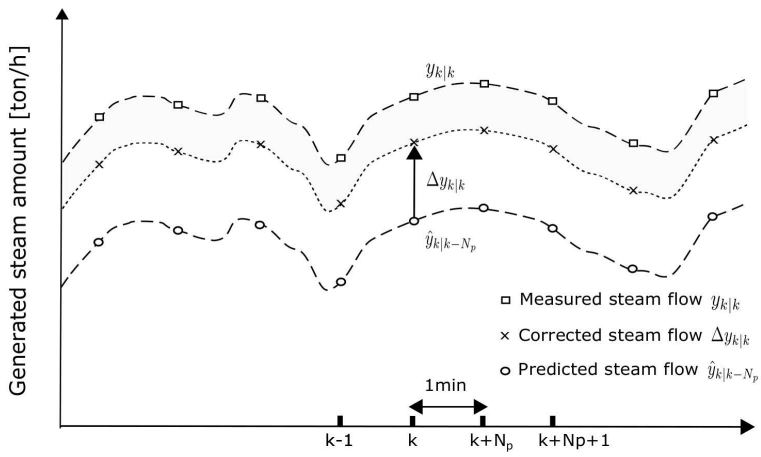

Figure 5.9: Optimization-based concept for approximating the solid biomass energy content in a grate-firing power plant [Belkhir and Frey, 2016b].

Consequently, the discussed concept leads to consider the last "puzzle" piece in developing the soft-sensor for the biomass power plant, which is critical for steam prediction, that is the dynamic model of a natural-circulation boiler for steam generation.

5.4.2 Prediction of steam generated

See Section 4.4.

5.5 Soft-sensor: A schematic overview

It has been demonstrated in this chapter that, by using only a few available process measurements and a mechanistic modeling approach, the calorific value of the biomass feedstock can be conveniently estimated. This allowed for having information about the major source of disturbance for the dynamic model of the grate fired unit developed in the previous chapter. To summarize, Figure 5.10 gives an overview of the different measured process variables and the calculated outputs by the developed soft-sensor, as well as parameters that can be fixed, such as the fuel

chemical composition and the inert fraction, which is obtained based on the monthly average of incombustible materials leaving the furnace.

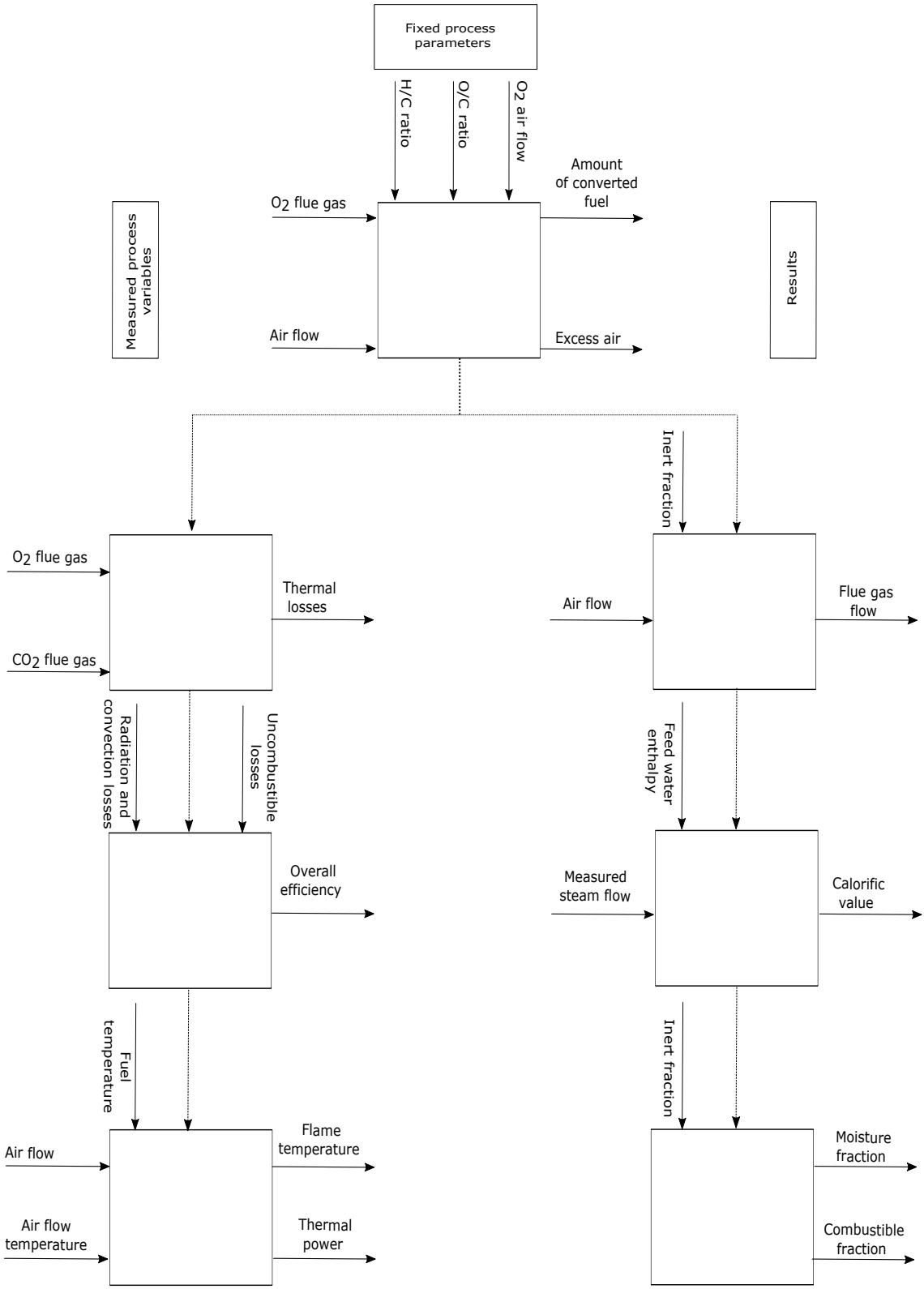

Figure 5.10: A schematic overview of the developed soft-sensor for estimating the calorific value of biomass and other process-related variables (adopted from [Van Kessel et al., 2004a].)

6 Simulation results and discussion

In this chapter, both the developed mathematical model of the biomass grate-fired system and the designed virtual sensor for estimating the energy content of the fuel mix delivered to the furnace will be numerically simulated using the retrieved process measurements from the the historian of the BMK Lünen power plant. As a consequence, the model validity will be achieved by comparing the predicted response by the implemented model against the measured one from the power plant. Additionally, step response experiments applied on the simulation model will be carried out while the system is at a given operating point. Such experiments consist of a step-wise increase in the values of the manipulated variables and observing the corresponding effects on the controlled ones.

6.1 Soft-sensor simulation

The designed soft-sensor in Chapter 5, that aims at estimating the energetic value of the biofuel and other process related variables, will be validated in this section. As already discussed, the sensor is comprised of two interlinked main parts: a static combustion model and a dynamic boiler model for steam prediction. For consistency reasons, the validation part of the latter will be reported in Subsection 6.3.1, but nevertheless, the model, i.e the boiler, will be used in the current section to close the estimation loop (see Figure 5.1).

6.1.1 Static combustion model

The static combustion model is simulated using the industrial data obtained from the biomass combustion power plant. The inputs for the model are: the amount of the atmospheric air (primary $\dot{m}_{\mathrm{pa}}$ and secondary $\dot{m}_{\mathrm{sa}}$) in [TNm^3/h][1], the re-circulation air $\dot{m}_{\mathrm{sa}}$ in [TNm^3/h], as well as the oxygen and carbon dioxide concentrations in [Vol. $-$ %]. The outputs are: the estimated mass flow rate of the wood chips $\dot{m}_{\mathrm{pa}}$ in [t/h], the amount of the total exhaust gas leaving the chimney $\dot{m}_{\mathrm{fg}}$ in [TNm^3/h], the excess air λ [-], the gas temperature T_g in [K], and finally the estimated heat power that $\dot{Q}_N$ in [MW] goes to the boiler section for an efficient heat exchange with the boiler tubes for steam production.

As the primary air is preheated at the current power plant, the water fraction in air can be neglected from the equations that describe the mechanistic model. Also, the variation of water content in the wood chips delivered between the different batches to the furnace is approximated by using Eq. (5.56). The fuel calorific value is obtained from the sensor[2] reading installed at the biomass heat recovery unit and it is used only for monitoring purposes. Therefore, the plausibility of the sensor reading will be verified, altogether with the estimated thermal power, by comparing the measured steam flow against the predicted one from the steam-boiler model

[1] Thousand of norm cubic meter per hour.
[2] The sensor structure is confidential and therefore cannot be discussed.

[Belkhir et al., 2015a].

It is worth mentioning that the amount of fuel burned at the BMK Lünen is unmeasured. Nevertheless, it is thought to be lying in the range of 17 (up to 20 [t/h])[3]. The estimated biomass flow rate fed to the furnace based on the static combustion model discussed in Section 5.3, the measured air amount (primary and secondary), and the measured oxygen fraction in the flue gas is shown in Figure 6.1.

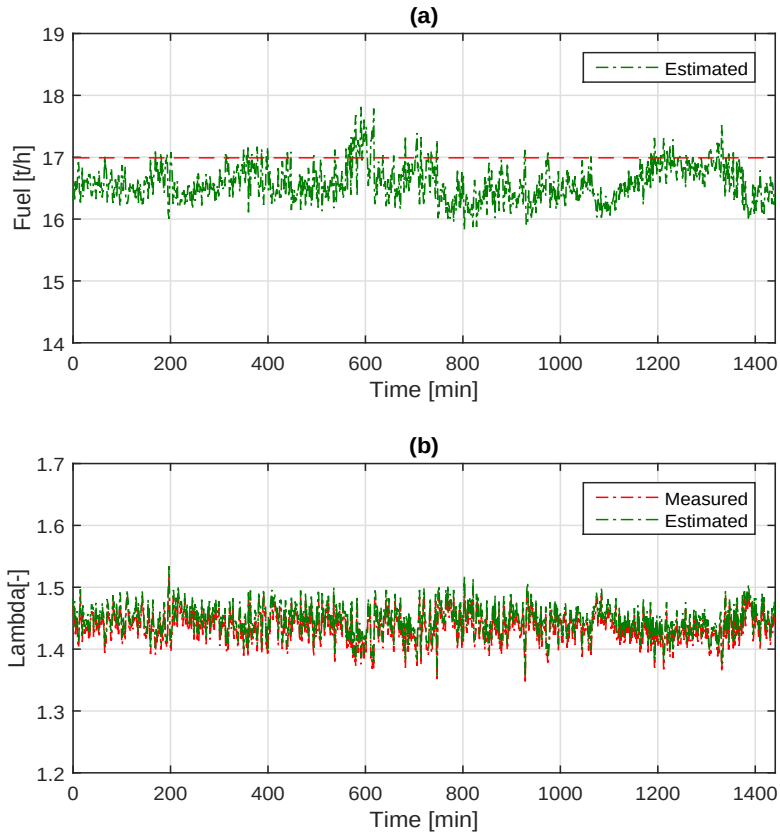

Figure 6.1: Estimated fuel flow rate and excess air by the static model.

As it can be seen from Figure. 6.1, the estimated value for the fuel mass flow by the soft-sensor lies very close to the interval mentioned by the plant operator. Moreover, the excess air λ, which represents the extra amount above the stoichiometric air requirement that has to be added to ensure both the complete thermal degradation of the biofuel and the safe process operations, correlates very well with the biomass flow rate and gas temperature (see Figure 6.2).

A decrease in the excess air indicates that more solid fuel is being fed and burned. Inversely, an increase in the excess air will indicate that a few amount of fuel is being currently burned; hence, more fuel has to be dosed inside the furnace to keep the steam production at the target level of demand.

[3]The mentioned interval is obtained through a personal communication with the plant operator.

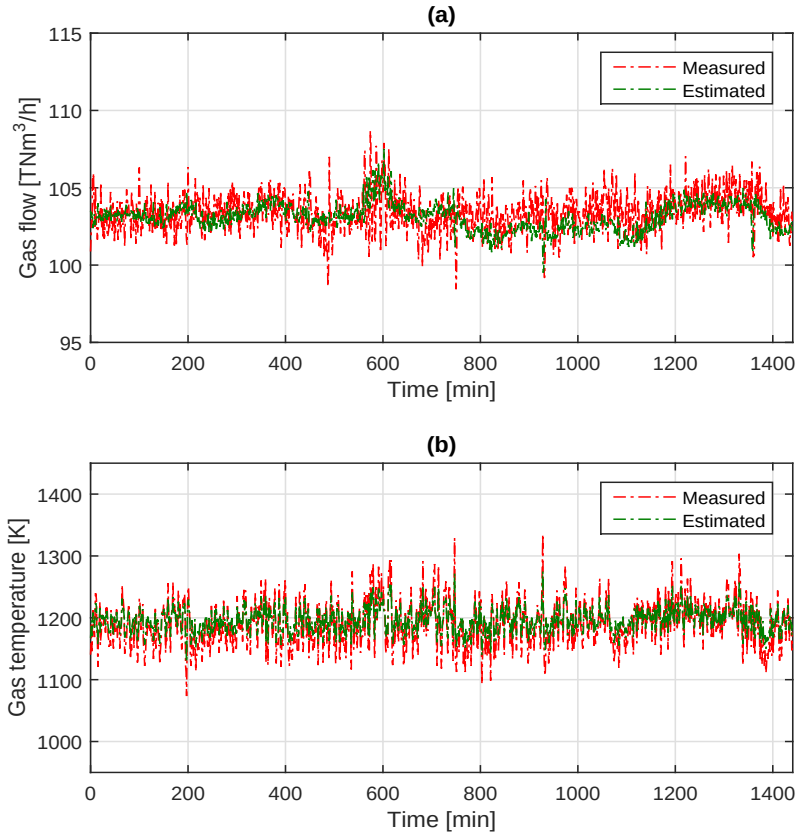

Figure 6.2: Estimated flue gas flow rate and gas phase temperature by the static model.

It can be inferred from Figure 6.2, that an increase or a decrease in the excess air amount will have a direct impact on the furnace temperature, an increase of the former will lead to a decrease of the latter, because extra amount of air will introduce a "cooling-effect" inside the combustion chamber (see also Subsection 5.3.2). In addition to this, an increase in the solid fuel flow rate leads to an increase in the amount of the exhaust gas at the chimney exit, and vice versa, since more fuel is being combusted, and therefore, more gas is being released from the solid bed.

The measured concentration of the carbon monoxide was close to zero, this indicates the good mixing conditions inside the chamber due to the secondary air being dosed in such a way to ensure turbulent mixing in the post-combustion phase, thus, an efficient oxidation of gaseous species is achieved. Consequently, the chemical loss $\mathcal{L}_{\text{ch}}$ by incomplete combustion in Eq. (5.48) can be neglected. Besides this fact, the loss due to incomplete combustion is very small in comparison to the flue gas loss, which is considered to be the major loss in any combustion power plant (see Subsection 5.3.3). Therefore, it can be omitted without introducing a significant error.

The computation of the thermal loss by sensible heat of the flue gas indicates its importance when estimating the overall efficiency (around 7.5%). The percentage of energy loss in a biomass power plant, due to the unburned carbon fraction in

the discharged ash, is difficult to assess in the current plant, but a good approximation of its value can be found in the literature. Generally, the approximate value of the incombustible fraction in the discharged ash is 1% of the total energy Baehr and Kabelac [2012], whereas for the radiation and convection losses, which occur due the heat transfer mechanism from the furnace surface to the surrounding, the chosen value here is 2%. Both the plant efficiency and the released thermal power are shown in Figure 6.3.

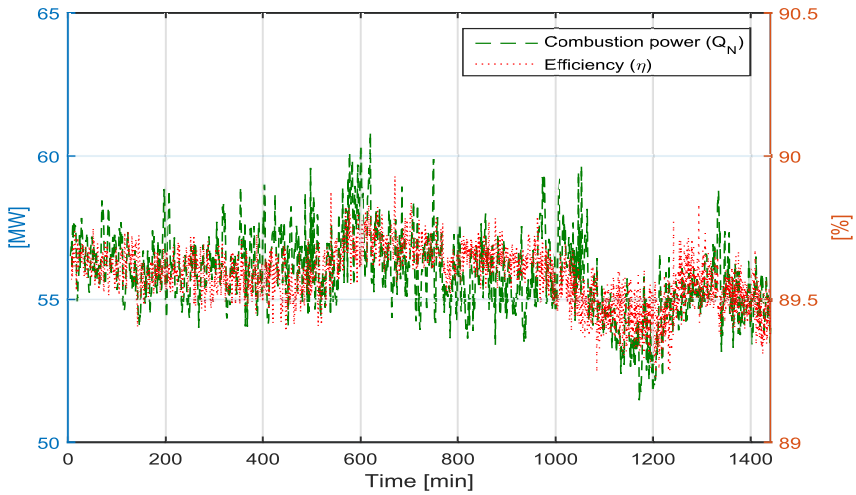

Figure 6.3: The released thermal combustion power and boiler efficiency as estimated by the implemented soft-sensor.

From Figure 6.3, it can be seen that the released thermal power and the efficiency are in correspondence with each other, if the boiler efficiency increases then the released thermal power increases too, and vice versa, an increase of the former is followed by an increase of the latter. Another striking fact, which can be observed from Figure 6.3, is that the boiler efficiency increases when the excess air in the combustion chamber decreases, and it decreases when the excess air increases (see also Figure 6.1). Therefore, it can be concluded that in order to have the most efficient combustion of the biomass fuel in the furnace, a balance between providing the optimal amount of air and the quantity of the provided fuel must be found, as more excess oxygen not consumed during the combustion process absorbs usable heat, and this useful energy will be carried away in the form of a stack loss (flue gas loss), which consequently decreases the plant efficiency.

Finally, the presented "open-loop" concept, shown in Figure 5.1, can be validated in two ways, these are [Van Kessel, 2003]:

1. Comparison of predicted steam production with the measured steam at the current combustion power plant.

2. Comparison of the estimated fuel flow with the measured fuel flow at the current combustion power plant.

As already stated, the biomass fuel flow at the current power plant cannot be measured. Hence, the first alternative is consequently used, since the steam measurements are readily-available in any combustion power plant. Moreover, the steam

measurements are often reliable and accurate. As it can be seen from Figure 6.4, the estimator, i.e. the soft-sensor predicts with a good accuracy the recorded steam amount generated for 10 hours operation of the power plant.

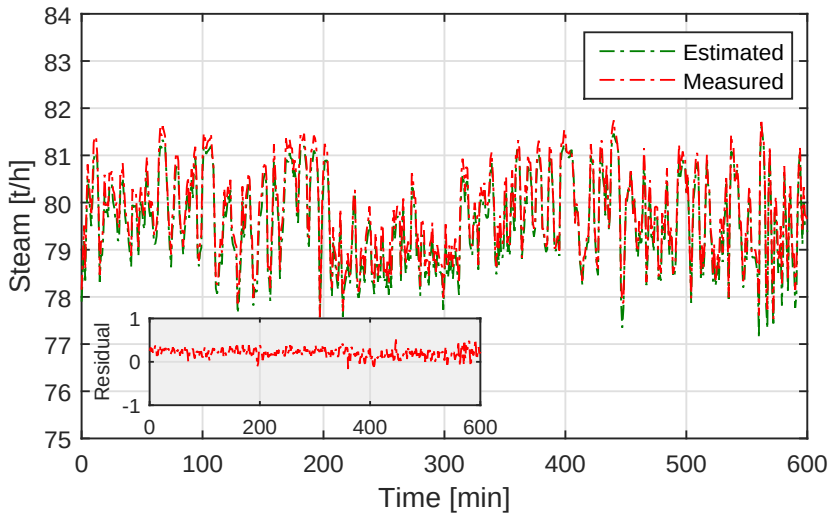

Figure 6.4: Comparison between measured and estimated steam flows.

6.1.2 Calorific value estimation

Knowing the biofuel's calorific value is of a prime interest, since in many operating biomass heat recovery power plants, its exact value is not known or at least could be approximated. Furthermore, even a very simplistic method such as laboratory sampling cannot be performed, due to the delay time introduced from one side, from another side, even if the fuel composition is supposed to be available after performing such an analysis, where many samples are taken to the lab for determining a representative composition of the solid fuel, it will then not be known at what time the analyzed fuel will be fed to the furnace.

It is for this purpose, the soft-sensor is developed for monitoring the fuel's energetic value, as soon as it enters the furnace, preferably within a matter of seconds or minutes, which makes from this a valuable information that can be fed back to the furnace dynamic model, in order to account for the uncertainty caused by the calorific value of the fuel mix, which varies even for the same type of biofuel.

Similar to the previous subsection, the fuel calorific value will be inferred in a "closed-loop" manner using an optimization-based scheme, based on the static combustion model, that estimates the released thermal power from the furnace, which consequently allows for the prediction of the steam amount generated by the steam-boiler dynamic model.

The closed-loop concept presented in Chapter 5, for estimating the fuel's energetic value, is now simulated using a new data set. Figure 6.4 shows the estimated biomass fuel flow based on the measured oxygen concentration in the flue gas and measured amount of air being injected into the combustion chamber.

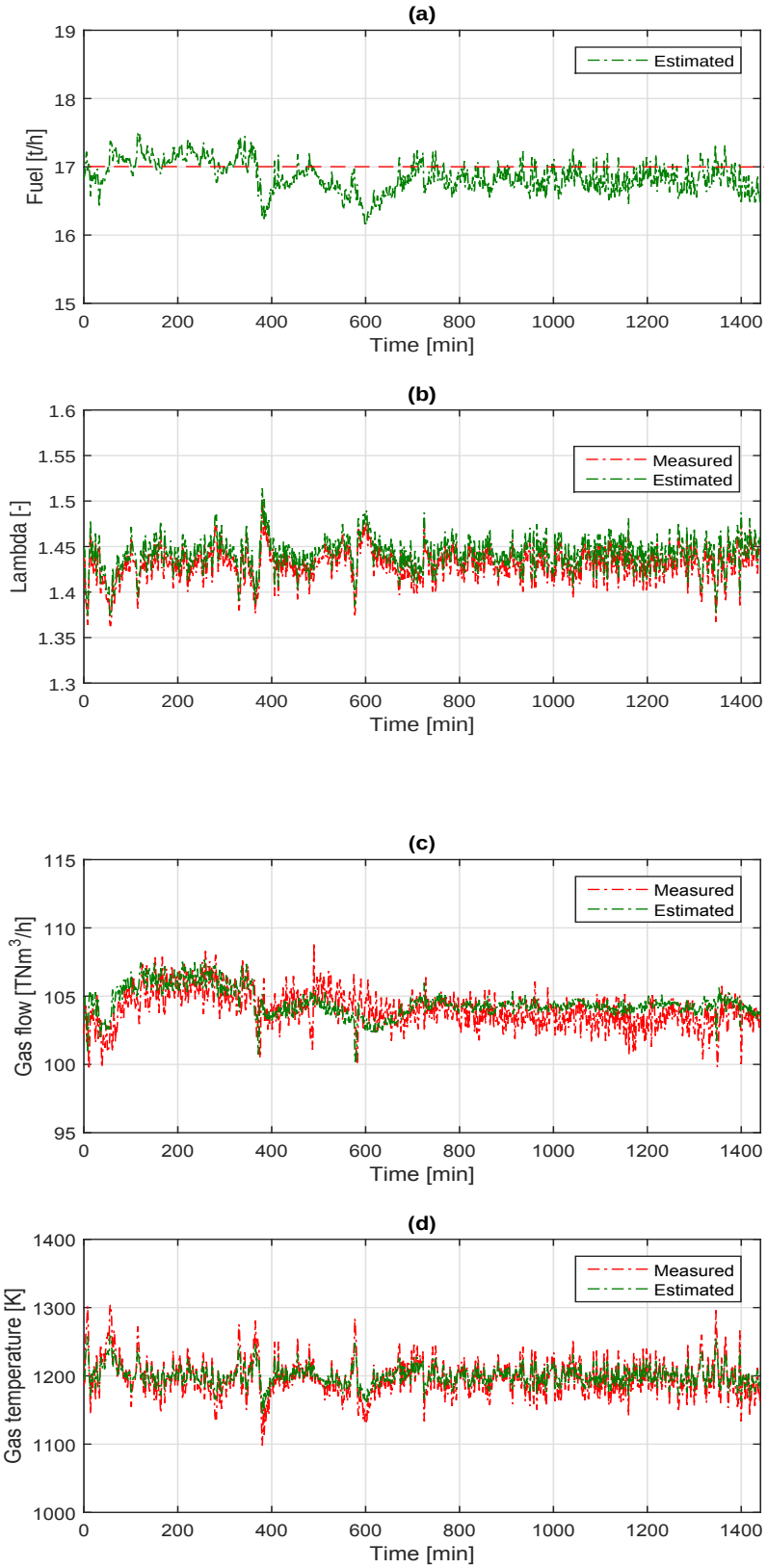

Figure 6.4: Comparison between measured and estimated process data: (a) Fuel flow, (b) excess air, (c) flue gas flow, (d) gas phase temperature (example 1).

Similar to the conducted discussion in Subsection 6.1.1, it can be also seen that the estimated value of the actual biomass flow rate is very close to 17[t/h]. Another fact, which can be readily seen from Figure 6.4; the fuel amount being currently burned inside the furnace is strongly related to the excess air, an increase or a decrease in excess air indicates a decrease or an increase in the fuel amount being fired.

Figure 6.4 (c) and (d) depicts the dynamic evolution of the flue gas flow and the flame temperature. Here, an increase in the flue gas amount can be related to an increase in the fuel amount being burned and the amount of air being injected into the furnace. Again, the flame temperature correlates very well with the excess air. An increase in the excess air leads to a decreasing flame temperature, due to the cooling effect introduced by blowing more air in the furnace and vice versa.

Figure 6.5 shows the estimated calorific value using the optimization-based concept presented in Chapter 5. As mentioned before, the sensor at the current combustion power plant is being used only for monitoring purpose of the energetic value of the biomass fuel. Unfortunately, due to the confidentiality reasons, the sensor structure is classified and therefore cannot be further discussed; however, its dynamic performance will be compared against the soft-sensor implemented in this thesis.

As it can be clearly seen from Figure 6.5, the estimated calorific value is in a good agreement with the measured value obtained from the current biomass heat recovery power plant. The fuel energetic value is around 14.5 [MJ/kg], which consequently indicates that the biomass fuel currently fired has moisture average content close to 20 %, and therefore, the combustible fraction will be around 67 %, since the inert fraction at the current biomass power plant is measured based on a monthly basis and it represents approximately 13%[4] from the total mass being fired.

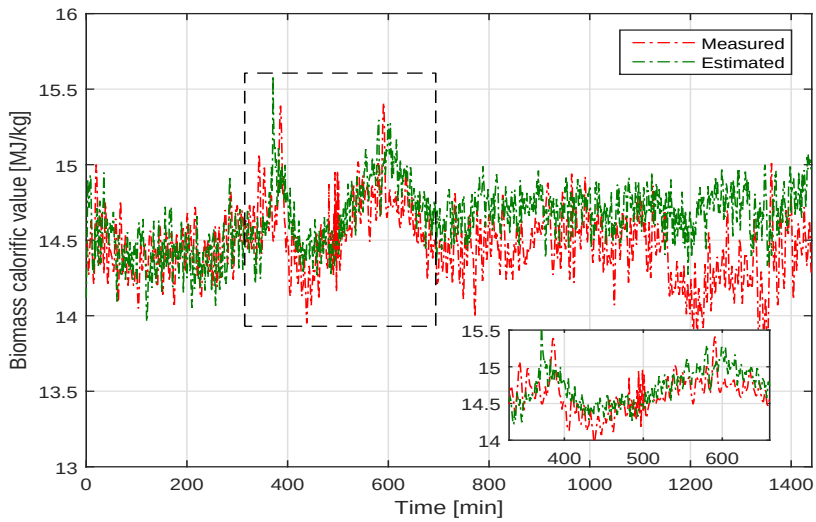

Figure 6.5: Comparison between estimated calorific value and the measured one as obtained from the plant (example 1).

[4]Inert fraction is set to a constant value.

In order to show the practicability of the proposed concept, the estimation loop is run using a new measured data set. The estimated process data is shown in Figure 6.5.

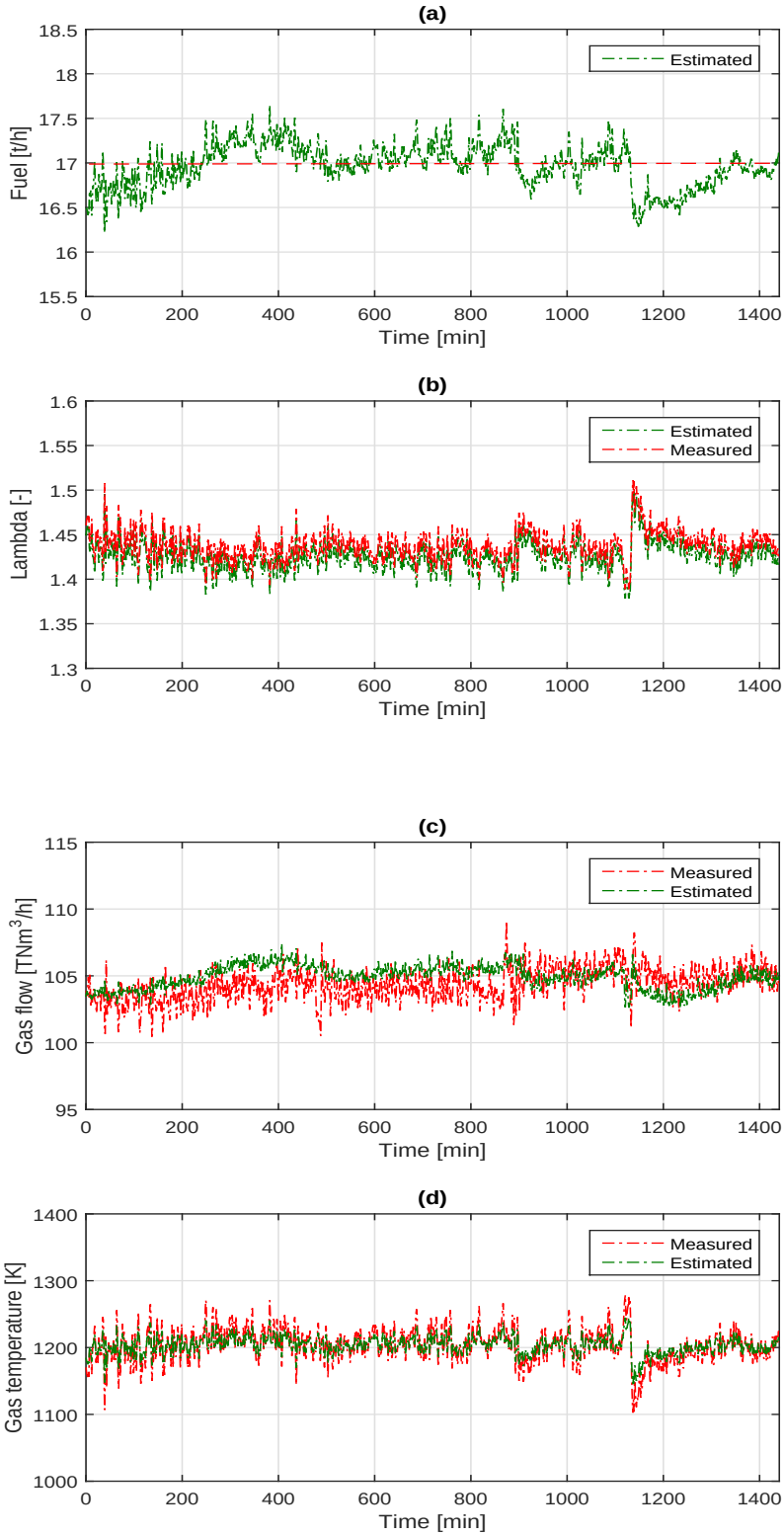

Figure 6.5: Comparison between measured and estimated process data: (a) Fuel flow, (b) excess air, (c) flue gas flow, (d) gas phase temperature (example 2).

Figure 6.6 and Figure 6.7 show again the estimated energetic content of the solid biomass currently being burned inside the furnace. As it can be seen, the estimated value by the soft-sensor follows the dynamics of the measured one with a good accuracy. Here, some outliers and missing data, which can be visibly detected, are present in the measured data obtained from the process database. These outliers are observations which deviate so much from other observations, in a way to arouse suspicions that they were generated by a different mechanism [Hawkins, 1980]. Such a mechanism can be, for example, anomalies due to incorrect reading from hardware instrumentation, transmission to plant data historian, or unusual disturbance.

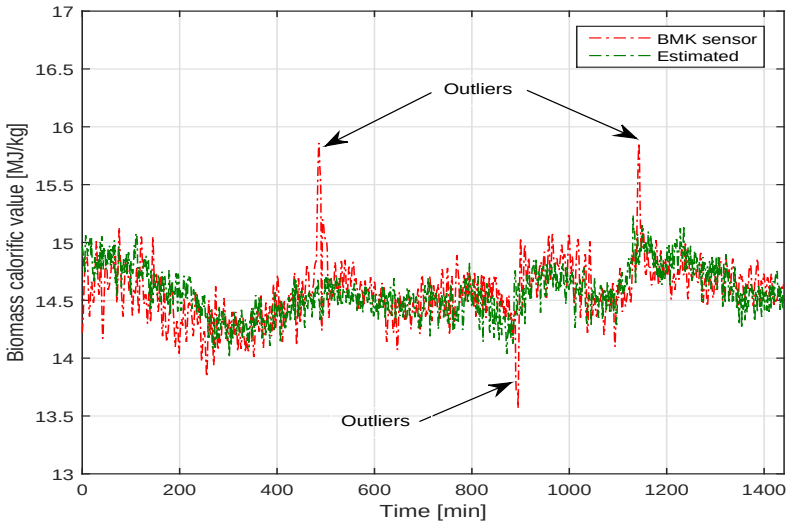

Figure 6.6: Comparison between estimated calorific value and the measured one as obtained from the plant (example 2).

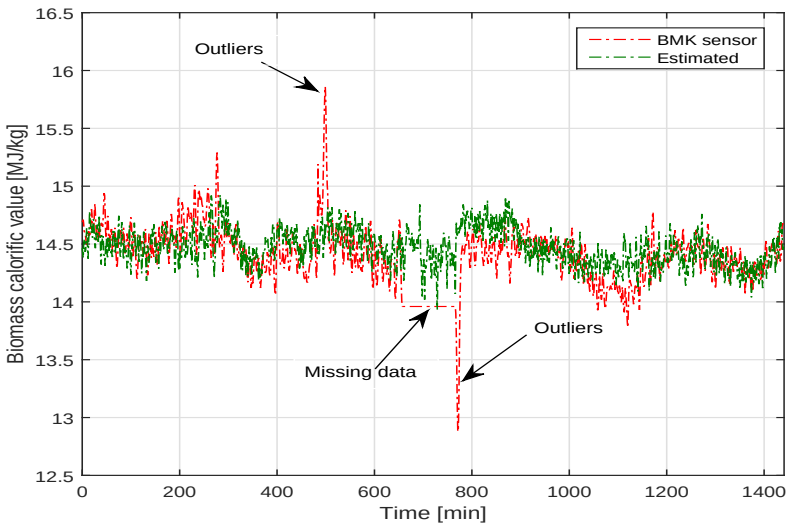

Figure 6.7: Comparison between estimated calorific value and the measured one as obtained from the plant (example 3).

6.1.3 Section summary

The simulation results of the soft-sensor concept in Chapter 5 were presented in this section. To a large extent, the objective was to show the performance of the developed soft-sensor in estimating calorific value of the solid fuel in a biomass heat recovery power plant. This concept was consolidated by means of giving various examples using different collected dataset which were obtained from the data historian.

In contrast to other related works, only a few key process measurements were used to feed in the inferential model. Here, the concept made use of a dynamic steam-boiler model to predict the generated steam amount, based on the estimated value of the released thermal power by a static combustion model from the furnace side, which consequently allowed for the computation of the fuel's energetic value by minimizing the difference between the measured steam value and the predicted one from the dynamic model. This goal was achieved by adopting an optimization-based scheme for this purpose.

As stated previously, the calculated value, which was obtained from minimizing the difference between the measured and predicted steam amount, allowed for the approximation of the energy content of the fuel. Consequently, the prediction of the fuel's calorific value can be achieved within one minute time horizon, since every new process measurement (either steam, or air and oxygen concentration in the flue gas), was available after one minute interval. The comparison of the estimated calorific value and the one obtained from the plant data historian revealed that the soft-sensor was able to track the dynamics of the measured one, and the presence of some anomalies in the measured data such as outliers and missing data, due to either a failure in hardware sensor reading or unusual disturbance. In this thesis, such a problem (missing data) was not present when using the developed soft-sensor for estimating the energy content of the fed biofuel, this might be explained by the few required physical instrumentation readings needed by the soft-sensor to estimate this value.

It was shown that other estimated process data by the implemented soft-sensor, such as the furnace temperature and flue gas flow at the chimney exit, follow the dynamics of their measured counterparts with a good accuracy. Additionally, the soft-sensor was capable of estimating the fuel amount currently fed and burned, which is unmeasured at the power plant. This goal was achieved based on measured air amount and oxygen and carbon dioxide concentration inside the grate-firing furnace. The biomass fuel amount correlated strongly with the oxygen concentration, an increase of the former led to a decrease of the latter and vice versa.

Finally, it can be stated that the implemented soft-sensor is able to leverage the available process measurements to estimate multifarious key process information, some of which cannot be directly measured in the plant, such as the amount of currently burned fuel and process performance indicators such as the thermal efficiency and the total released thermal power. Furthermore, the soft-sensor can be used as a diagnostic tool in order to asses the performance of the already existing physical sensors in the power plant, or can be integrated in a control concept to effectively control the combustion-air system and the biomass feed rate.

6.2 Understanding the plant dynamics

Traditionally and as previously stated, mathematical development for dynamic systems, such as for the biomass heat recovery power plant case, deals with the building of a model, this is achieved in terms of having a set of mathematical equations, which can be manipulated logically in order to answer questions about a given system. Consequently, a next step that follows the modeling part is the simulation part that aims at answering those questions without conducting experiments on the real plant.

To do so, in Section 6.2, step response experiments will be applied on the simulation model while the system is at a given operating point. Such tests are comprised of stepwise increase on the independent variables, also known as manipulated variables, and observing the corresponding effects on the controlled variables in order to explain the dynamic behavior of the plant, and thereby, answering the question of why the process is behaving the way it is. Here, typical manipulated variables in a biomass combustion power plant are: the fuel dosage, the primary air flow, the secondary air flow, the recirculation flue gas, and the grate speed. The controlled variables are divided into two main aspects: (a) environmental, which is represented by the appropriate oxygen concentration and temperature in the post-combustion chamber, and (b) operational, which is represented by the required steam amount to the turbine engine or district heating.

6.2.1 Step response experiments

Plant response to a step increase in fuel dosage

Figure 6.8 depicts the dynamic response of the large-scale combustion plant to a 10% stepwise change in fuel dosage. In all upcoming experiments the model parameters are kept constant, including the fuel calorific value, and therefore, these experiments are considered to be a representative of the open-loop response of the plant [Koppejan and Van Loo, 2012].

Here, the model exhibits an initial (inverse) response for the steam flow rate produced as a result of an increase in the fuel flow amount, this inverse response was also reported in the models of [Manca et al., 1998],[Van Kessel, 2003] for a municipal waste incinerator. It is generally presumed that the steam amount increases as the fuel flow increases, but this inverse behavior can be explained by the fact that the fuel is fed at the ambient temperature and with a moisture fraction that requires a part of energy to be drawn from the total available thermal energy in order to increase the fuel's temperature and starting the drying process of the wet biomass fuel.

Once the water is retrieved, the biomass fuel will catch fire followed by a positive increase in the amount of generated steam, and a steady state is reached after 50 min. Finally, the oxygen consumption in the furnace exhibits an opposite behavior in comparison to the generated steam, this due to the reason that more fuel is being combusted, and therefore, more oxygen is being consumed inside the furnace.

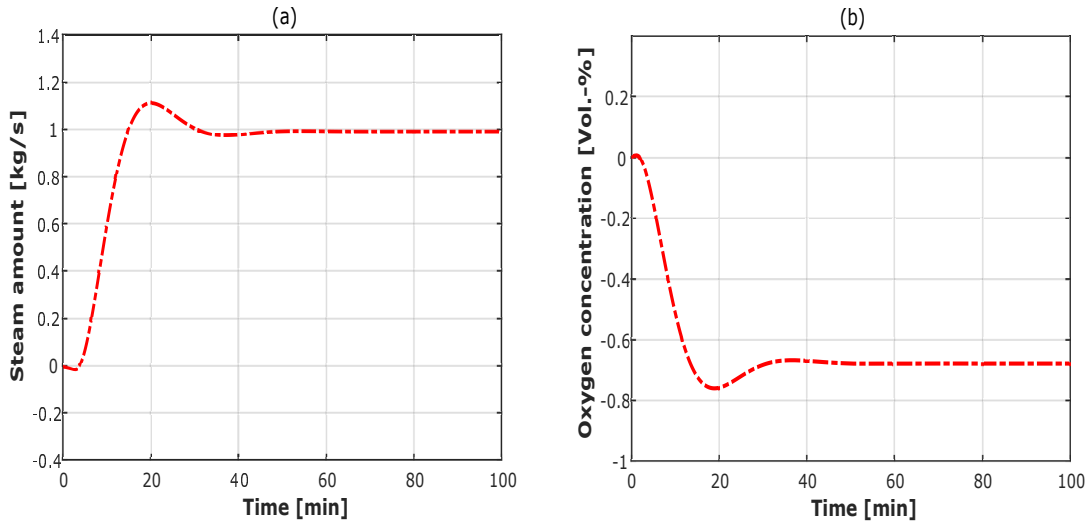

Figure 6.8: Dynamic response of a biomass combustion power plant to a 10 % stepwise increase in solid fuel flow rate on: (a) steam amount, (b) oxygen concentration.

Plant response to a step increase in primary air

In the second step response experiments on the dynamic model, the primary air flow rate was similarly step-wise increased by 10%. The dynamic behavior of the plant to an increase in the primary air from below the moving grate is shown in Figure 6.9.

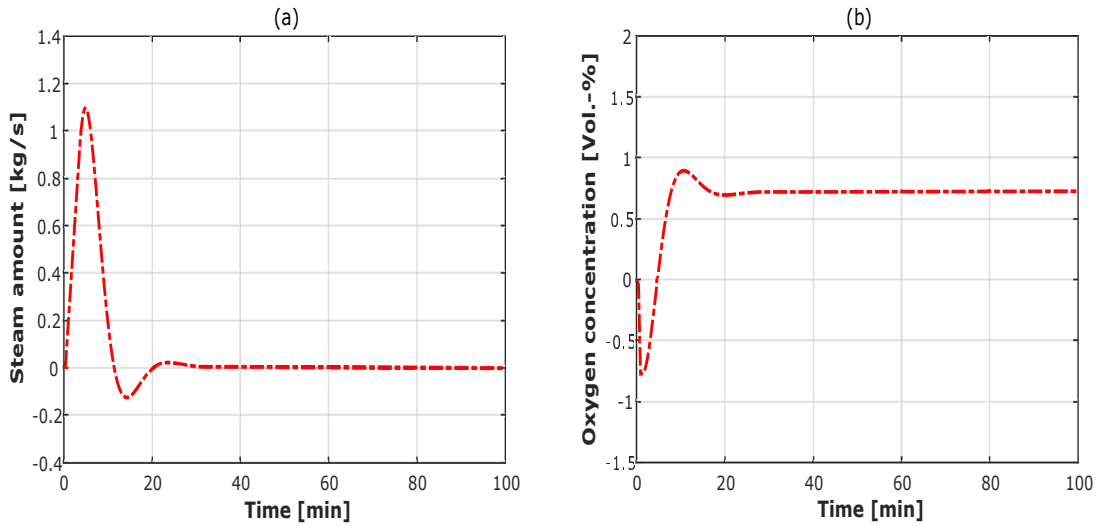

Figure 6.9: Dynamic response of a biomass combustion power plant to a 10 % stepwise increase in primary air flow rate on: (a) steam amount, (b) oxygen concentration.

As it can be seen from Figure 6.9, the generated steam amount will increase as a result of an increase in the primary air, whereas the oxygen decreases and then it increases again. At a first glance, this might seem surprising, since more oxygen carried with the atmospheric air will certainly lead to an overall increase in the oxygen concentration inside the furnace. However, this behavior can be traced back

to the porous nature, i.e. the voids occupied by the gases, of the burning bed on the moving grate, and the fact that the primary air is blown in a forced flow regime, which will induce a kind of "agitation" inside the bed; hence, more oxygen will reach the solid surface of the biomass particles leading to an increase in the burning rate, therefore, more thermal energy as well as steam will be generated, before it decreases again and the steady state settle back to its initial value after 30 min, since the amount of fuel is being constant and no more fuel is added.

For the oxygen after the observed sharp decrease, it increases again and it reaches a new steady state. It should be noted that an excessive amount of primary air will lead to a possibility of "cold-blowing" the fire, which consequently leads to a decreasing steam amount and unburned fuel that has to cope with at the end of the grate [Koppejan and Van Loo, 2012].

Plant response to a step increase in grate speed

The third step response experiment on the model consists of increasing the grate speed also step wise by 10 %. The dynamic behavior of the plant as consequence to this experiment is depicted in Figure 6.10.

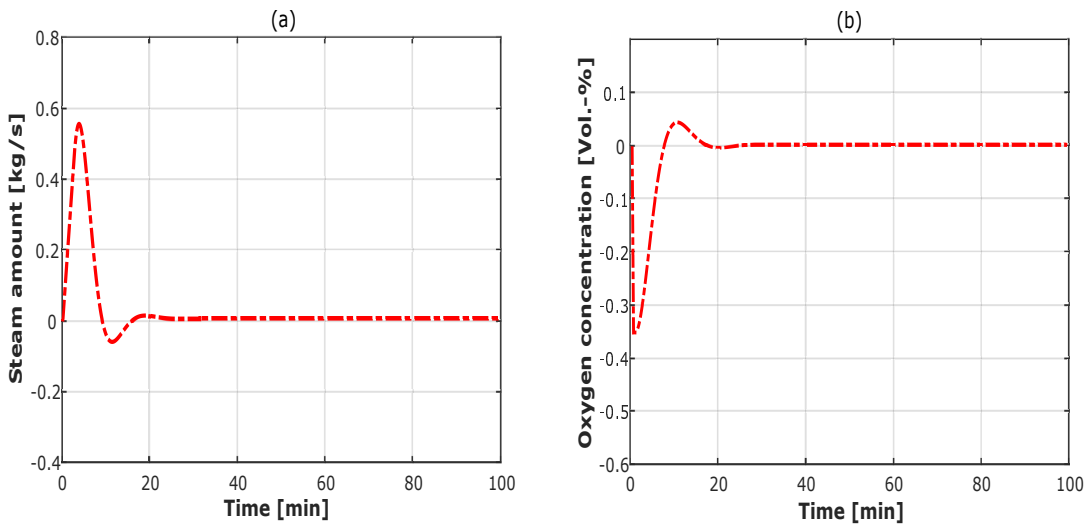

Figure 6.10: Dynamic response of a biomass combustion power plant to a 10 % stepwise increase in grate speed on: (a) steam amount, (b) oxygen concentration.

As it can be observed from Figure 6.10, increasing the grate speed will have a temporary positive effect on the amount of steam being generated from the boiler, followed by a sharp decrease in the oxygen concentration in the furnace.

Such plant behavior is similar to the effect of primary air on these two controlled variables, increasing the grate speed will also introduce a "mixing effect" in the solid bed; hence, more oxygen will reach the surface of biomass particles, and the fire will intensify as a reason of a temporary increase in the combustion rate, due to the solid-oxidizer interaction.

Similar to primary air case, and in contrast to the responses of the fuel flow, both steam flow and oxygen concentration show no static gain, as an increased speed will not lead to more fuel being dosed inside the combustion furnace [Koppejan and Van Loo, 2012]. After approximately 25 min the steam amount and the oxygen concentration settle back to their initial steady state, which means that the dynamics of the grate speed is much faster than the two former ones.

Plant response to a step increase in secondary air

The last step response experiment on the dynamic model is presented by the stepwise increase of the secondary air flow rate in the post-combustion phase. Similarly to the previous experiments, the dynamic behavior of the amount of steam being generated and oxygen concentration is shown in Figure 6.11.

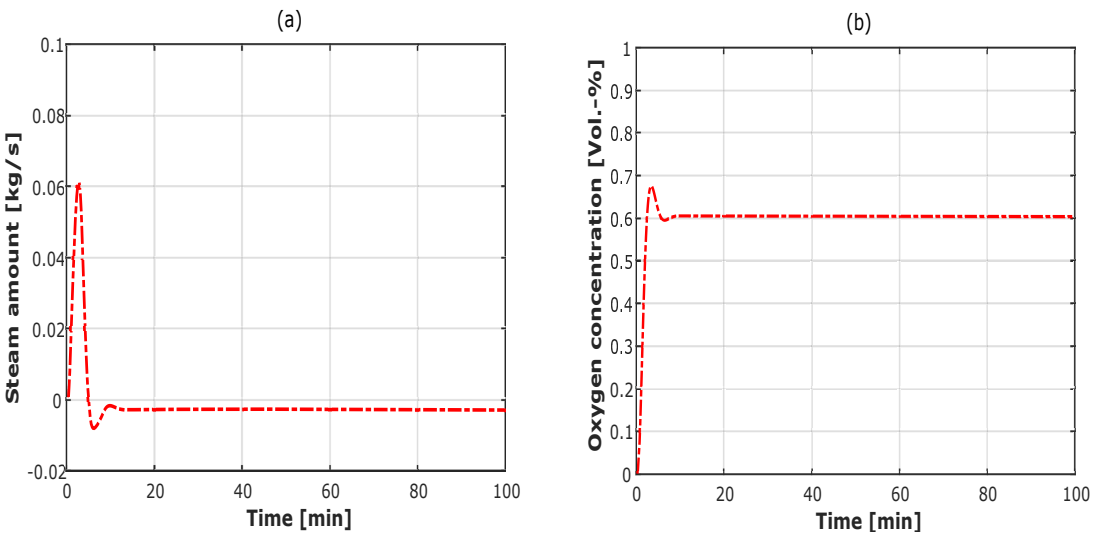

Figure 6.11: Dynamic response of a biomass combustion power plant to a 10 % stepwise increase in secondary air flow rate on: (a) steam amount, (b) oxygen concentration.

As it can clearly be seen from Figure 6.11, the secondary air has barely any effect on the generated steam amount, since it is not related to the combustion process taking place in the bed, but it is mainly used to ensure a complete burnout of incombustible gaseous species, which emanate from the solid phase, as a reason of either a local lack in providing enough atmospheric air, or the air cannot reach a part of the solid on the moving grate.

The observed slight increase in the produced steam might be explained by the sudden increase in the flue gas amount before the cooling effect introduced by the secondary air takes place and a new steady state is achieved. The secondary air also has a direct impact on the oxygen concentration, an increase of the former will immediately lead to an increase of the latter, and therefore, an increase in the secondary air will lead to a positive static gain on oxygen concentration inside the combustion chamber.

6.2.2 Section summary

In Section 6.2, four step response experiments were conducted on the model in order to gain insight on how the biomass combustion power plant outputs would behave as the manipulated inputs are changed stepwise. The plant output variables of interest were the amount of generated steam, due to its economical relevance, and the oxygen concentration in the outlet gas, which governs the ecological aspects in the heat recovery power plant, i.e., emissions.

The first experiment carried out on the model was a 10 % stepwise increase in the amount of dosed biomass in the furnace. The model exhibited an "inverse response" for the generated steam amount as a consequence of this action, which means that the generated steam did not immediately increase as a result of an increase in the fuel flow rate, but it decreased for a while before inverting the trend and then reaching at the end of a transient phase a final value higher than the initial one, as the fuel was fed to the furnace at ambient temperature and with a moisture fraction. These two require a part of the internal available thermal energy to be stripped off in order to start the drying process, before the solid bed combustion mechanism eventually increases the gas temperature and the produced steam amount, as a result of the fuel being dried and then burned.

The second conducted experiment was also a 10 % stepwise increase in the primary air flow, which is injected from beneath the moving grate. Contrary to one's logic, the oxygen concentration was temporary dropped due to the porous nature of the solid bed and the fact that the dosed atmospheric air is injected in a forced regime, which introduced a kind of "agitation" inside the burning bed; therefore, more oxygen reached the surface of solid biomass particles leading to an increase in the reaction rate and more released thermal energy, which consequently increased the gas temperature and the generated steam amount. This explains why the fed air is used for the short-term control strategy for the steaming capacity and for the long-term control for the O_2-concentration in the furnace. Similar to the last experiments, a step wise increase of 10 % in the grate speed led to a temporary drop in the O_2-concentration and an increase in the amount of generated steam, due to the introduced "mixing effect" in the solid bed, which consequently led to more solid fuel interaction with the oxidizer, and the release of a more thermal energy. This explains why the generated steam amount was temporary increased before it decreased, thereby, reaching back its initial start value, since no more solid fuel was fed inside the combustion furnace in order to increase the amount of generated steam.

The last step response experiment, which was carried on the model, was also a 10 % stepwise increase in the secondary air that is dosed in the post-combustion phase to achieve good mixing conditions and a complete burnout of incombustible gaseous species, that may leave the solid bed without being fully oxidized. The secondary air had barely any effect on the amount of steam generated, but it influenced directly the O_2-concentration. Of course, more secondary air led to an observed cooling-effect inside the chamber, which was manifested by a slight decrease in the generated steam amount. Therefore, both the secondary and primary air have to be controlled in a counter balance to each other in order to maintain a constant O_2-concentration.

6.3 Power plant simulation

In this part, validation results of both dynamic models of the combustion furnace and the steam-boiler, using the model parameter estimation and model validation procedure discussed in Section 4.5, will be presented. Here, the degree to which the simulation model mimics the real world from the perspective of the intended use of the model will be achieved by giving different illustrative simulation examples and by using different gathered data obtained from the large-scale combustion power plant. Consequently, the model validity will be achieved through the comparison of predicted response from the model against the real plant response.

It is worth to mention that the conduction of large step response experiments on the real combustion power plant, in order to isolate the effect of the disturbances acting on the process when the inputs are considerably changed, were not possible for safety and economical reasons. Therefore, and as an alternative, only data where the power plant exhibited a large variation in the process operation were selected from the plant data historian, including a start-up data case. Furthermore, the reason behind selecting such data for model validation is for the sake of showing that the dynamic response obtained from the model follows its real counter part.

6.3.1 Boiler model

Figure 6.12 illustrates the measurement data used for parameter identification and validation part for the steam boiler model discussed in Section 4.4.

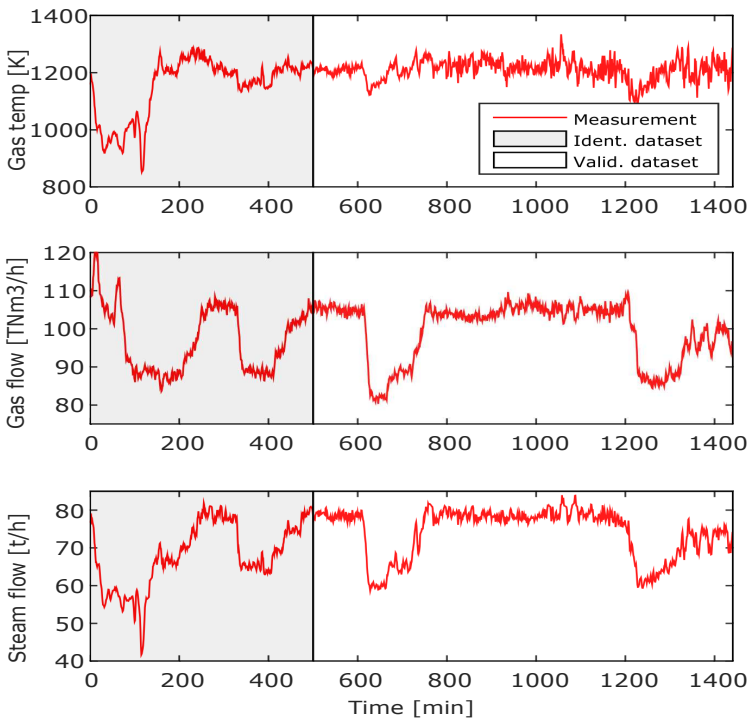

Figure 6.12: Process measurements for the boiler model validation: (a) gas temperature, (b) flue gas flow, (c) steam flow rate.

As it can be seen, the selected process measurement exhibits the strong variation in the process operation, which makes it suitable for the identification and validation task. Additionally, the data is divided into two data sets, one for identifying the model parameter A_{dr} and the second for model validation. The inputs for the model were the gas temperature and the flue gas flow to the boiler section, the output is the generated steam amount. The flue gas temperature at the boiler exit is measurable at the current power plant (see Figure 6.13), but it can be set to a constant value $T_{fg} = 162\,°\mathrm{C}$ without introducing a significant error, since the gas temperature is much higher than the temperature at the boiler exit. Each of the aforementioned process measurements were recorded at one minute interval for 24 hours.

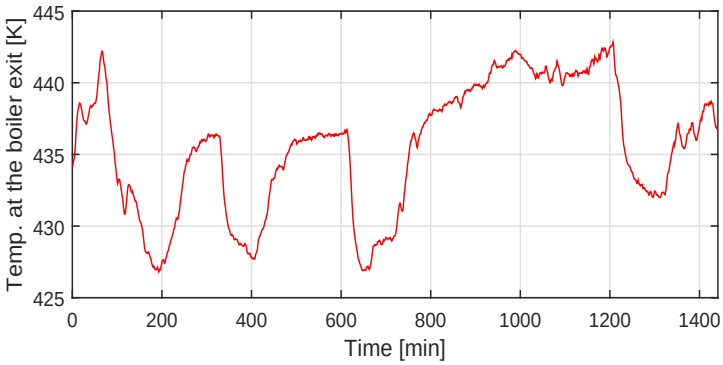

Figure 6.13: Measured temperature at the exit of boiler section.

A crucial step that directly follows the model calibration part is the model validation, which will decide the quality of the model obtained by the modeling task and the model parameter estimation part, or revealing some shortcomings. The steam-boiler model performance is illustrated in Figure 6.14. It can be then deduced that the estimated parameter A_{dr} from the identification step works also well on the independent data set (validation data) series shown in Figure 6.12, and the captured process dynamic is similar to the measured one by the physical sensor.

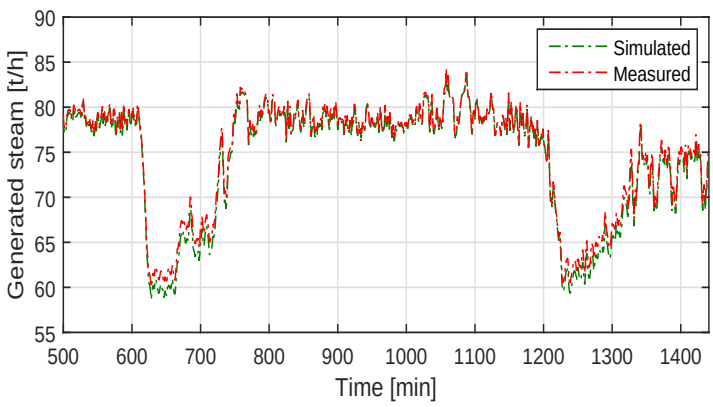

Figure 6.14: Measured and simulated steam flow rate from the validated dynamic model.

6.3.2 Furnace model

The identification and the validation of the furnace dynamic model, presented in Section 4.2, were conducted using gathered measurements from the combustion power plant logged at 1 minute interval. Similar to the steam boiler model, the calibration procedure discussed in Section 4.5 was used to determine the model parameters. The inputs for the model were the primary, the secondary air and the recirculated flue gas flows with their corresponding temperatures, and finally the estimated biomass flow rate and the energetic content of the biofuel. The actual process observations, to which the model response has to be compared for establishing the adequacy of the identified dynamic model, are: the flue gas flow, the oxygen concentration in the post-combustion phase, and the gas temperature respectively. The collected measurements were again splitted into two parts: one for identification, and the second for model validation part.

Figure 6.15 illustrates the model response and the actual process response. As it can be seen, the predicted outputs from the model are fitted to the process output measured data based on minimization of the loss function that dictates the adequacy of the identified model parameters.

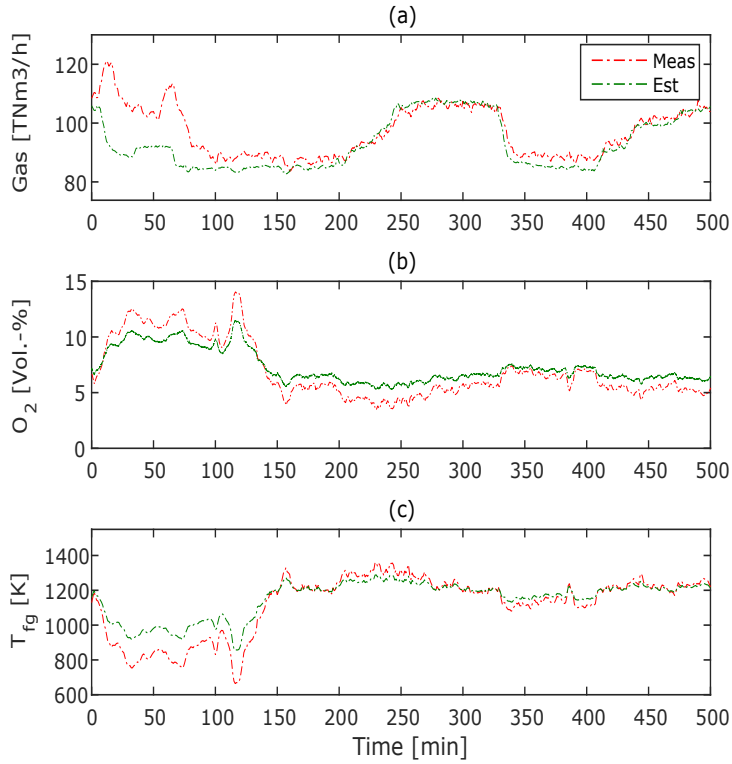

Figure 6.15: The measured and estimated model responses in the identification phase (data set one).

After calibrating the model in the identification step, an independent data set (validation data) was applied on the identified model in order to decide on the quality of the model obtained. The model performance as a result of this step is illustrated in Figure 6.16. As it can be seen from the figure, the identified model performs also well on the validation data series.

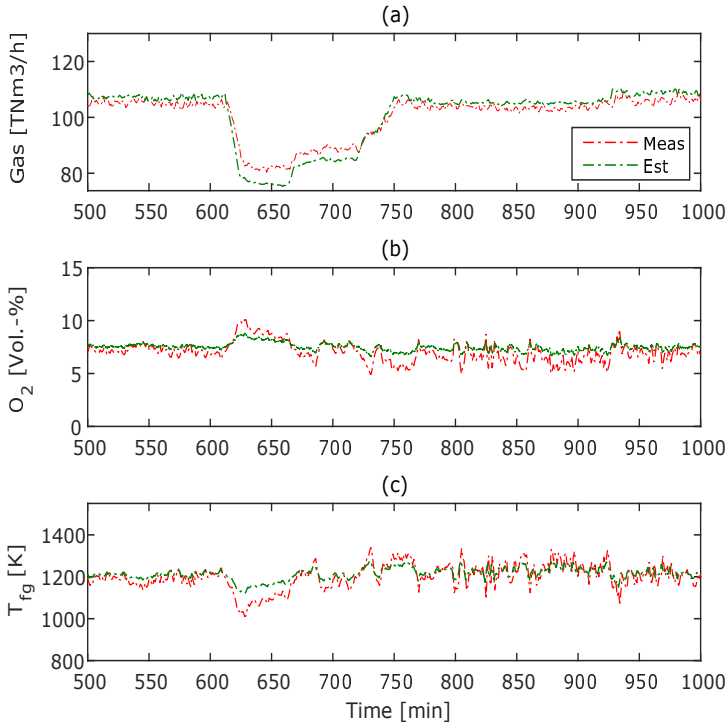

Figure 6.16: The measured and estimated model responses in the validation phase (data set one).

The furnace model was again calibrated with another measured process data. The performance of the model for the identification part is shown in Figure 6.17.

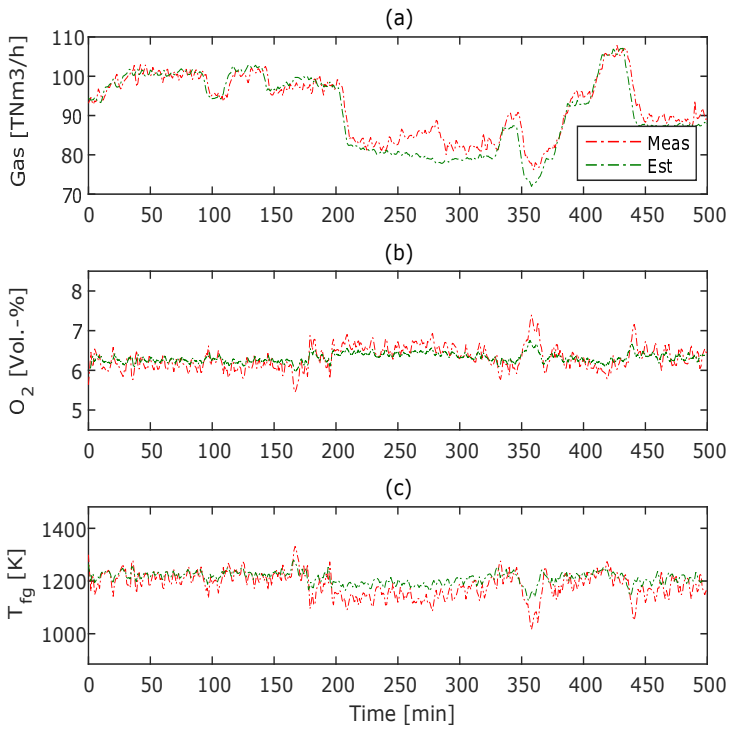

Figure 6.17: The measured and estimated model responses in the identification phase (data set two).

The comparison between measured outputs and modeled response from the validation step are plotted in Figure 6.18. As it can been seen, the performance of the model with properly tuned parameters from the identification step is satisfactory.

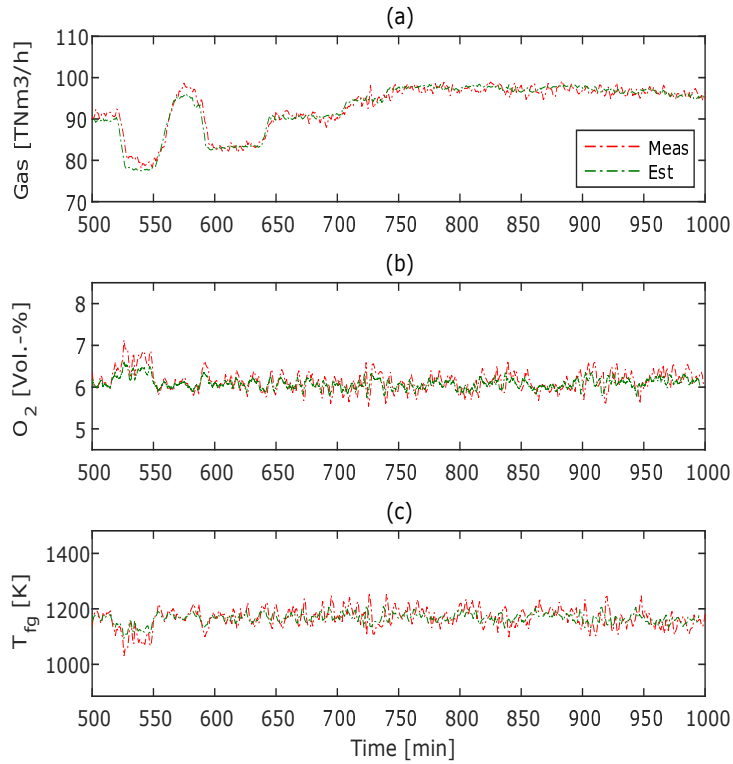

Figure 6.18: The measured and estimated model responses in the validation phase (data set two).

Since the plant is comprised of two major parts, the furnace and the boiler dynamic models, this calls for the simulation of the overall combustion power plant model. The comparison between the estimated steam amount by the boiler model and plant measurement is depicted in Figure 6.19. As it can also be seen, the captured process dynamic by the model is quite similar to the measured one by the physical sensor in the power plant.

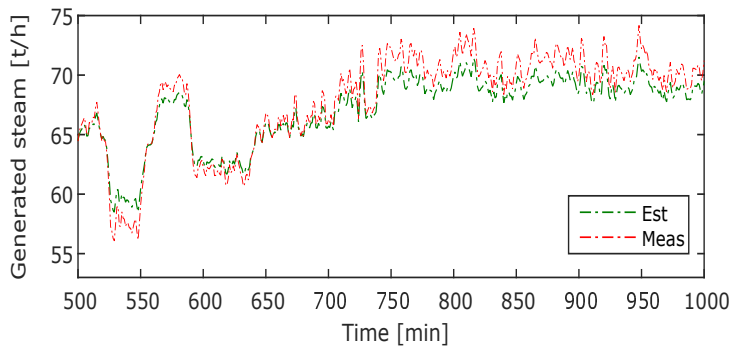

Figure 6.19: Measured and estimated steam flow by the combustion power plant dynamic model (data set two).

Finally, the model is tested with measurement during the startup of the power plant, the aim of such test is to check how well the dynamic model will perform during the

startup phase of the plant, which can be considered a challenging situation for the model. The simulation results are depicted in Figure 6.20. As it can be seen from the figures, the model response is quite satisfactory for the startup case, and that the process dynamics are captured well by the plant's model.

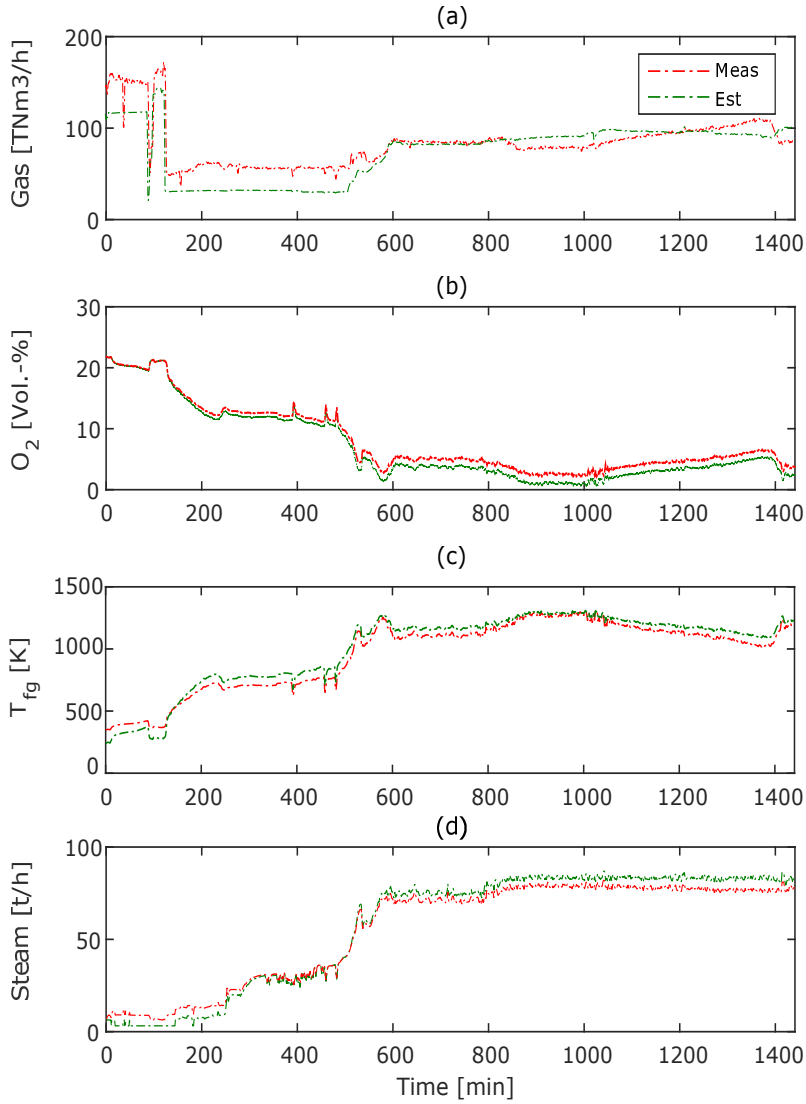

Figure 6.20: Comparison between measured and simulated responses during a startup phase of the combustion power plant.

6.3.3 Section summary

In this section, both implemented dynamic models for the grate fired furnace and the steam-boiler with a natural circulation have been validated using measured data from the real plant. The validity of the proposed model for the power plant has been demonstrated by giving different examples where the plant exhibited a large variation in the process operation, this included also a startup phase of the unit. From the simulation results, it can be concluded that the system dynamics are well captured by the simulation model, making from the latter a suitable candidate to further investigate the possibility of improving the economical aspect of the combustion site by the deployment of advanced process control techniques for this purpose.

7 Summary and future work

In this work, mathematical modeling of a large-scale biomass firing power plant has been carried out in order to derive a suitable dynamic model, which is capable enough to characterize and capture the dynamics of the real combustion system and over a wide range of operating conditions of the power plant, while keeping the modeling task at acceptable levels of model details to meet the objectives which the model has been built for, i.e., improving plant performance through advanced model-based control strategies. Therefore, the modeling task involved making some assumptions and approximations to lessen the confronted complexity.

Additionally, the model has been built based upon the gained knowledge from the physical system and its behavior, this entails also the underlying principles related to time-dependent laws for the conservation balances in the control volume that defines how the system interacts with its surrounding and other key controlling factors, which include heat and mass transfer mechanisms inside the combustion furnace. It is by the application of these fundamental laws on the control volume that a set of mathematical equations describing the grate-firing system and the steam-boiler has been derived. Such a modeling approach led to a lumped parameter model with a relatively low complexity.

Furthermore, the modeling task of the combustion chamber involved the development of different "submodels" for the individual processes and components that comprise the system, such as radiative and convective heat transfer models in the furnace and the solid bed respectively, the models that describe the drying process of the fresh fuel and the thermal decomposition of its dried part, as well as the residence time model for describing the average time the biofuel spends inside the combustion chamber as a function of the grate geometry. These individual submodels when coupled with each other, resulted in a model for the entire biomass grate fired system.

In order to integrate more information about the main source of acting disturbance on the process operation, that is the energy value of the fuel mix, which commonly varies between the different batches delivered to the furnace and depends linearly on the moisture content, the dynamic model of the grate firing power plant has been extended by designing a soft-sensor using a mechanistic approach and measurements in the flue gas for this purpose. In this approach, the developed soft-sensor was based upon two interlinked main parts: (a) a static combustion model for estimating the released thermal power from burning the solid biomass, and (b) a dynamic steam-boiler model for predicting the amount of generated steam based on the estimated thermal power from the furnace side. This allowed for the calculation of the calorific value of the solid biomass based on minimizing the difference between the measured and predicted steam values by applying an optimization-based scheme. The value which minimized this difference was then assumed to correspond to the fuel's moisture content.

Future work entails the implementation of an advanced control strategy, namely the model predictive control as an appealing control technique, which allows for an optimal handling of the multiple and conflicting objectives and process constraints. Such technique uses the available numerical model to predict the plant's behavior and compute the optimal trajectory for the manipulated variables that meet the aforementioned goals by solving an optimization problem. This may lead to even consider the derivation of a more simpler model from the detailed one by reduction in dimension and complexity for an efficient numerical calculation when computing the optimal trajectories for the manipulated variables.

Bibliography

Y. Abbi. *Energy Audit: thermal power, combined cycle, and cogeneration plants.* The Energy and Resources Institute (TERI), 2012.

E. Achenbach. Heat and flow characteristics of packed beds. *Experimental Thermal and Fluid Science*, 10(1):17–27, 1995.

E. Adam and J. Marchetti. Dynamic simulation of large boilers with natural recirculation. *Computers & chemical engineering*, 23(8):1031–1040, 1999.

E. Agora. Understanding the Energiewende. *FAQ on the Ongoing Transition of the German Power System. Agora Energiewende, Berlin*, 2015.

I. Akkurt, B. Mavi, A. Akkurt, C. Basyigit, S. Kilincarslan, and H. Yalim. Study on z dependence of partial and total mass attenuation coefficients. *Journal of Quantitative Spectroscopy and Radiative Transfer*, 94(3):379–385, 2005.

K. H. Asli. *Water Hammer Research: Advances in Nonlinear Dynamics Modeling.* CRC Press, 2013.

ASME PTC 4-2008 . Fired Steam Generators: Performance Test Codes, The American Society of Mechanical Engineers , 2009.

K. J. Åström and R. D. Bell. Drum-boiler dynamics. *Automatica*, 36(3):363–378, 2000.

G. Ayalew and S. M. Ward. Development of a prototype infrared reflectance moisture meter for milled peat. *Computers and electronics in agriculture*, 28(1):1–14, 2000.

V. Babrauskas. Ignition of wood: a review of the state of the art. *Journal of Fire Protection Engineering*, 12(3):163–189, 2002.

H. D. Baehr and S. Kabelac. *Thermodynamik: Grundlagen und technische Anwendungen.* Springer-Verlag, 2012.

P. Barale, C. Fong, M. Green, P. Luft, A. McInturff, J. Reimer, and M. Yahnke. The use of a permanent magnet for water content measurements of wood chips. *Lawrence Berkeley National Laboratory*, 2001.

C. Baskar, S. Baskar, and R. S. Dhillon. *Biomass conversion: The interface of biotechnology, chemistry and materials science.* Springer Science & Business Media, 2012.

P. Basu. *Biomass gasification, pyrolysis and torrefaction: practical design and theory.* Academic press, 2013.

R. Bauer, M. Gölles, T. Brunner, N. Dourdoumas, and I. Obernberger. Modelling of grate combustion in a medium scale biomass furnace for control purposes. *Biomass and Bioenergy*, 34(4):417–427, 2010.

C. E. Baukal Jr. *Industrial burners handbook*. CRC press, 2003.

C. E. Baukal Jr. *The John Zink Hamworthy Combustion Handbook: Volume 1-Fundamentals*. CRC Press, 2012.

L. L. Baxter. Ash deposition during biomass and coal combustion: a mechanistic approach. *Biomass and Bioenergy*, 4(2):85–102, 1993.

K. R. Beebe and B. R. Kowalski. An introduction to multivariate calibration and analysis. *Analytical Chemistry*, 59(17):1007A–1017A, 1987.

A. Bejan and A. D. Kraus. *Heat transfer handbook*, volume 1. John Wiley & Sons, 2003.

F. Belkhir and G. Frey. Soft-sensing of key process variables in a biomass combustion plant. In *2016 7th International Renewable Energy Congress (IREC)*, pages 1–6, March 2016a. doi: 10.1109/IREC.2016.7478861.

F. Belkhir and G. Frey. Model-driven soft sensor for predicting biomass calorific value in combustion power plants. In *Industrial Electronics and Applications (ICIEA), 2016 IEEE 11th Conference on*, pages 807–812. IEEE, 2016b.

F. Belkhir, C. Gierend, and G. Frey. Component oriented modeling of biomass incineration plants. In *ICINCO (1)*, pages 396–404, 2013.

F. Belkhir, D. Kraus Cabo, F. Felgner, and G. Frey. Optimal startup control of a steam power plant using the jmodelica platform. In *Proceedings of the 8th Vienna International Conference on Mathematical Modeling (MATHMOD)*, pages 204–209, 2015a.

F. Belkhir, J. Meiers, F. Felgner, and G. Frey. A biomass combustion plant model for optimal control applications-the effect of key variables on combustion dynamics. In *Renewable Energy Congress (IREC), 2015 6th International*, pages 1–6. IEEE, 2015b.

T. L. Bergman, F. P. Incropera, and A. S. Lavine. *Fundamentals of heat and mass transfer*. John Wiley & Sons, 2011.

G. L. Borman and K. W. Ragland. *Combustion engineering*. McGraw-Hill Science/Engineering/Math, 1998.

M. L. Brown, W. S. Bulpitt, J. L. Walsh Jr, and T. F. McGowan. *Biomass and alternate fuel systems: an engineering and economic guide*. John Wiley & Sons, 2011.

F.-J. Brüggemeier. Sun, water, wind: Development of the energy transition in germany. *Friedrich Ebert Stiftung*, 2015.

D. A. Burns and E. W. Ciurczak. *Handbook of near-infrared analysis*. CRC press, 2007.

I. T. Cameron and K. Hangos. *Process modelling and model analysis*, volume 4. Academic Press, 2001.

K. Carlsson. Gas cleaning in flue gas from combustion of biomass. *Deliverable 2E-3 of the EU project ThermalNet, EcoExpert*, 2008.

F. Casella and A. Leva. Object-oriented modelling & simulation of power plants with modelica. In *Decision and Control, 2005 and 2005 European Control Conference. CDC-ECC'05. 44th IEEE Conference on*, pages 7597–7602. IEEE, 2005.

Y. A. Cengel, M. A. Boles, and M. Kanoğlu. *Thermodynamics: an engineering approach*, volume 5. McGraw-Hill New York, 2002.

J. Cheng. *Biomass to renewable energy processes.* CRC press, 2009.

T. H. Christensen et al. *Solid waste technology & management*, volume 1. Wiley Online Library, 2011.

E. Dahlquist. *Technologies for converting biomass to useful energy: combustion, gasification, pyrolysis, torrefaction and fermentation.* CRC Press, 2013a.

E. Dahlquist. *Biomass as energy source: resources, systems and applications.* CRC Press, 2013b.

S. Das and P. N. Suganthan. Differential evolution: a survey of the state-of-the-art. *IEEE transactions on evolutionary computation*, 15(1):4–31, 2011.

W. De Jong and J. R. Van Ommen. *Biomass as a Sustainable Energy Source for the Future: Fundamentals of Conversion Processes.* John Wiley & Sons, 2014.

K. G. Denbigh and J. C. R. Turner. *Chemical reactor theory: an introduction.* CUP Archive, 1984.

L. Devi, K. J. Ptasinski, and F. J. Janssen. A review of the primary measures for tar elimination in biomass gasification processes. *Biomass and bioenergy*, 24(2): 125–140, 2003.

R. Dolezal. Dampferzeugung. *Verbrennung, Feuerung, Dampferzeuger*, 1985.

S. Döring. *Pellets als Energieträger: Technologie und Anwendung.* Springer-Verlag, 2010.

S. Döring. *Power from pellets: technology and applications.* Springer Science & Business Media, 2012.

F. Dunlap. *The specific heat of wood.* Number 110. US Dept. of Agriculture, Forest Service, 1912.

H. Effenberger. *Dampferzeugung.* Springer-Verlag, 2013.

G. Emig and E. Klemm. *Technische Chemie: Einführung in die chemische Reaktionstechnik.* Springer-Verlag, 2006.

EN 12953-11. Shell boilers - Part 11: Acceptance tests, European Committe for Standardization, 2003.

AG. Energiebilanzen. Bruttostromerzeugung in Deutschland von 1990 bis 2016 nach energieträgern. *Available online at http://www.ag-energiebilanzen.de/*, 2016.

B. Epple, R. Leithner, W. Linzer, and H. Walter. *Simulation von Kraftwerken und wärmetechnischen Anlagen.* Springer-Verlag, 2009.

L. Fortuna, S. Graziani, A. Rizzo, and M. G. Xibilia. *Soft sensors for monitoring and control of industrial processes.* Springer Science & Business Media, 2007.

G. Frey and F. Belkhir. *Produktivität - Qualität - Effizienz Innovative Prozesse für die Produktion von morgen. in: R. Müller and J. Flackus (Eds.)*, chapter Modellbasierte Regelung von Biomasseverbrennungsanlagen, pages 230–248. ISBN 978-3-8440-3509-4 (Print), Shaker Verlag , Herzogenrath, Germany, 2015.

V. Ganapathy. *Industrial boilers and heat recovery steam generators: design, applications, and calculations.* CRC Press, 2002.

S. Gaur and T. B. Reed. An atlas of thermal data for biomass and other fuels. Technical report, National Renewable Energy Lab., Golden, CO (United States), 1995.

V. Gnielinski. Berechnung mittlerer Wärme-und Stoffübergangskoeffizienten an laminar und turbulent überströmten Einzelkörpern mit Hilfe einer einheitlichen Gleichung. *Forschung im Ingenieurwesen A*, 41(5):145–153, 1975.

V. Gnielinski, A. Mersmann, and F. Thurner. *Verdampfung, Kristallisation, Trocknung.* Springer-Verlag, 2013.

M. Gölles. *Modellierung einer Biomasse-Kleinfeuerungsanlage als Grundlage für modellbasierte Regelungsstrategien.* PhD thesis, Teschnische Universität Graz, 2008.

M. Gölles, S. Reiter, T. Brunner, N. Dourdoumas, and I. Obernberger. Model based control of a small-scale biomass boiler. *Control engineering practice*, 22:94–102, 2014.

D. Y. Goswami and F. Kreith. *Handbook of energy efficiency and renewable energy.* Crc Press, 2007.

P. Grammelis. *Solid biofuels for energy.* Springer, 2010.

D. M. Hawkins. *Identification of outliers*, volume 11. Springer, 1980.

S. Hermansson, F. Lind, and H. Thunman. On-line monitoring of fuel moisture-content in biomass-fired furnaces by measuring relative humidity of the flue gases. *Chemical Engineering Research and Design*, 89(11):2470–2476, 2011.

C. Higman and M. Van der Burgt. *Gasification.* Gulf professional publishing, 2011.

H. Hottel and A. Sarofim. Models of radiative transfer in furnaces. *Journal of engineering physics*, 19(3):1102–1114, 1970.

H. C. Hottel. *Radiant heat transmission*, volume 3. McGraw-Hill New York, 1954.

M. Hultnäs and V. Fernandez-Cano. Determination of the moisture content in wood chips of scots pine and norway spruce using mantex desktop scanner based on dual energy x-ray absorptiometry. *Journal of wood science*, 58(4):309–314, 2012.

S. Ikonen, L. Stormbom, and T. Ranta-aho. Chemical interference test results of a novel humidity sensor. In *5th International Symposium on Humidity and Moisture, ISHM*, 2006.

W. L. James, Y.-H. Yen, and R. J. King. *A microwave method for measuring moisture content, density, and grain angle of wood*, volume 250. US Dept. of Agriculture, Forest Service, Forest Products Laboratory, 1985.

B. Jenkins and P. Mullinger. *Industrial and process furnaces: principles, design and operation.* Butterworth-Heinemann, 2011.

B. Jenkins, L. Baxter, and T. Miles. Combustion properties of biomass. *Fuel processing technology*, 54(1):17–46, 1998.

P. D. Jensen, H. Hartmann, T. Böhm, M. Temmerman, F. Rabier, and M. Morsing. Moisture content determination in solid biofuels by dielectric and NIR reflection methods. *Biomass and Bioenergy*, 30(11):935–943, 2006.

R. Jeschar, R. Alt, and E. Specht. *Grundlagen der Wärmeübertragung.* Viola-Jeschar-Verl, 1990.

J. M. Jones, A. R. Lea-Langton, L. Ma, M. Pourkashanian, and A. Williams. *Pollutants Generated by the Combustion of Solid Biomass Fuels.* Springer, 2014.

F. Joos. *Technische Verbrennung.* Springer, 2006.

P. Kadlec, B. Gabrys, and S. Strandt. Data-driven soft sensors in the process industry. *Computers & Chemical Engineering*, 33(4):795–814, 2009.

M. Kaltschmitt, D. Thrän, and K. Smith. Renewable energy from biomass. *Encyclopedia of Physical Science and Technology, ed. by RA Meyers*, pages 203–228, 2002.

M. Kaltschmitt, H. Hans, and H. Hermann. *Energie aus Biomasse- Grundlagen, Techniken und Verfahren.* Springer-Verlag, 2009.

J. Karl. *Dezentrale Energiesysteme: Neue Technologien im liberalisierten Energiemarkt.* Walter de Gruyter, 2012.

D. L. Karlen. *Cellulosic Energy Cropping Systems.* John Wiley & Sons, 2014.

B. Kavalov and S. D. Peteves. *Bioheat applications in the European Union: an analysis and perspective for 2010.* European commission, Institut for Energy, Patten, The Netharlands, 2004.

R. B. Kemp. *Handbook of thermal analysis and calorimetry: from macromolecules to man*, volume 4. Elsevier, 1999.

S. Kieseler, Y. Neubauer, and N. Zobel. Ultimate and proximate correlations for estimating the higher heating value of hydrothermal solids. *Energy & Fuels*, 27 (2):908–918, 2013.

C.-K. Kim, J.-K. Oh, J.-P. Hong, and J.-J. Lee. Dual-energy x-ray absorptiometry with digital radiograph for evaluating moisture content of green wood. *Wood Science and Technology*, pages 1–11, 2015.

M. Kind, A. Mersmann, and J. Stichlmair. *Thermische Verfahrenstechnik: Grundlagen und Methoden.* Springer, 2005.

V. Kishore. *Renewable energy engineering and technology: principles and practice.* The Energy and Resources Institute (TERI), 2010.

J. B. Kitto and S. Stultz. *Steam: its generation and use.* Babcock & Wilcox Company, 1992.

D. L. Klass. *Biomass for renewable energy, fuels, and chemicals.* Academic press, 1998.

H. H. Klee. Mathematical modeling of continuous dynamic systems. *Mathematical Modelling*, 8:468–471, 1987.

E. Klose, H. Göhler, and M. Born. Heizwertformeln-Genauigkeit und Grenzen der anwendbarkeit. *Energietechnik*, 39(12):450–453, 1989.

F. F. Kollmann and W. A. Côté Jr. Principles of wood science and technology. vol. i. solid wood. In *Principles of Wood Science and Technology. Vol. I. Solid Wood.* Springer-Verlag, 1968.

J. Koppejan and S. Van Loo. *The handbook of biomass combustion and co-firing.* Routledge, 2012.

J. Kortela and S. Jämsä-Jounela. Fuel moisture soft-sensor and its validation for the industrial biopower 5 chp plant. *Applied energy*, 105:66–74, 2013.

J. Kortela and S.-L. Jämsä-Jounela. Fault-tolerant model predictive control (ftmpc) for the biograte boiler. In *2015 IEEE 20th Conference on Emerging Technologies & Factory Automation (ETFA)*, pages 1–6. IEEE, 2015.

U. Kortela and A. Marttinen. Modelling, identification and control of a grate boiler. In *American Control Conference, 1985*, pages 544–549. IEEE, 1985.

R. Kramer. *Chemometric techniques for quantitative analysis.* CRC Press, 1998.

A. W. Kraszewski. Microwave aquametry-needs and perspectives. *Microwave Theory and Techniques, IEEE Transactions on*, 39(5):828–835, 1991.

F. Krüll. *Verfahren zur numerischen Simulation von Müllrostfeuerungen.* Shaker, 2001.

R. Kullenberg, M. Hultnäs, V. Fernandez, M. Nylinder, S. Toft, and F. Danielsson. Dual-energy x-ray absorptiometry analysis for the determination of moisture content in biomass. *Journal of Biobased Materials and Bioenergy*, 4(4):363–366, 2010.

M. Lackner, F. Winter, and A. K. Agarwal. Handbook of combustion. *Methods*, 1: 4, 2013.

K. Langeheinecke, P. Jany, and E. Sapper. *Thermodynamik für Ingenieure*. Springer, 1993.

B. Leblon, O. Adedipe, G. Hans, A. Haddadi, S. Tsuchikawa, J. Burger, R. Stirling, Z. Pirouz, K. Groves, J. Nader, and A. LaRocque. A review of near-infrared spectroscopy for monitoring moisture content and density of solid wood. *The Forestry Chronicle*, 89(5):595–606, 2013.

B. Leckner. Spectral and total emissivity of water vapor and carbon dioxide. *Combustion and flame*, 19(1):33–48, 1972.

A. Leva, C. Maffezzoni, and G. Benelli. Validation of drum boiler models through complete dynamic tests. *Control Engineering Practice*, 7(1):11–26, 1999.

C. Maffezzoni. Boiler-turbine dynamics in power-plant control. *Control Engineering Practice*, 5(3):301–312, 1997.

D. Manca, M. Rovaglio, G. Pazzaglia, and G. Serafini. Inverse response compensation and control optimization of incineration plants with energy production. *Computers & chemical engineering*, 22(12):1879–1896, 1998.

R. B. Mazess, H. S. Barden, J. P. Bisek, and J. Hanson. Dual-energy x-ray absorptiometry for total-body and regional bone-mineral and soft-tissue composition. *The American journal of clinical nutrition*, 51(6):1106–1112, 1990.

S. McAllister, J.-Y. Chen, and A. C. Fernandez-Pello. *Fundamentals of combustion processes*. Springer Science & Business Media, 2011.

P. McKendry. Energy production from biomass (part 2): conversion technologies. *Bioresource technology*, 83(1):47–54, 2002a.

P. McKendry. Energy production from biomass (part 1): overview of biomass. *Bioresource technology*, 83(1):37–46, 2002b.

M. F. Modest. The weighted-sum-of-gray-gases model for arbitrary solution methods in radiative transfer. *Journal of heat transfer*, 113(3):650–656, 1991.

M. F. Modest. *Radiative heat transfer*. Academic press, 2013.

Z. Morvay and D. Gvozdenac. *Applied industrial energy and environmental management*, volume 2. John Wiley & Sons, 2008.

T. Naes, T. Isaksson, T. Fearn, and T. Davies. *A user friendly guide to multivariate calibration and classification*. NIR publications, 2002.

A. Nakayama and A. Shenoy. Combined forced and free convection heat transfer in power-law fluid-saturated porous media. *Applied scientific research*, 50(1):83–95, 1993.

S. Nelson. *Dielectric Properties of Agricultural Materials and Their Applications*. Academic Press, 2015.

W. R. Niessen. *Combustion and incineration processes: applications in environmental engineering*. CRC Press, 2010.

T. Nussbaumer and J. Good. Wirkungsgradbestimmung bei Holzfeuerungen. *Schweizer Ingenieur und Architekt (11) März*, 1994.

T. Nuusbaumer. Combustion and co-combustion of biomass. In *Proceedings of 12th European Conference on Biomass for Energy, Industry and Climate Protection*, pages 17–21, 2002.

J. Nyström and E. Dahlquist. Methods for determination of moisture content in woodchips for power plants: a review. *Fuel*, 83(7):773–779, 2004.

I. Obernberger. Decentralized biomass combustion: state of the art and future development. *Biomass and bioenergy*, 14(1):33–56, 1998.

I. Obernberger. Reached developments of biomass combustion technologies and future outlook. In *Proc. of the 17th European Biomass Conference*, 2009.

I. Obernberger, T. Brunner, and G. Bärnthaler. Chemical properties of solid biofuels-significance and impact. *Biomass and Bioenergy*, 30(11):973–982, 2006.

D. O'Shea. *An Introduction to Dynamical Systems and Mathematical Modelling.* State University of New York. Research Foundation, 1992.

N. Ouelhazi, G. Arnaud, and J. Fohr. A two-dimensional study of wood plank drying. the effect of gaseous pressure below boiling point. *Transport in Porous Media*, 7(1):39–61, 1992.

N. Paces and M. Kozek. Modeling of a grate-firing biomass furnace for real-time application. In *International Symposium on Models and Modeling Methodologies in Science and Engineering (MMMse 2011)*, volume 6, 2011.

A. Pandey, T. Bhaskar, M. Stöcker, and R. Sukumaran. *Recent advances in thermochemical conversion of biomass.* Elsevier, 2015.

C. Peishi and D. C. Pei. A mathematical model of drying processes. *International Journal of heat and mass transfer*, 32(2):297–310, 1989.

N. Petchers. *Combined heating, cooling & power handbook: Technologies & applications: An integrated approach to energy resource optimization.* The Fairmont Press, Inc., 2003.

G. Petrecca. *Industrial Energy Management: Principles and Applications: Principles and Applications.* Springer Science & Business Media, 2012.

K. Price, R. M. Storn, and J. A. Lampinen. *Differential evolution: a practical approach to global optimization.* Springer Science & Business Media, 2006.

A. Rasmuson, B. Andersson, L. Olsson, and R. Andersson. *Mathematical Modeling in Chemical Engineering.* Cambridge University Press, 2014.

L. Rosendahl. *Biomass combustion science, technology and engineering.* Elsevier, 2013.

F. Rosillo-Calle and J. Woods. *The biomass assessment handbook.* Earthscan, 2012.

M. Rovaglio, D. Manca, and G. Biardi. Dynamic modeling of waste incineration plants with rotary kilns: Comparisons between experimental and simulation data. *Chemical Engineering Science*, 53(15):2727–2742, 1998.

M. Ruusunen. Real-time moisture content monitoring of solid biomass in grate combustion. In *Proceedings of the 17th World Congress of the IFAC, July*, pages 6–11, 2008.

D. Sartoris and D. Resnick. Dual-energy radiographic absorptiometry for bone densitometry: current status and perspective. *American Journal of Roentgenology*, 152(2):241–246, 1989.

M. Scheftelowitz, J. Daniel-Gromke, N. Rensberg, V. Denysenko, K. Hillebrand, K. Naumann, D. Ziegler, J. Witt, M. Beil, and W. Beyrich. Stromerzeugung aus biomasse (vorhaben iia biomasse) zwischenbericht juni 2015. *DBFZ, Leipzig*, 2015.

R. Scholz, M. Beckmann, and F. Schulenburg. Abfallbehandlung in thermischen verfahren. *Verbrennung, Vergasung, Pyrolyse, Verfahrens-und Anlagenkonzepte. Teubner-Reihe UMWELT, Stuttgart/Leipzig/Wiesbaden: BG Teubner GmbH*, pages 1–460, 2001.

C. Schörghuber, M. Reichhartinger, M. Horn, M. Gölles, and R. Seeber. Control of a biomass-furnace based on input-output-linearization. In *Control Conference (ECC), 2015 European*, pages 3508–3513. IEEE, 2015.

W. Schupe and R. Jeschar. Vereinfachte Berechnung des Strahlungswärmeübergangs in Industrieöfen und Vergleich mit Messungen in einer Versuchsbrennkammer. *Gaswärme International*, 4(24):64–75, 1975.

A. R. Sharp, M. T. Riggin, R. Kaiser, and M. H. Schneider. Determination of moisture content of wood by pulsed nuclear magnetic resonance. *Wood and Fiber Science*, 10(2):74–81, 1978.

Y. Shastri, A. Hansen, L. Rodríguez, and K. Ting. *Engineering and Science of Biomass Feedstock Production and Provision.* Springer, 2014.

C. Sheng and J. Azevedo. Estimating the higher heating value of biomass fuels from basic analysis data. *Biomass and Bioenergy*, 28(5):499–507, 2005.

R. Siegel and J. R. Howell. *Thermal radiation heat transfer*, volume 3. National Aeronautics and Space Administration, 1971.

C. Skaar et al. *Wood-water relations.* Springer-Verlag, 1988.

E. Specht. *Kinetik der Abbaureaktionen.* Cuvillier Verlag, 1993.

H. Spliethoff. *Power generation from solid fuels.* Springer Science & Business Media, 2010.

K. S. Stadler, J. Poland, and E. Gallestey. Model predictive control of a rotary cement kiln. *Control Engineering Practice*, 19(1):1–9, 2011.

P. Stephan, S. Kabelac, M. Kind, H. Martin, D. Mewes, and K. Schaber. *VDI heat atlas*. Springer, Berlin, 2010.

G. Stephanopoulos. *Chemical process control*, volume 2. Prentice hall New Jersey, 1984.

C. Stevens and R. C. Brown. *Thermochemical processing of biomass: conversion into fuels, chemicals and power*. John Wiley & Sons, 2011.

R. Strzalka, T. G. Erhart, and U. Eicker. Analysis and optimization of a cogeneration system based on biomass combustion. *Applied Thermal Engineering*, 50(2):1418–1426, 2013.

J. A. Suykens. *Advances in learning theory: methods, models, and applications*, volume 190. IOS Press, 2003.

T. Tanaka and Y. Kawai. A new method for nondestructive evaluation of solid wood moisture content based on dual-energy x-ray absorptiometry. *Wood science and technology*, 47(6):1213–1229, 2013.

P. J. Thomas. *Simulation of industrial processes for control engineers*. Butterworth-Heinemann, 1999.

D. A. Tillman. *Wood Combustion: Principle, Processes, and Economics*. Academic Press, 1981.

X. Tong, H. Chen, J. Hu, Y. Bi, Z. Sun, and W. Fan. The efficient and sustainable pyrolysis and gasification of biomass by catalytic processes. *ChemBioEng Reviews*, 2(3):157–174, 2015.

G. I. Torgovnikov. *Dielectric Properties of Wood-Based Materials*. Springer, 1993.

S. R. Turns et al. *An introduction to combustion*, volume 287. McGraw-hill New York, 1996.

A. TyssØ. Modelling and parameter estimation of a ship boiler. *Automatica*, 17(1): 157–166, 1981.

A. Ullberg, R. Kullenberg, E. ODÉN, and F. Danielsson. Method and apparatus for measuring moisture content in a biological material, 2010. WO Patent App. PCT/EP2009/062,767.

E. K. Vakkilainen and P. Ahtila. Modern method to determine recovery boiler efficiency. *O PAPEL*, 72(12):58–65, 2011.

R. P. Van Der Lans, L. Pedersen, A. Jensen, P. Glarborg, and K. Dam-Johansen. Modelling and experiments of straw combustion in a grate furnace. *Biomass and Bioenergy*, 19(3):199–208, 2000.

L. Van Kessel. *Stochastic Disturbances and Dynamics of Thermal Processes: With Application to Municipal Solid Waste Combustion*. Technische Universiteit Eindhoven, 2003.

L. Van Kessel, A. Arendsen, and G. Brem. On-line determination of the calorific value of solid fuels. *Fuel*, 83(1):59–71, 2004a.

L. Van Kessel, A. Arendsen, P. de Boer-Meulman, and G. Brem. The effect of air preheating on the combustion of solid fuels on a grate. *Fuel*, 83(9):1123–1131, 2004b.

S. V. Vassilev, D. Baxter, L. K. Andersen, and C. G. Vassileva. An overview of the chemical composition of biomass. *Fuel*, 89(5):913–933, 2010.

R. Viskanta and M. Mengüç. Radiation heat transfer in combustion systems. *Progress in Energy and Combustion Science*, 13(2):97–160, 1987.

P. Von Böckh and T. Wetzel. *Heat transfer: basics and practice*. Springer Science & Business Media, 2011.

N. Wakao and S. Kagei. *Heat and mass transfer in packed beds*, volume 1. Taylor & Francis, 1982.

J. Warnatz, U. Maas, R. W. Dibble, and J. Warnatz. *Combustion*, volume 3. Springer, 2001.

K. Warne, G. Prasad, S. Rezvani, and L. Maguire. Statistical and computational intelligence techniques for inferential model development: a comparative evaluation and a novel proposition for fusion. *Engineering Applications of Artificial Intelligence*, 17(8):871–885, 2004.

H. Watter. Nachhaltige Energiesysteme. *Vieweg+ Teubner— GWV Fachverlage GmbH, Wiesbaden*, 2009.

H. Windisch. *Thermodynamik: ein lehrbuch für ingenieure*. Walter de Gruyter, 2014.

C. Wolf. *Erstellung eines Modells der Verbrennung von Abfall auf Rostsystemen unter besonderer Berücksichtigung der Vermischung*. PhD thesis, Universität Duisburg-Essen, Fakultät für Ingenieurwissenschaften, 2005.

C. Wolf and R. Koralewska. Anwendungsorientierte modellierung und simulation der verbrennungsvorgänge in abfallverbrennungsanlagen. *Chemie Ingenieur Technik*, 77(10):1557–1564, 2005.

C. Yin, L. A. Rosendahl, and S. K. Kær. Grate-firing of biomass for heat and power production. *Progress in Energy and Combustion Science*, 34(6):725–754, 2008.

C.-Y. Yin. Prediction of higher heating values of biomass from proximate and ultimate analyses. *Fuel*, 90(3):1128–1132, 2011.

References related to this thesis

F. Belkhir and G. Frey. Soft-sensing of key process variables in a biomass combustion plant. In *2016 7th International Renewable Energy Congress (IREC)*, pages 1–6, March 2016a. doi: 10.1109/IREC.2016.7478861

F. Belkhir and G. Frey. Model-driven soft sensor for predicting biomass calorific value in combustion power plants. In *Industrial Electronics and Applications (ICIEA), 2016 IEEE 11th Conference on*, pages 807–812. IEEE, 2016b

G. Frey and F. Belkhir. *Produktivität - Qualität - Effizienz Innovative Prozesse für die Produktion von morgen. in: R. Müller and J. Flackus (Eds.)*, chapter Modellbasierte Regelung von Biomasseverbrennungsanlagen, pages 230–248. ISBN 978-3-8440-3509-4 (Print), Shaker Verlag , Herzogenrath, Germany, 2015

F. Belkhir, J. Meiers, F. Felgner, and G. Frey. A biomass combustion plant model for optimal control applications-the effect of key variables on combustion dynamics. In *Renewable Energy Congress (IREC), 2015 6th International*, pages 1–6. IEEE, 2015b

F. Belkhir, D. Kraus Cabo, F. Felgner, and G. Frey. Optimal startup control of a steam power plant using the jmodelica platform. In *Proceedings of the 8th Vienna International Conference on Mathematical Modeling (MATHMOD)*, pages 204–209, 2015a

F. Belkhir, C. Gierend, and G. Frey. Component oriented modeling of biomass incineration plants. In *ICINCO (1)*, pages 396–404, 2013

A Nomenclature

Latin symbols

Symbol	Unit	Meaning
A	m^2	Surface
A_{dr}	J s/kg	Lumped parameter
a	m^2/kg	Interfacial surface area
c_p	J kg/K	Specific heat capacity
c_{O_2}	mol/m^3	Oxygen concentration in flue gas
d_p	mm	Particle diameter
H_U, H_L	kJ/kg	Higher and lower heating values
h	J/kg	Specific enthalpy
K_{evap}	kg/s	Water evaporation rate
k_d	m/s	Mass transfer coefficient
L	m	Length
$L^+_{O_2}$	kg_{O_2}/kg_B	Theoretical oxygen amount
L^+_A	kg_A/kg_B	Theoretical air
$\mathcal{L}$	-	Thermal and chemical losses
M_i	kg/mol	Molar mass of species i
$\dot{m}$,Φ	kg/s	Mass flow rate
Nu	-	Nusselt number
n_G	-	Number of roller grates
n_i	mol	Amount of substance of species i
Pr	-	Prandtl number
p	Pa	Pressure
$\dot{Q}$	W	Heat flow supplied or extracted
R_{thd}	kg/m^2 s	Thermal decomposition rate
R	J/mol K	Universal gas constant
Re	-	Reynolds number
$r_{O_2}^{\nu_{O_2}}$	mol/s	Consumption rate of oxygen
Sc	-	Schmidt number
Sh	-	Sherwood number
s_{eq}	m	Equivalent layer thickness
T	K	Temperature
u	m/s	Fluid superficial velocity
V	m^3	Volume
W	m	Width
v_G	m/s	Grate speed
X	-	Specific humidity of air
x_i	-	Mole fraction of species i
x,y,z	m	Spatial coordinates
y	-	Humidity of fuel

Greek symbols

Symbol	Unit	Meaning
γ_{C}	$\mathrm{kg_C/kg_B}$	Mass fraction C
γ_{H}	$\mathrm{kg_H/kg_B}$	Mass fraction H
γ_{O}	$\mathrm{kg_O/kg_B}$	Mass fraction O
γ_{N}	$\mathrm{kg_N/kg_B}$	Mass fraction N
γ_{S}	$\mathrm{kg_S/kg_B}$	Mass fraction S
Δh_v^{w}	kJ/kg	Enthalpy of vaporization of water
Δh_{R}	J/kg	Enthalpy of reaction
Δ_{rec}	-	Distribution factor of flue gas
λ	-	Excess air ratio
λ_{pa}	W/m K	Thermal conductivity of air
τ	s	Residence time of the reactor
$\nu_{\mathrm{O_2}}$	$\mathrm{kg_{O_2}/kg_B}$	Specific oxygen demand
ν_{pa}	$\mathrm{m^2/s}$	Kinematic viscosity of air
ρ	$\mathrm{kg/m^3}$	Density
β	m/s	Mass transfer coefficient
δ	°deg	Grate inclination angle
τ	s	Residence time
ϵ	-	Emissivity coefficient
ϕ_s	-	Wall/solid surface ratio
ζ	$\mathrm{m^2/s}$	Thermal diffusivity
φ_{sw}	-	View factor
κ	$\mathrm{W/m^2\,K}$	Heat transfer coefficient
ΔT_{LM}	K	Logarithmic mean temperature
Ψ	-	Bed porosity
$\bar{\alpha}$	-	Parameter
$\xi_{\mathrm{O_2}}^{A}$	-	Mass fraction of oxygen in air
φ	-	Relative humidity of air
η	-	Efficiency

Acronyms

BFB	Bubbling-fluidized bed
CFB	Circulating-fluidized bed
CFD	Computer fluid dynamics
CSTR	Continuous stirred tank reactor
CVS	Calorific value sensor
HHV	Higher heating value
LCV	Lower calorific value
PF	Pulverized-fuel
VOC	Volatile organic compound
wb	Wet basis
wf	Water free
wt	Weight
WSGGM	Weighted sum of grey gases model

Subscript and Superscript

A	Air
ad	Adiabatic
a, b, c	Stoichiometric coefficients in $C_aH_bO_c$
B	Biomass/boiler
b	Bed
C	Combustion
c	Condensation
ch	chemical
conv	Convection
db	Dry basis
daf	Dry and ash free
dr	Drum
ds	Dry substance
eff	Effective
el	Electric
evap	Evaporation
F	Furnace
FC	Fixed carbon
fg	Flue gas
fw	Feed water
G	Grate
g	Gas
in	Input
L	Lower
l	Laminar
$\mathcal{L}$	Loss
m	Metal
out	Output
p	Particle

pa	Primary air
rec	Recirculation air
s	Solid
sa	Secondary air
sat	Saturation
sp	Sphere
st	Steam
t	Turbulent
thd	Thermal decomposition of dry biomass
tr	Triple point pressure
tot	Total
U	Upper
v	Vaporization
VM	Volatile matter
w	Water
w	Wall
$+$	Stoichiometric combustion

B Appendix II

Table B.1: Ultimate and proximate analyses of various wood and woody biomass fuels (adapted from [Vassilev et al., 2010]).

Fuel type	Proximate analysis [a]			Ultimate analysis [b]				
	VM	FC	Ash	C	O	H	N	S
Alder-fir sawdust	76.6	19.2	4.2	53.2	40.2	6.1	0.5	0.04
Balsam bark	77.4	20.0	2.6	54.0	39.5	6.2	0.2	0.10
Beech bark	73.7	18.5	7.8	51.4	41.8	6.0	0.7	0.11
Birch bark	78.5	19.4	2.1	57.0	35.7	6.7	0.5	0.10
Christmas trees	74.2	20.7	5.1	54.5	38.7	5.9	0.5	0.42
Elm bark	73.1	18.8	8.1	50.9	42.5	5.8	0.7	0.11
Eucalyptus bark	78.0	17.2	4.8	48.7	45.3	5.7	0.3	0.05
Fir mill residue	82.0	17.5	0.5	51.4	42.5	6.0	0.1	0.03
Forest residue	79.9	16.9	3.2	52.7	41.1	5.4	0.7	0.10
Hemlock bark	72.0	25.5	2.5	55.0	38.8	5.9	0.2	0.10
Land clearing wood	69.7	13.8	16.5	50.7	42.8	6.0	0.4	0.07
Maple bark	76.6	19.4	4.0	52.0	41.3	6.2	0.4	0.11
Oak sawdust	86.3	13.4	0.3	50.1	43.9	5.9	0.1	0.01
Oak wood	78.1	21.4	0.5	50.6	42.9	6.1	0.3	0.10
Olive wood	79.6	17.2	3.2	49.0	44.9	5.4	0.7	0.03
Pine bark	73.7	24.4	1.9	53.8	39.9	5.9	0.3	0.07
Pine chips	72.4	21.6	6.0	52.8	40.5	6.1	0.5	0.09
Pine pruning	782.2	15.1	2.7	51.9	41.3	6.3	0.5	0.01
Pine sawdust	83.1	16.8	0.1	51.0	42.9	6.0	0.1	0.01
Poplar	85.6	12.3	2.1	51.6	41.7	6.1	0.6	0.02
Poplar bark	80.3	17.5	2.2	53.6	39.3	6.7	0.3	0.10
Sawdust	84.6	14.3	1.1	49.8	43.7	6.0	0.5	0.02
Spruce bark	73.4	23.4	3.2	53.6	40.0	6.2	0.1	0.10
Spruce wood	81.2	18.3	0.5	52.3	41.2	6.1	0.3	0.10
Tamarack bark	69.5	26.3	4.2	57.0	32.0	10.2	0.7	0.11
Willow	82.5	15.9	1.6	49.8	43.4	6.1	0.6	0.06
Wood	84.1	15.7	0.2	49.6	44.1	6.1	0.1	0.06
Wood residue	78.0	16.6	5.4	51.4	41.9	6.1	0.5	0.08
Mean	78.0	18.5	3.5	52.1	41.2	6.2	0.4	0.08
Minimum	69.5	12.3	30.1	48.7	32.0	5.4	0.1	0.01
Maximum	86.3	26.3	16.5	57.0	45.3	10.2	0.7	0.42

[a] Dry basis (d.b).
[b] Dry, ash-free basis (d.a.f).

C Appendix I

Table C.1: Combustion characteristics of untreated biomass fuels (adapted from [Döring, 2012]).

Fuel/Type of biomass	LHV MJ/kg	HHV MJ/kg	Ash content %	Volatile components %	Ash deformation DT[a] °C	HT[b] °C	FT[c] °C
Needlewood (with barkless)	19.1	20.5	0.63	-	-	-	-
leafwood(with barkless)	18.9	20.1	0.3	-	-	-	-
Bark needlewood)	19.2	20.4	1.5	77.2	1,440	1,460	1,490
Bark (leafwood)	19.0	20.0	1.5	-	-	-	-
Forest offcuts	18.7	19.7	5.0	-	-	-	-
Spurce(with bark)	18.8	20.2	0.6	82.9	1,426	-	1,583
Beech (with bark)	18.4	19.7	0.5	84.0	-	-	-
Poplar (short rotation)	18.4	19.8	2.0	81.2	1,335	-	1,475
Willow (short rotation)	18.4	19.9	2.0	80.3	1,283	-	1,490
Rye straw	17.4	18.5	4.8	76.4	1,002	1,147	1,188
Wheat straw	17.2	18.5	5.7	77.0	998	1,246	1,302
Triticale straw	17.1	18.3	5.9	75.2	911	1,125	1,167
Barley straw	17.5	18.5	4.8	77.3	980	1,113	1,173
Rapessed straw	17.6	18.8	5.0	75.8	1,273	-	1,403
Corn straw	17.7	18.9	6.7	76.8	1,050	1,120	1,140
Sunflower straw	15.8	16.9	12.2	72.7	839	1,178	1,270
Hemp straw	17.0	18.2	4.8	81.4	1,336	1,420	1,456
Whole rye plants	17.7	19.02	4.2	79.1	-	-	-
Whole wheat plants	17.1	18.7	4.1	77.6	977	1,155	1,207
Whole triticale plants	17.0	18.4	4.4	78.2	833	982	1,019
Rye seeds	17.1	18.4	2.0	80.9	710	-	810
Wheat seeds	17.0	18.4	2.7	80.0	687	887	933
Triticale seeds	16.9	18.2	2.1	81.0	730	795	840
Rape seeds	26.6	28.1	4.3	85.2	-	-	-
Miscanthus	17.7	19.0	4.0	77.6	973	1,097	1,170
Grass (hay) mixed	17.1	18.0	7.0	-	-	-	-

[a] DT: Deformation temperature.
[b] HT: Hemisphere temperature.
[c] FT: Flow temperature.